MASSACHUSETTS INSTITUTE OF TECHNOLOGY
LINCOLN LABORATORY

AIRBORNE LASERNAV II ACCURACY EVALUATION: Modeling Considerations, Parameterizations, and Indicated Performance (via Kalman filter analysis)

T. H. Kerr

NAV ACCURACY EVALUATIONS IN SUPPORT OF ETB DATA COLLECTION MISSIONS

15 February 1991

LEXINGTON MASSACHUSETTS

ABSTRACT

The purpose of this memo is threefold: (1) to offer the system models that we are using to represent the performance of our airborne LASERNAV II inertial navigation system (INS) in operation; (2) to establish the associated navigation accuracy provided by this system; and (3) to recommend the type and frequency of external navaid fixes to be used to update this navigation system in order to adequately support data collection missions for the Electronic Terrain Board (ETB). An INS is strongly cross-coupled in the various channels of gyro input axes and accelerometer input axes that typically defy simple back-of-the-envelop analysis and prediction of results. However, there is an established tradition of properly handling such situations that we are tying into to expedite obtaining of evaluation/prediction results. The conventions and error models that account for the behavior of the gyros and accelerometers were developed by others over the last 30 years and have been independently cross-checked and streamlined here. While plenty of $\sim$ 19 to 25 state variable error models exist for airborne navigation systems, we made a concerted effort to make our model state size here as low as possible (whittled down to 12 states) yet still retain the essence of our airborne Electronic Terrain Board (ETB) imaging data collection application.

Certain intermediate problems were encountered as we proceeded along the principal evaluation path and solutions are worked out as part of the solution process in determining how to best proceed. Proper scaling and units to use are also established here, as needed for insertion as input to the software.

Representative quantitative results are offered here to illustrate the Kalman filter-based accuracy assessment of the performance of, first, a template model or guide of a typical airborne Inertial Navigation System (INS) while proceeding along various flight paths (of 4 to 8 hr mission duration) and experiencing differing conditions of no NAV updates at all, one update per hour, and two updates per hour; then, an evaluation of the performance of our LASERNAV II navigation system (undergoing periodic updates from appropriate fix sources at acceptable rates for missions of 3 to 4 hr duration). Recommendations for the detailed planning and layout of ETB data collection missions are made here based on these results. Subsidiary studies are also identified here that are natural to support decisions on how the LASERNAV II can best be used to support aiding the cameras or other sensors to compensate for the deleterious effects of aircraft motion.

TABLE OF CONTENTS

TABLE OF CONTENTS
(Continued)

LIST OF ILLUSTRATIONS

LIST OF ILLUSTRATIONS
(Continued)

LIST OF ILLUSTRATIONS
(Continued)

LIST OF ILLUSTRATIONS
(Continued)

LIST OF TABLES

1. INTRODUCTION AND OVERVIEW

A simplified linearized error model is being used to represent Honeywell's LASERNAV II as the model is exercised, within a Kalman filter/covariance analysis, to accurately predict expected navigation accuracy attainable during Electronic Terrain Board (ETB) data collection missions (our main objective). The LASERNAV II Navigation Management System is to be installed aboard a Grumman G-1 Gulfstream aircraft that is already equipped with multispectral imaging sensors. LASERNAV is to be used in a supporting role to both provide standard NAV information during data collection missions and possibly to provide motion compensation for airborne cameras and other sensors. Depending on the degree of navigation accuracy predicted by our simulated LASERNAV II performance evaluation, this information can be useful (1) in designating number of and locations for navigation waypoints as part of mission trajectory planning in covering a 10 km $\times$ 10 km area patch via row-wise overflights (row width reflecting the sweepwidth of the particular sensor used); (2) to allow dovetailing of sensor swaths (avoid redundant data overlap with previous rows collected vs. prevent data gaps between successive adjacent rows); (3) in specifying rate of external radio position fix taking to maintain sufficient navigation accuracy to enable tight row dovetailing (critical at end-of-row 3 minute aircraft turns to initiate start of next row as a backsweep); (4) in deciding the preferred location of visual fix updates; and (5) in deciding whether or not real-time navigation data tags should also be inserted within our imaging sensor recording tapes (for auxiliary scene orientation in post-processing).

The purpose of this memo is threefold: (1) to describe the system models that we are using to represent the performance of the airborne LASERNAV II inertial navigation system (INS) in operation; (2) to establish the associated navigation accuracy provided by this system; and (3) to recommend the type and frequency of external navaid fixes to be used to update this navigation system in order to adequately support data collection missions for the Electronic Terrain Board (ETB). An INS is strongly cross-coupled in the various channels of gyro input axes and accelerometer input axes that typically defy simple back-of-the-envelop analysis and prediction of results (see verification of this assertion as [14]). The gyros of an Inertial Navigation System are usually used to establish the stable platform [1] upon which the triad of accelerometers are mounted as the

[1]We recognize that the LASERNAV II is *actually* mechanized as a strapdown system, where the gyros are rigidly bolted physically to the aircraft frame in a particular known orientation and the input axes of the three accelerometers that are installed are also of known orientation with respect to the gyro input axes for proper decomposition of measured accelerations and their subsequent accumulation (integration up) into corresponding components of, first, velocity and then ultimately into components of aircraft position location. We explicitly realize here and exploit the fact for our convenience in numerical evaluation that *ultimate navigation accuracy does not depend upon how the gyros and accelerometers are mechanized* (of the several conventions available) *but does depend fundamentally on the quality of the underlying constituent gyro and accelerometer components* (i.e.,

motion sensing elements. The input axes of the gyros affects the orientation of the input axes of the accelerometers used to sense and measure platform accelerations (subjected to two subsequent integrations to provide velocity and position), which affects the computed gyro-induced platform tilts, which affects the positioning of the sensitive input axes of the gyros, and so on in round-robin fashion. The strong coupling between the gyro drift errors, accelerometer biases errors, and platform tilts or misalignments (contained or captured in the linear error model representation of the INS) allows mere navaid fixes of position to propagate or translate into corrections of *position, velocity, and tilt.* While there are three standard alternate conventions for representing tilts (as either Ψ, Θ, or Φ a'la Pinson/Leondes', Britting's [8], Pitman's [9], Wrigley's, or Farrell's [7] textbook convention) the convention used here [2], which is fast becoming almost universal [3], is to represent gyro behavior using Ψ-angles as *the misalignment between the true frame and the computer frame* (idealization) upon which the computer-based corrections are calculated. The reason it is possible for just position fixes to suffice in correcting gyro-induced platform tilts is because of the inherent *controllability and observability* that exists in the underlying structure of the linearized INS error model [4] and the navaid measurement models of navigation. While *observability and controllability* have been *assumed* to exist for years for Nav error models (without adverse consequences) it has only somewhat recently been rigorously proved in [19], [20], [137] by Itzhack Bar-Itzhack (but the new analytic insight thus availed has now allowed more efficient utilization of the underlying structure in Bar-Itzhack's NAV alignment applications). Recall that observability and controllability

---

associated residual gyro drift-rates and biases as well as any scale factor errors). To expedite a numerical evaluation here we have treated the LASERNAV II as if it were a Local Level system since (1) its final outputs are converted to this form (as latitude and longitude); (2) explicit treatment of strapdown mechanization (as in [115]) is computationally more intensive than other mechanizations (since internal sampling is, of necessity, at a much higher rate than in other mechanizations in order to follow aircraft maneuvers) so to avoid explicit strapdown mechanization during off-line analysis evaluations is a desirable simplification; (3) linearized error models (upon which the associated Kalman navigation filters are based) are of a common form independent of the details of the (nonlinear) mechanization option selected (e.g., [95]), although some specifics of the output sample functions can sometimes have uniquely distinguishable characteristics.

[2]Battles for consistency and relevance of conventions adopted have already been fought and won (viz., [99]-[101]).

[3]Please see [86] for a confirming modern derivation from first principles of the important error equations of navigation (with the claim of providing one new relationship). Although now out of print, the 1963 reference [96] (by the navigation manager at Autonetics) is still highly regarded as a classic in readability in this thorny application area.

[4]While alternative navigation mechanizations exist that on the face of it appear to be drastically different such as Space Stable, Free Inertial, Local Level, Wander-Azimuth, North-Slaved, etc., the associated underlying linear error model equations for each have similar characteristics.

conditions being satisfied are sufficient to guarantee both (1) existence of the solution to the associated Riccati equation from which the covariance of estimation error evolves with time (and from which the time-varying Kalman gains are calculated) and (2) also suffices to guarantee long-term stability or well-behavedness of the Kalman filter in tracking the *true* states (of the error model).

There is an established tradition (covered below in Sections 2, 3, and 4) for properly handling such situations that we are tying into to expedite obtaining of evaluation/prediction results. The conventions and error models that account for the behavior of the gyros and accelerometers were developed by others (C. S. DRAPER LABORATORY, LITTON, AUTONETICS/RI, SINGER-KEARFOTT, TASC, WPAFB/FDL, UNISYS, DRC, NORTHROP, COLLINS/RI, INTERMETRICS INC.) over the last 30 years and have been independently cross-checked and streamlined here. While plenty of $\sim$ 19 to 25 state variable error models exist for airborne navigation systems ([2]-[6], also see Table III of [13] for an extremely convenient overview comparison of twelve different candidate filters for airborne navigation systems, all having slight variations in state selections), we made a concerted effort to make our model state size here as low as possible (whittled down to 12 states) yet still retain the essence of our airborne Electronic Terrain Board (ETB) imaging data collection application. The principal path being used is exposed in this memo as necessary and natural intermediate benchmarks are documented as we check and cross-check the numbers in the matrices that we use as input for the PC-based computer program in generating our first cut results.

Certain intermediate problems were encountered as we proceeded along the principal evaluation path and solutions are worked out, as summarized here, as part of a disciplined approach to the solution process in determining how to best proceed. Additionally, offering easy to read top down documentation here of "where we are and how we got there" helps to expose soft spots, gaps, or holes in our reasoning and by so doing to expedite shoring them up early on. We indicate in Section 6.1 how to properly handle some of the otherwise vaguely delineated parameters of the INS model since we know that explicit total delineation is needed in successfully applying the theory of Kalman filter/covariance analysis, embodied in the associated software package (i.e., all necessary inputs must be supplied and requisite conditions satisfied in order to use it). Proper scaling and units to use are also established in Section 5, as needed for insertion as input to the software in order to obtain the output answers in the units that we want.

Representative quantitative results are offered here in Section 7 to illustrate the Kalman filter-based accuracy assessment of the performance of, first, a template model or guide of a typical airborne Inertial Navigation System (INS) while proceeding along various flight paths (of 4 to 8 hr mission duration) and experiencing differing conditions of no NAV updates at all, one update per hour, and two updates per hour; then, an evaluation of the performance of a LASERNAV II navigation system (undergoing periodic updates from appropriate fix sources at acceptable rates for our ETB data collection missions of 3 to 4 hr duration). Also included here in Section 8 is a list of the goals that we used as a guide for improvement in introducing more model realism and software convenience (beyond what we initially had) as we tailored our tools to handle the larger scale ETB application that we are faced with. This list also suggests refinements for subsequent (second cut)

evaluations. Subsidiary studies are also identified in Section 8 that are natural to support decisions on how the LASERNAV II can best be used to support aiding the cameras or other sensors to compensate for the deleterious effects of aircraft motion. A concise summary highlighting the results and conclusions of this investigation are offered in Section 9. Recommendations for the detailed planning and layout of ETB data collection missions are made in Section 9.3 based on these results.

2. SUMMARY OF NONLINEAR DIFFERENTIAL EQUATION MODEL THAT DESCRIBES THE LASERNAV II ACCURACY ERROR

2.1 An Encapsuled Overview of an Inertial Navigation System

A typical Inertial Navigation System (INS), as in Fig. 1, consists of a platform instrumented by gyroscopes and mounted with accelerometers that can accurately sense accelerations. The accelerometers have known orientations, as maintained by the gyro-instrumented platform. The sensed accelerations are converted to the navigation frame (if necessary), and integrated to provide good estimates of velocity and position of the vehicle (see Fig. 2). The purpose of the gimbals depicted in Fig. 1 for Pitch and Roll is explained in Section 3.2 (see footnote 9).

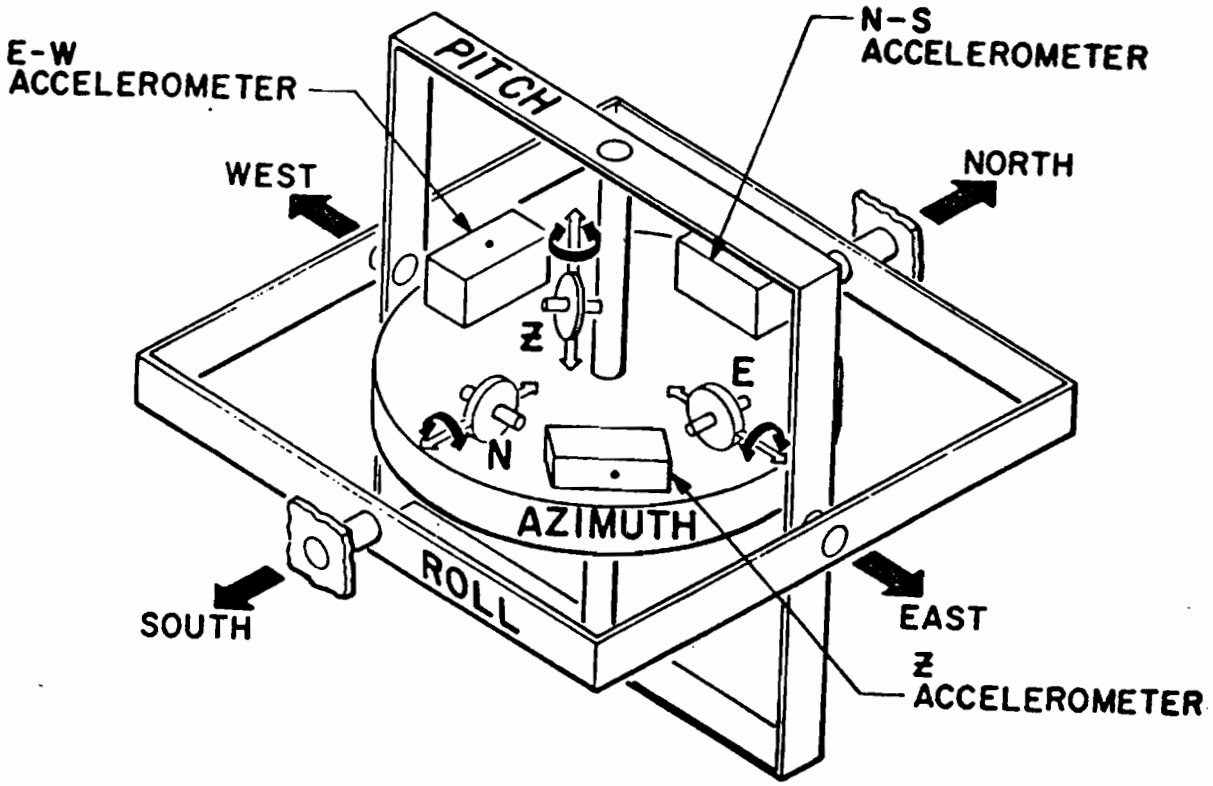

Figure 1. Platform and Structure of a Typical Conventional Airborne Local Level INS Mechanization

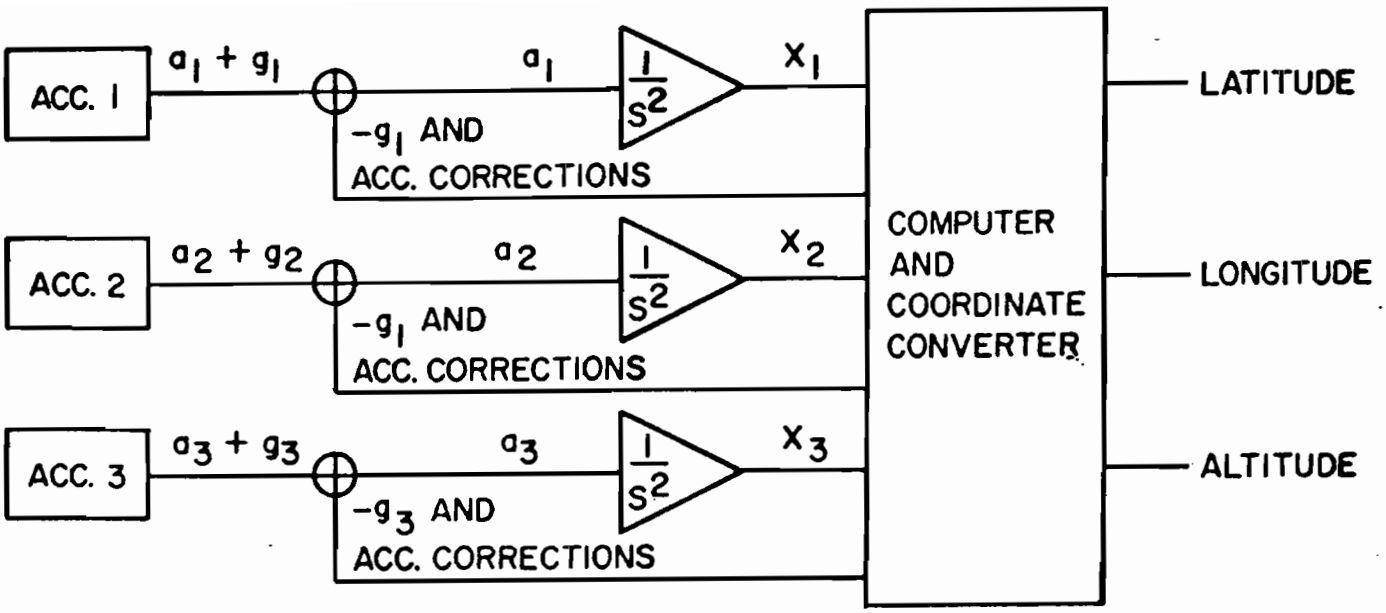

Figure 2. Simplified View of Inputs and Outputs of an INS

Typically, the "effective" INS vertical channel (most severely affected by anomalous gravity effects of the three INS channels [114]) exhibits degradations and tends to grow erroneously with time unless damped by a suitably accurate external reference of altitude (such as from an Air Data System/baro-altimeter [112], laser radar altimeter, or GPS [116], as described in Appendix A). Once compensated by external means and made benign, the vertical accelerometer output can be ignored, as is standard practice in simplified Local Level INS analysis (see Fig. 3) and all attention is focused on the N-S and E-W accelerometers, as the fundamental inputs of greatest importance. Due to small misalignments of the stabilized platform, the presence of possible scale factor errors, and fundamental imperfections in gyro and accelerometer construction and placement within the system, gyros ultimately exhibit drifting effects that cause any INS to experience some degree of cumulative error that increases with the passage of time. Thus, the system must be corrected by occasional position updates or fixes, derived from external sensor subsystems used as navigation aids (navaids, as described in Appendix A), in order to prevent unbounded error growth.

INS drifting is usually tracked (and can therefore be compensated for to an extent) in a Kalman-like filter (included as part of the INS software), based on the characteristic INS error

equations describing the drift experienced by an INS using the particular mechanization employed. The resulting uncompensated or residual drift characterizes the ultimate navigation accuracy provided by the entire navigation system as a functioning coherent unit with or without external navaid fix/updates. The three standard types of gyros are conventional gimballed gyros, conventional strapdown gyros, and strapdown ring laser gyros (RLGs) such as is used in the current LASERNAV II system under investigation. An INS provides pitch, roll, heading, acceleration, velocity, and position of the aircraft and the LASERNAV II can provide this information at the rapid rate of at least 5 times per second, if so desired [5].

2.2 The Fundamentals of INS Error Models

This introductory paragraph, as paraphrased from [19], summarizes pertinent bridging links to how inertial navigation systems are analyzed. Most of the published work on INS error analysis adopt the psi-angle approach and use the velocity error version of the translatory error equations. This model is also used in the present analysis. In addition, components of the platform-to-computer-frame attitude difference or errors are used as the variables of the attitude error equations as a convenient convention that is fast becoming almost universal usage. Although this angular difference is conceptual and cannot be physically instrumented and measured, it possesses the advantage that the translatory error is not coupled into the attitude error equations. The physical attitude difference (or errors) between the platform and a Local Level North-pointing coordinate system (see Fig. 3) can be calculated using the position and attitude errors obtained from the solution of these INS error equations.

The above mentioned convenient selection yields a complete terrestrial INS error model expressed by the following general equations (that account for the crucial Coriolis effect of a rotating non-inertial frame):

$$\begin{aligned} \dot{v} + (\bar{\Omega} + \omega) \times v &= \nabla - (\Psi \times f) + \Delta g \,, \\ \dot{r} + (\rho \times r) &= v \,, \\ \dot{\Psi} + (\omega \times \Psi) &= \epsilon \,, \end{aligned} \tag{1}$$

[5] Data output rates of the LASERNAV II are sometimes faster than merely 5 Hz, depending upon which databus is used to interface to the INS as being either ARINC 429 [28, Table 630] (notably offering 50 Hz for body pitch, roll, and yaw, and the corresponding associated rates), ARINC 419 [28, Table 638] (offering 5 Hz ground present position and velocity but 25 Hz heading rate, bearing, and roll), or ARINC 561 [28, Table 644] (offering 5 Hz for present position and velocity but 25 Hz for bearing to waypoints and roll, heading), while the LASERNAV II itself has an inherent 50 Hz rate (while internal dither to prevent laser lock-up is at 400 Hz).

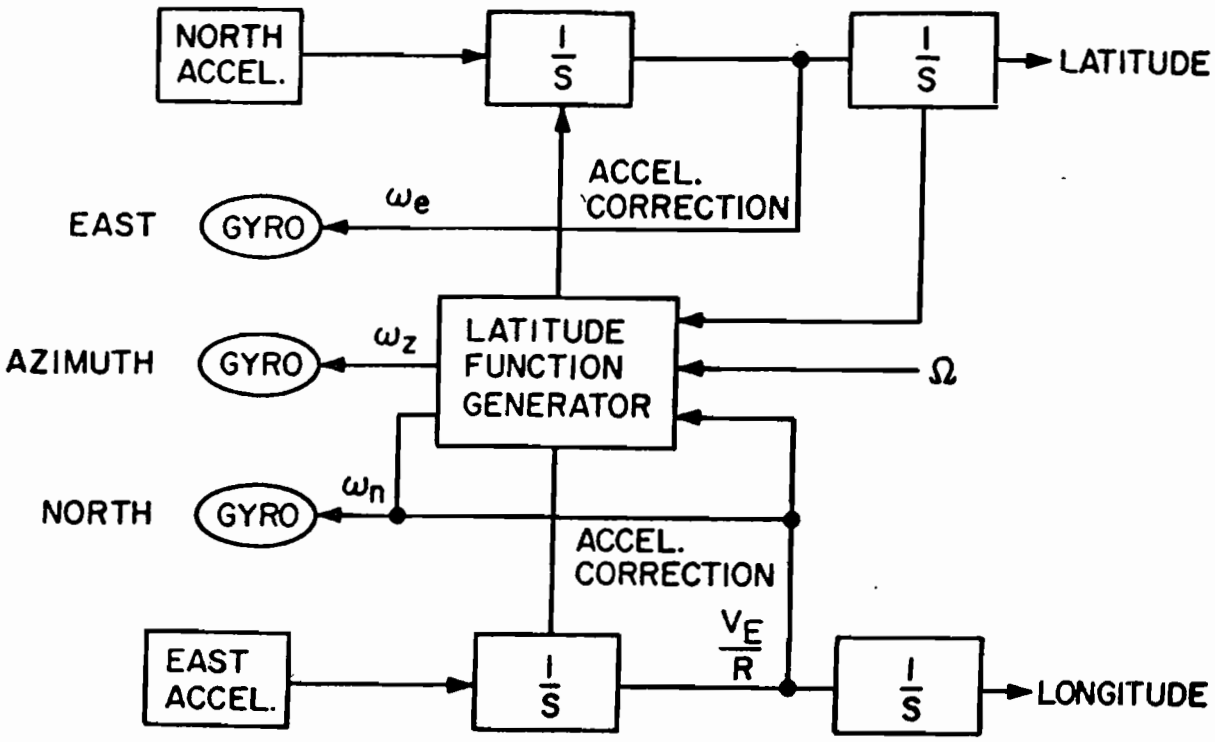

Figure 3. Simplified Block Diagram of Conventional Airborne Local-Level INS

where v, r, and Ψ are, respectively, the velocity, the position, and the attitude error vectors; $\bar{\Omega}$ is the earth rate vector; ω is the angular rate vector of the *true* coordinate system with respect to an inertial frame; ∇ is the accelerometer error vector; f is the specific force vector (accelerations other than gravity experienced by the aircraft during maneuvers); Δg is the error in the computed gravity vector; ρ is the vector of the rate of turn of the true frame with respect to the earth; and finally, ϵ is the gyro drift-rate vector. It can be shown [2] that in the local North, East, Down coordinate system that

$$\bar{\Omega} = \begin{bmatrix} \Omega\cos(L) \\ 0 \\ -\Omega\sin(L) \end{bmatrix}, \tag{2}$$

where L is the local latitude. The vector ω is computed as follows:

$$\omega = \bar{\Omega} + \rho \,, \tag{3}$$

where

$$\rho = \begin{bmatrix} \dot{\lambda}\cos(L) \\ -\dot{L} \\ -\dot{\lambda}\sin(L) \end{bmatrix} \,, \tag{4}$$

where λ represents longitude and $\dot{\lambda}$ represents the rate-of-change in aircraft longitude. In Sections 3 and 4, ϕ will represent longitude and λ will represent latitude. The nonlinear error model of an INS is now complete and will be linearized in Section 4 to be compatible with what is needed in a Kalman filter mechanization.

3. ESSENTIALS OF A KALMAN FILTER MECHANIZATION

A Kalman filter (see Fig. 4) is an efficient and convenient computational scheme for providing the optimal estimate of the system state and an associated measure of the goodness of that estimate (the variance or covariance). In order to implement a Kalman filter, the actual continuous-time system must be adequately characterized by a linear (or linearized) ordinary differential equation model, represented in state space at time t in terms of a vector $x(t)$, and having associated initial conditions specified, and availing sensor output measurements $z(t)$ (functions of the state plus additive measurement noise). It is mandatory that the Kalman filter itself actually contain within it an analytical mathematical model of the system and sensors in order to perform its computations, and it must possess a statistical characterization of the covariance intensity level of the additive white Gaussian measurement and process noises present as well to enable an implementation.

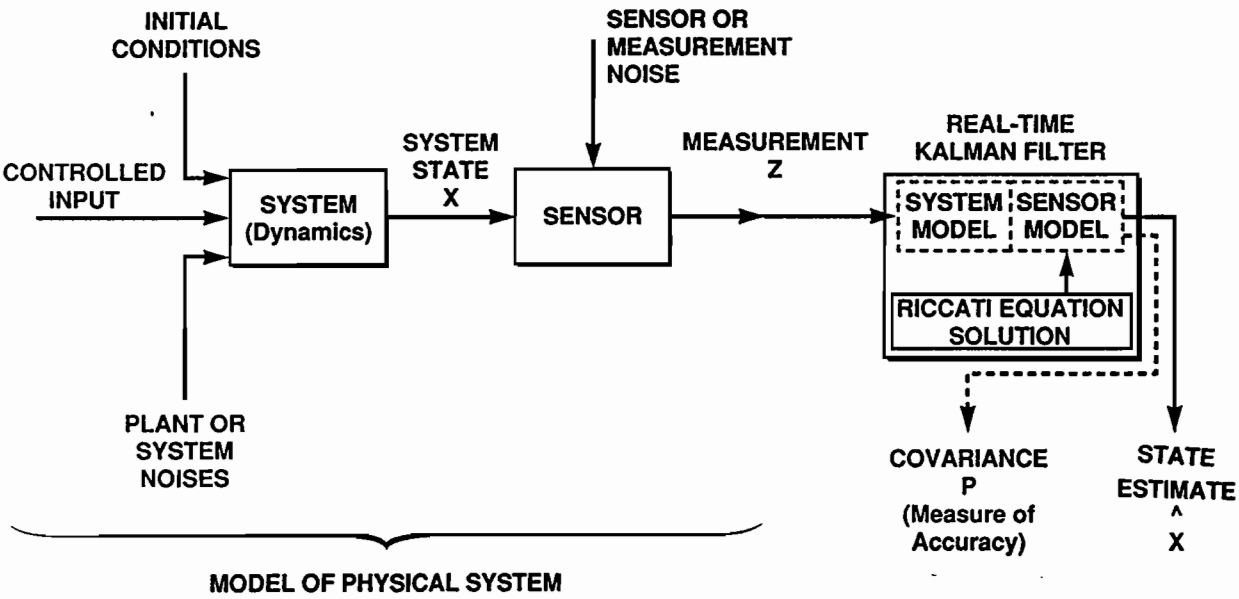

Figure 4. Overview Functional Block Diagram of the Internal Structure of a Kalman Filter

The standard linear dynamical system for which Kalman-type filters are designed has a discrete-time representation consisting of an n-dimensional state vector x_k and an m-dimensional measurement vector z_k of the following well-known form:

$$\text{System}: \quad x_{k+1} = \Phi(k+1,k)x_k + w_k, \tag{5}$$

$$\text{Measurement}: \quad z_k = H_k x_k + v_k, \tag{6}$$

with known initial condition $x(0) \sim \mathcal{N}(\overline{x}(0), P(0))$ and where $\Phi(k+1,k)$ is the known *transition matrix* and the process and measurement noises, w_k and v_k, respectively, are zero mean, white Gaussian noises (independent of the Gaussian initial condition) of known covariance intensity levels Q_k and R, respectively. The two symmetric matrices $P(0)$ and Q_k must be positive semidefinite and the third symmetric matrix R must usually be positive *definite*. Proper computational tests for these requisite properties exist and diagonal matrices that are used as software input for Q_c, R, and $P(0)$ in the present investigation have a definiteness that is always immediately identifiable. The usual conditions of observability/controllability (or less restrictive detectability/stabilizability conditions) are assumed to be satisfied here by the system of Eqs. 5 and 6 without concern since navigation systems have been historically treated as such and are generally structurally well-behaved along these lines, as analytically confirmed in [19], [20], [137]. The above conditions being satisfied guarantee that the covariance calculations from the associated Riccati equation (to be defined below) will be well-behaved and consequently that the resulting Kalman filter will be stable [6].

Equation 5 above is a discrete-time difference equation that corresponds to the solution of an associated underlying continuous-time state variable differential equation (describing the system) of the form:

$$\frac{d}{dt}x = F(t)x + w'(t), \tag{7}$$

---

[6]The conditions have been loosened somewhat over the years to be more easily met in practice, but with weakened hypotheses comes slightly weaker conclusions on the ultimate performance of the Kalman filter. With weaker hypotheses (such as in [18]) instead of being able to make the standard guarantee that the filter is *exponentially asymptotically stable* in converging to proper estimates at a *fast* rate, it can only be validly concluded that the filter is merely stable and will eventually give good estimates if one waits long enough *and the particular application can tolerate such possible delays.* The rigorous demonstrations or proofs of these conclusions on the stability exhibited by the Kalman filter estimates usually utilize Lyapunov functions.

where the *transition matrix* for the general time-varying case of $F(t)$ is obtained by integration of the homogenous part of Eq. 7 over the time interval of interest prior to the next available measurement to be used by the filter. If $F(t)$ is constant, then the appropriate transition matrix simplifies to just an evaluation of the fairly well-known matrix exponential as

$$\Phi(k+1,k) = e^{F\Delta}, \tag{8}$$

where Δ is the appropriate time-step between measurements. Similarly, the appropriate discrete-time process noise covariance intensity level, Q_k, to use in the Kalman filter mechanization equations corresponding to Eq. 5 is obtained by integration of the continuous-time process noise covariance intensity level, $Q_c(t)$, associated with the continuous-time white Gaussian noise $w'(t)$ of Eq. 7 as [3, p. 171, Eq. 4-127b]:

$$Q_k = \int_{t_k}^{t_{k+1}} \Phi(t_{k+1},\tau) Q_c(\tau) \Phi^T(t_{k+1},\tau)\, d\tau, \tag{9}$$

where $\Delta = t_{k+1} - t_k$.

The standard familiar Kalman filter implementation/mechanization equations for periodic measurements available every Δ units of time are as portrayed in Table 1 and the associated block diagram implementation is as depicted in Fig. 5 (c.f., [3, p. 217, Fig. 5.4]). Starting from the initial conditions of $\hat{x}(0) = \overline{x}(0)$ and $P_{0|0} = P(0)$, the two Kalman filter computations that provide the P's (filter covariance of estimation error) and the $\hat{x}$'s (optimal estimate of the state x from the filter proper) are to continue to alternate between the computations of the propagate and update steps of Table 1.

TABLE 1

Standard Kalman Filter Implementation/Mechanization Equations

	PROPAGATE STEP	UPDATE STEP
COVARIANCE	$P_{k\|k-1} = \Phi(k,k-1)P_{k-1\|k-1}\Phi^T(k,k-1) + Q_k$	$P_{k\|k} = [I - K_k H_k]P_{k\|k-1}[I - K_k H_k]^T + K_k R K_k^T$
FILTER GAIN	$K_k = P_{k\|k-1}H_k^T[H_k P_{k\|k-1} H_k^T + R]^{-1}$	
FILTER	$\hat{x}_{k\|k-1} = \Phi(k,k-1)\hat{x}_{k-1\|k-1}$	$\hat{x}_{k\|k} = \hat{x}_{k\|k-1} + K_k(z_k - H_k\hat{x}_{k\|k-1})$

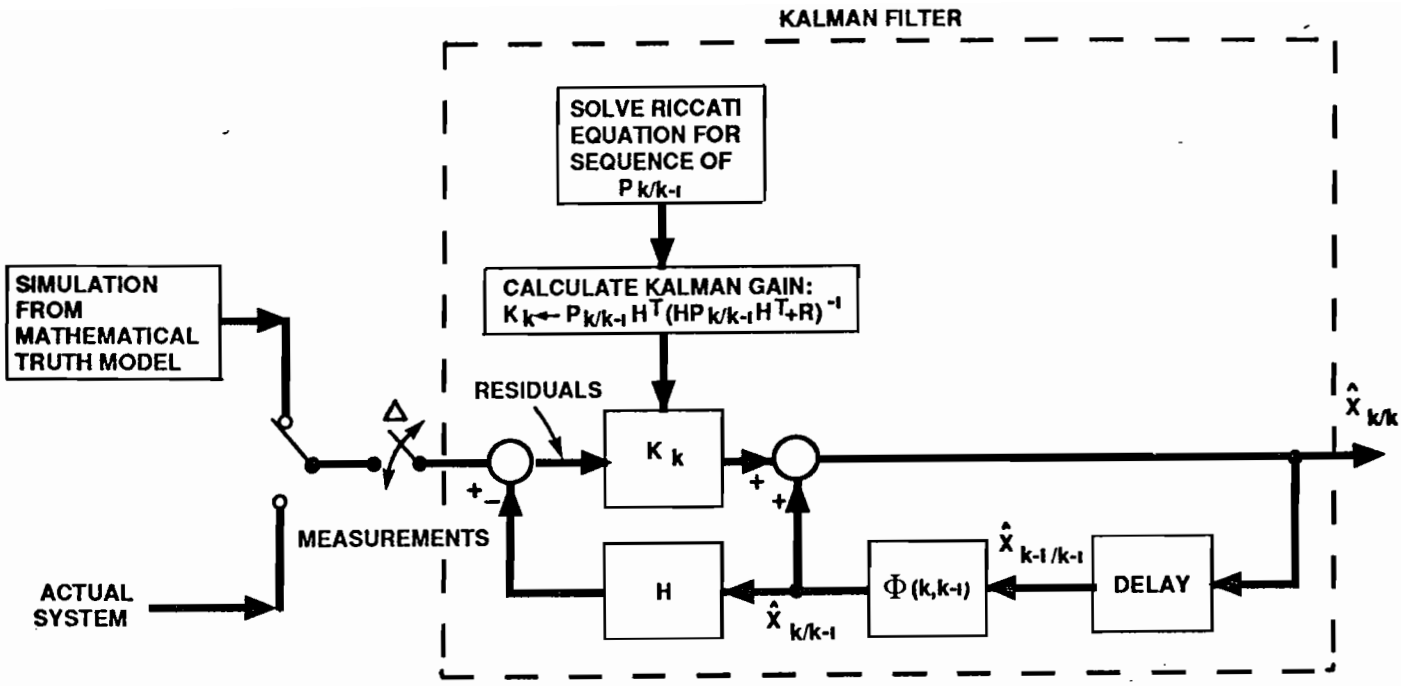

Figure 5. Block Diagram of Standard Discrete-Time Kalman Filter Mechanization (applicable to either a pure simulation or for use with the actual system)

The covariance update equation is

$$P_{k|k} = [I - K_k H_k] P_{k|k-1}$$

$$= [I - K_k H_k] P_{k|k-1} [I - K_k H_k]^T + K_k R K_k^T, \tag{10}$$

while the above two forms are mathematically equivalent, it is the more complex final expression (known as Joseph's form) that more effectively resists the deleterious effect of roundoff in machine computations [3, p. 237] and, due to its form or structure (as the sum of two positive definite matrices rather than as the difference of two such matrices one line above) enforces the desirable feature of positive definiteness (that should be exhibited by valid covariance matrices) and is therefore the preferred implementation. Combining both the propagate and update steps of Table 1 for the

calculation of $P_{k+1|k}$ yields the following single expression for the discrete-time Riccati equation:

$$\begin{aligned} P_{k+1|k} &= \Phi(\mathrm{k}+1,\mathrm{k})[\mathrm{P_{k|k-1}} - \mathrm{P_{k|k-1}H_k^T}[\mathrm{H_kP_{k|k-1}H_k^T} + \mathrm{R}]^{-1}\mathrm{H_kP_{k|k-1}}]\Phi^{\mathrm{T}}(\mathrm{k}+1,\mathrm{k}) + \mathrm{Q_k} \\ &= \Phi(\mathrm{k}+1,\mathrm{k})\{[\mathrm{I} - \mathrm{K_kH_k}]\mathrm{P_{k|k-1}}[\mathrm{I} - \mathrm{K_kH_k}]^{\mathrm{T}} + \mathrm{K_kRK_k^T}\}\Phi^{\mathrm{T}}(\mathrm{k}+1,\mathrm{k}) + \mathrm{Q_k}\,. \end{aligned} \quad (11)$$

This single equation can be used to provide $P_{k|k-1}$ for all the k's of interest. Notice from Fig. 5 that the discrete-time Kalman filter only explicitly uses $P_{k|k-1}$ in its mechanization as used to provide the Kalman gain and doesn't explicitly use $P_{k|k}$ except as an intermediate calculation.

For the sake of simplicity, the Kalman filter mechanization equations above were depicted for the case of periodic measurements being available every Δ units of time. The Kalman filter is by no means restricted to just this periodic measurement case and can handle asynchronous measurement availability of any known time spacing of measurements or even synchronized simultaneous measurements from several different sensors at a time. It is precisely this aspect that makes it lucrative as the unifying basis of multisensor data fusion from several otherwise independent navigation sensors [13]. To put it simply, the Kalman filter is a computational scheme for keeping all the bookkeeping straight and can frequently be implemented in real-time. As output, the Kalman filter provides its "best estimate" and an associated covariance which serves as a gauge of how much faith or trust should be ascribed to this estimate. Covariance analysis, corresponding to the top row of Table 1 and also used in the investigation of this report, as a subset of a full Kalman filter, usually focuses attention on only the variances and/or standard deviations associated with the entries on the main diagonal of $P_{k+1|k}$.

3.1 Covariance Analysis Input Requirements (Same as Needed to Unambiguously Specify a Linear Kalman Filter)

The minimum information needed to completely specify a Kalman filter is summarized here as being:

- *Specification of* the state variables x to be used in the application. (Answer for this ETB data collection navigation support application is provided here in Section 3.2.)
- *Specification of* the system and measurement structure (corresponding either to Eqs. 5 or 7 for the system and to Eq. 6 for the measurement). (Answers for this ETB data collection navigation support application are provided here in Sections 4.1 and 4.2.)
- *Full specification of* the parameter values and matrix entries of either $\Phi(k+1,k)$ or, equivalently, of $F(t)$ (and the time-step Δ or equivalent measurement event time information) or of the vector entries of the nonlinear function $f(x)$ (see Eq. 25 which will subsequently be linearized in Section 4 to eventually be of the form of either $F(t)$ or $\Phi(k+1,k)$ and necessary quantification is completed in Section 5.3.3).
- *Specification of* all the parameter values of the covariance intensities R and Q_k or Q_c (unless there is no process noise, thus $Q_c = 0$ and the Information filter form

of Kalman filtering can be used instead). (Answers for this ETB data collection navigation support application are provided here in Sections 5.1, 5.2, 5.3.4, 5.3.5.)

- *Optional specification of* initial conditions $\overline{x}(0)$ (strictly speaking, this is not needed for just a covariance analysis) and a positive definite $P(0)$ (which is needed in a covariance analysis, as provided for this ETB support application in Section 5.3.2, Eq. 50 and is refined in Eq. 64 by the two phase methodology espoused in Section 6.1). Although *some* value for each of these two quantities *needs to be assigned* (perhaps by guessing) to get the filter started, it is known that a Kalman filter is robust with respect to incorrect initial guesses [7] of these initial conditions [18] and, following an initial transient, the Kalman filter will eventually converge to the proper estimates. However, the better the initial guess, the less time elapses before the filter provides its proper best estimates. Any known initial uncertainty should be utilized and incorporated within the initial $P(0)$ (unless it is completely unknown and is expected to be quite large, then the Information filter form can be used to assume it to be equivalently $\mathcal{I}(0,0) = 0$ without incurring any numerical difficulties of computer register floating point "overflow").

- *Verification* that the system and measurement structure and parameter values for the application satisfy requisite "regularity conditions", namely controllability/observability (detectability/stabilizability) to be certain that the resulting Kalman filter is well-posed and that no numerical difficulties will be encountered in a correctly implemented version in the internal calculations of $P_{k|k-1}$ and $P_{k|k}$ and subsequently of K_k.

This last step is frequently skipped in some applications under the assumption that everything is satisfactory. This skipping is frequently justified if the application area is well studied, as the standard navigation application is (but, as mentioned in Section 1, has just now been analytically completed in [19], [20], [137] a full 25 years after it has been in routine use worldwide).

---

[7] Even an initial guess of $P(0)$ needs to be positive definite because there are n^2 possible solutions of the Riccati equation but only one (unique) correct positive definite solution that evolves with time as long as the initial condition $P(0)$ is positive definite (and the system and measurement equations exhibit controllability and observability, as is already assumed to be the case in this Section). In lieu of no other information being available, a good positive definite initial condition guess to use would be a diagonal matrix with all entries positive; however, we have the diagonal matrix completely specified in Eq. 50 for our LASERNAV II application and have the nondiagonal version exhibited in Eq. 64, as computed on an IBM PC using our software enhancements to [85].

3.2 The System Model

For aircraft navigation applications and supporting investigations there are several different conventions to choose from (e.g., [1], [2], [3, pp. 289-359], [4, pp. 30-31], [5, pp. 31-33], [6, pp. 2-8 to 2-11], [7], [8], [9]). Reference 1 provides a particularly convenient convention to use that doesn't require too large a state size [8] and involves use of the following system of nonlinear differential equations to characterize the behavior of the airborne navigation system when interest is focused only on the subsequent errors incurred in latitude (λ), longitude (ϕ), North velocity (V_N), and ground East velocity (V_{GE}) of the aircraft:

$$\dot{\lambda} = \frac{V_N}{(R_o + h)}, \tag{12}$$

$$\dot{\phi} = \frac{V_{GE}}{(R_o + h)\cos(\lambda)}, \tag{13}$$

$$\dot{V}_N = A_N - (\omega_A + \Omega \sin(\lambda))V_{GE} - E_N - g\,\psi_E + A_E\,\psi_A, \tag{14}$$

$$\dot{V}_{GE} = A_E - (\omega_A + \Omega \sin(\lambda))V_N - E_E + g\,\psi_N - A_N\,\psi_A, \tag{15}$$

where $g = 32.095$ ft/sec^2 $= 9.78049$ m/sec^2 is the acceleration of gravity and

$$\omega_E \equiv \frac{-V_N}{(R_o + h)}, \tag{16}$$

$$\omega_N \equiv \Omega \cos(\lambda) + \frac{V_{GE}}{(R_o + h)}, \tag{17}$$

$$\omega_A \equiv \omega_N \tan(\lambda), \tag{18}$$

where the magnitude of the velocity (i.e., speed) is

$$V = \sqrt{V_N^2 + V_{GE}^2}, \tag{19}$$

and $\Omega = \frac{2\pi \text{ radians}}{24 \text{ hrs}} = 0.2617$ rad/hr $= 0.2506844773°$/min $= 7.292115856 \times 10^{-5}$ rad/sec is the earth rotation rate and $R_o = 6378.145$ km $= 2.092567257 \times 10^7$ ft (= 3963.195563 mi) is the mean radius of the earth and h= altitude of the aircraft above the surface of the earth. The time-varying

---

[8] The computational burden of the Kalman filter/covariance analysis software (to be used as our working tool for runs performed on the PC) goes as $O(n^3)$, where n is the dimension of the state variable model ultimately used. Ref. 1 had a model of state size 14 but our specialization avoids use of Doppler radar and Loran and subsequently has been whittled down to state size 12.

dynamics of gyro misalignment are further characterized by three differential equations describing the time evolution of the three coupled ψ-angles (*as expressed in terms of the true gyro frame to computer frame (i.e., computed) misalignments*):

$$\dot{\psi}_E = D_E - \omega_N \psi_A + \omega_A \psi_N + T_E - \omega_E , \tag{20}$$

$$\dot{\psi}_N = D_N - \omega_A \psi_E + \omega_E \psi_A + T_N - \omega_N , \tag{21}$$

$$\dot{\psi}_A = D_A + \omega_N \psi_E - \omega_E \psi_N + T_A - \omega_A , \tag{22}$$

where the T_i's are the "effective gyro torquing rates [9] based on indicated values of the ω_i's (see Fig. 6)), the D_i's are bias drift-rates of the gyros, the E_i's are the bias errors of the accelerometers, and ψ_E, ψ_N, and ψ_A are the misalignments about the East, North, and Vertical (Azimuth) axes, respectively. Further, all of the component bias terms are assumed to be unknown random constants, which therefore satisfy the following considerably simpler differential equations (see [2, pp. 79, 83]):

$$\dot{D}_E = \dot{D}_N = \dot{D}_A = \dot{E}_E = \dot{E}_N = 0 . \tag{23}$$

Hence according to the bare-bones model offered in [1, p. 431], a reasonable representation of the airborne navigation accuracy error can be obtained from the 12-component state vector defined as follows [10]:

---

[9]The accelerometers are mounted on a platform within a gimbal structure that is compensated in such a manner that the platform remains normal to the earth's gravitational field by being held tangent to the earth's surface at all times. In the LASERNAV II system, the mechanization is evidently strapdown (accounting for the fast rate of body angle readouts of 50 Hz from a ARINC 429 databus interface) while the ultimate position outputs are latitude and longitude, only available at a much slower output rate of approximately 2 to 5 Hz (corresponding to after-the-fact conversion to a Local Level convention). Because of this inherent strapdown mechanization that doesn't need to be precessed, the T_i's in Eqs. 20 to 22 are taken to be zero here in this LASERNAV II application.

[10]While the vertical channel of the INS is unstable [96], it is a standard assumption [89] that altitude information is available from another source such as a barometric altimeter (for use and stablization [97]). Thus, only the two horizontal channels of the INS position and velocity are considered here (as in [1], [89]) in our INS error model, while it is necessary that all three channels of tilts and gyro drifts be considered.

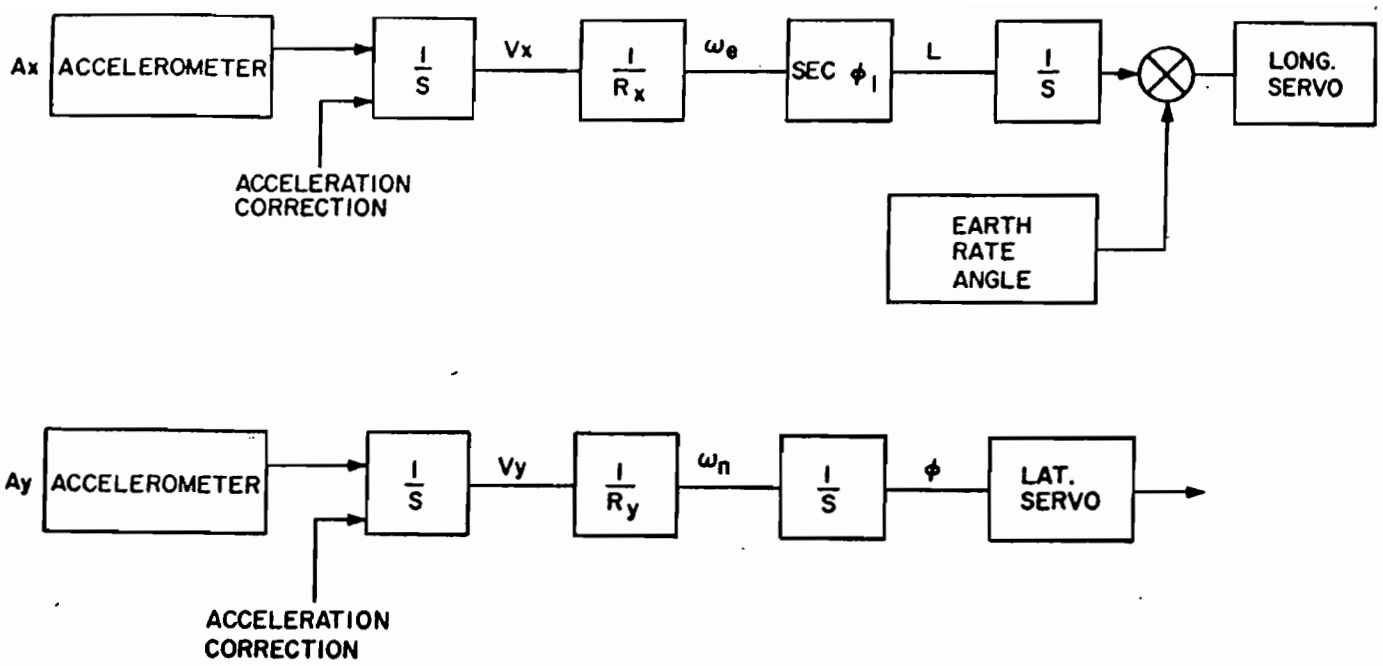

Figure 6. Functional Diagram of the Effective Processing Flow for Computing Gyro Torquing Signals Used in Compensating Conventional Gyros used in a Local Level INS

$$\begin{bmatrix} x_1 \\ x_2 \\ x_3 \\ x_4 \\ x_5 \\ x_6 \\ x_7 \\ x_8 \\ x_9 \\ x_{10} \\ x_{11} \\ x_{12} \end{bmatrix} \triangleq \begin{bmatrix} \lambda \\ \phi \\ V_N \\ V_{GE} \\ \psi_E \\ \psi_N \\ \psi_A \\ D_E \\ D_N \\ D_A \\ E_E \\ E_N \end{bmatrix} = \begin{bmatrix} \text{Latitude of aircraft} \\ \text{Longitude of aircraft} \\ \text{North velocity of aircraft} \\ \text{ground East velocity of aircraft} \\ \text{gyro psi} - \text{angle misalignment, East} \\ \text{gyro psi} - \text{angle misalignment, North} \\ \text{gyro psi} - \text{angle misalignment, Azimuth} \\ \text{gyro drift} - \text{rate bias, East} \\ \text{gyro drift} - \text{rate bias, North} \\ \text{gyro drift} - \text{rate bias, Azimuth} \\ \text{accelerometer bias, East} \\ \text{accelerometer bias, North} \end{bmatrix} . \quad (24)$$

3.3 The Corresponding Measurement Model

Equations 12 to 15, and 20 to 23 when used, per the state assignments of Eq. 24, are of the form of the following nonlinear ordinary differential equation:

$$\dot{x}(t) = f(x) + G(t)u(t)\,, \tag{25}$$

where $u(t)$ is zero mean white Gaussian noise; and for the measurement equation development: the DRAPER Airborne Profiling System (APS) reports [10], [11], [12] acknowledge use of ground-based retroreflectors as a position update to an airborne INS as the only known precedent found in the open literature [11] but which doesn't discuss the presumed mathematical model associated with a visual update from a *landmark of known surveyed location.* For pertinent contributions to this model, the literature of *Search and Screening*, developed during and following WW II, and recently made available in a more up-to-date easy to read form [16 Appendix E], [17], [58] is utilized in Section 5.3.5. The measurement equation and quantification for standard VOR/DME use as position update is provided in [13]. The measurement equation is of the form of a nonlinear algebraic equation:

$$z(t) = h(x) + v_i(t)\,, \tag{26}$$

where $v_i(t)$ are zero mean white Gaussian noises, independent of the $u(t)$ in Eq. 25 and $i = 1$ or 2 corresponds, respectively, to whether VOR/DME or a *visual update* [12] is being used. For both VOR/DME and visual update use,

$$h(x) = \begin{bmatrix} x_1 \\ x_2 \end{bmatrix}\,, \tag{27}$$

while for VOR/DME use

---

[11] WPAFB indicated that some technical aspects were offered on the topic of *use of a visual update* in the vintage 1976 nav system (see [3, p. 361, Item 32]) used on the F-111 (which we have now followed up on in [57]) and later in the 1980's for the B-1 Bomber, while the tactical LANTRIN system has two pods, one for navigation and the other usually used for steering a designator to a point target, but this second pod could also be used in a mode to aid the first by providing slant-range visual fixes or updates off of landmarks of known location.

[12] In military terminology, this operational procedure has been referred to by pilots and airborne navigators as "mark-on-top".

$$v_1(t) \sim \mathcal{N}(0, R_1)\,, \tag{28}$$

and for optical sightings

$$v_2(t) \sim \mathcal{N}(0, R_2)\,, \tag{29}$$

where R_1 and R_2 will be further specified below in Section 5.3.5. The above system and measurement equation [13] together with their partial derivatives (i.e., the corresponding Jacobian matrices F and H, as prescribed in Section 4) and the corresponding *a priori* statistics (initial conditions and covariances to be specified in detail for the generic LASERNAV II system in Section 5.3 are all that are required for realizing the complete accuracy error analysis using Kalman filter/covariance analysis (as available for the PC in a validated basic program entitled *Kalman Filtering Software* [85], as supplied by *Optimization Software, Inc.*).

3.4 Comments on Mechanizing an On-line Kalman Filter for Aircraft Navigation

The above filter navigation error model utilized in this investigation was for theoretical analysis only. There are allowable variations in how a Kalman filter *is to actually be used* in airborne navigation applications (as admirably explained in detail in [3, Chapter 6, Sections 6.3 to 6.6, pp. 291-321]; however, this topic won't be addressed here since explicit real-time filter design is not our current concern). This topic is mentioned here in passing since *it will be* a downstream issue for others using the results of our investigation. What we do in this investigation in Sections 6 and 7 is perform navigation performance evaluations (or predictions) before the fact (as explained/justified in [3, Section 6.8, pp. 325-341]) under the assumption that the true error model and the error model utilized by the Kalman filter *are identical* [14]. Using covariance analysis, we obtain the theoretically computed ensemble averaged covariances in Sections 6.1 and 7.2 without having to deal with messy intermediate sample functions from numerous Monte-Carlo trials.

---

[13] Additional confirmation from C. S. Draper Laboratory was solicited to substantiate that the essence of a RLG has indeed been captured in our model of Section 3.2.

[14] Our assumption that the truth model and the filter model *are identical* is not necessary and explicit differences, if known, can be accounted for and handled by our PC-software (derived from [85] in the manner explained in Sections 8.1 and 8.2) and may result in evaluation differences of as much as $\pm$ 20 % as an estimated worst case departure ([98], [87]); however, the assumption invoked here of being identical is both convenient and computationally expedient being of order n^3 instead of $(n+m)^3$ [98, pp. 251-254], where n and m ($m \leq n$) are the dimensions of the truth model and filter model, respectively.

Our evaluation procedure uses a well-known property frequently exploited to an advantage for navigation applications, namely, that the conditional mean [15] and the conditional (and/or the unconditional) variance (i.e., covariance) of a Gaussian process are independent and that, moreover, the variance (i.e., in this case, the covariance of estimation error of the Kalman filter) is independent of the actual measurements received (but is a function of their specified frequency (i.e., sample rate) and quality (as reflected in their known measurement covariances, R)). Our concentration or focus entirely on covariance analysis in this report is theoretically justified due to the accepted form of linear error models for navigation applications being Gauss-Markov processes (of the form of Eqs. 25 and 26) yielding Gaussian processes as evolutionary solutions. The conditional means (i.e., the state estimates outputted by the Kalman filter) most assuredly *do depend* on the actual values of the measurements received, but the covariance of estimation error does not. Since it is the variance (or more specifically its square root as the standard deviation that appropriately reflects ultimate system accuracy achievable or system uncertainty), our focus on only covariance analysis is theoretically justified. Moreover, alternatives in how a real-time Kalman filter is actually implemented for navigation sometimes reduces to answering questions of whether estimates are periodically subtracted off from whole-value navigation outputs (as a deterministic control action as discussed in [98, p.254, Eq. 7.2-22] to enforce the small angle assumption utilized elsewhere) which likewise requires the corresponding periodic zeroing of Kalman filter estimates. Whether the estimates (i.e, the mean) *is* or *is not* periodically zeroed does not affect the covariance analysis that we employ (which is independent of the mean) so we leave this question open in this investigation since it doesn't currently affect us.

[15] Conditioned on the accumulated measurements $\mathcal{Z}_k = \{z(i) \mid 0 \leq i \leq k,$ where t_k is present time.$\}$.

4. SIMPLIFIED LINEARIZED CONSTANT COEFFICIENT DIFFERENTIAL EQUATION MODEL OF THE LASERNAV II ACCURACY ERROR USED FOR KALMAN FILTER/COVARIANCE ANALYSIS

To linearize the general system of Eq. 25 about the operating point $\bar{x}$, the state space trajectory resulting from applying the control $\bar{u}(t)$, a Taylor series approximation is used and expanded about $\bar{x}$ as

$$\dot{\bar{x}}+\partial\dot{x} = f(\bar{x}+\partial x)+G(t)\,[\bar{u}(t)+\partial u(t)] = f(\bar{x})+\frac{\partial f}{\partial x}|_{x=\bar{x}}\,(\bar{x}+\partial x-\bar{x})+H.O.T.+G(t)\,[\bar{u}(t)+\partial u(t)]\ , \quad (30)$$

and the original

$$\dot{\bar{x}} = f(\bar{x}) + G(t)\bar{u}(t) \quad (31)$$

is then subtracted en masse from Eq. 30 to result in

$$\partial\dot{x} = \frac{\partial f}{\partial x}|_{x=\bar{x}}\,\partial x + G(t)\,\partial u(t)\ , \quad (32)$$

where the higher order terms ($H.O.T.$) are ignored and dropped from further consideration because they are small in comparison to primary terms. In keeping with established tradition, instead of writing the exacting expression ∂x for all the deviations in the now linearized versions of Eq. 32, we just drop the symbol ∂ throughout for convenience while acknowledging that it is actually the deviations that we now have in these states of the linearized model (expressed in the same units, until rescaled in Section 5):

$$\begin{bmatrix} x_1 \\ x_2 \\ x_3 \\ x_4 \\ x_5 \\ x_6 \\ x_7 \\ x_8 \\ x_9 \\ x_{10} \\ x_{11} \\ x_{12} \end{bmatrix} \triangleq \begin{bmatrix} \partial\lambda \\ \partial\phi \\ \partial V_N \\ \partial V_{GE} \\ \partial\psi_E \\ \partial\psi_N \\ \partial\psi_A \\ \partial D_E \\ \partial D_N \\ \partial D_A \\ \partial E_E \\ \partial E_N \end{bmatrix} = \begin{bmatrix} \text{deviation in Latitude of aircraft} \\ \text{deviation in Longitude of aircraft} \\ \text{deviation in North velocity of aircraft} \\ \text{deviation in ground East velocity of aircraft} \\ \text{deviation in gyro psi} - \text{angle misalignment, East} \\ \text{deviation in gyro psi} - \text{angle misalignment, North} \\ \text{deviation in gyro psi} - \text{angle misalignment, Azimuth} \\ \text{deviation in gyro drift} - \text{rate bias, East} \\ \text{deviation in gyro drift} - \text{rate bias, North} \\ \text{deviation in gyro drift} - \text{rate bias, Azimuth} \\ \text{deviation in accelerometer bias, East} \\ \text{deviation in accelerometer bias, North} \end{bmatrix} .$$

This version of a linear error model is now compatible with the form needed for Kalman filtering, as discussed in Section 3.

4.1 The Linearized System Matrix F

The linearized dynamics matrix F used in the transition matrix calculation of

$$\dot{\Phi}(t,\tau) = F(t)\Phi(t,\tau)\ ,\ \Phi(s,s) = I_{n\times n} \tag{33}$$

is obtained by direct differentiation of Eqs. 12 to 15 and 20 to 23 (as summarized/collected in the state variable representation at the bottom of p. 23, in the same order as Eq. 24). The resulting 12×12 matrix (resulting from forming the requisite Jacobian by performing the indicated differentiations) is given by

$$F = \left[\begin{array}{c:c} F_1 & F_2 \\ \cdots & \cdots \\ 0_{5\times 7} & 0_{5\times 5} \end{array}\right], \tag{34}$$

where the (7×7) F_1 and (7×5) F_2 are given below.

$$F_1 = \left[\begin{array}{ccccccc} 0 & 0 & \frac{1}{(R_o+h)} & 0 & 0 & 0 & 0 \\ \frac{1}{(R_o+h)}V_{GE}\tan(\lambda)\sec(\lambda) & 0 & 0 & \frac{1}{(R_o+h)}\sec(\lambda) & 0 & 0 & 0 \\ -(2\Omega\cos(\lambda)+\frac{1}{(R_o+h)}(\sec(\lambda))^2)V_{GE} & 0 & 0 & -2\omega_A & -g & 0 & A_E \\ (2\Omega\cos(\lambda)+\frac{1}{(R_o+h)}(\sec(\lambda))^2)V_N & 0 & \omega_A+\Omega\sin(\lambda) & -\omega_E\tan(\lambda) & 0 & g & -A_N \\ \Omega(\psi_A\sin(\lambda)+\psi_N\cos(\lambda))+\frac{1}{(R_o+h)}V_{GE}\psi_N(\sec(\lambda))^2 & 0 & \frac{1}{(R_o+h)} & \frac{1}{(R_o+h)}(\psi_N\tan(\lambda)-\psi_A) & 0 & \omega_A & -\omega_N \\ -\psi_E(\Omega\cos(\lambda)+\frac{1}{(R_o+h)}V_{GE}(\sec(\lambda))^2)+\Omega\sin(\lambda) & 0 & \frac{-1}{(R_o+h)}\psi_A & \frac{-1}{(R_o+h)}(\psi_E\tan(\lambda)+1) & -\omega_A & 0 & \omega_E \\ -\psi_E\Omega\sin(\lambda)-\Omega\cos(\lambda)-\frac{1}{(R_o+h)}V_{GE}(\sec(\lambda))^2 & 0 & \frac{1}{(R_o+h)}\psi_N & \frac{1}{(R_o+h)}(\psi_E-\tan(\lambda)) & \omega_A & -\omega_E & 0 \end{array}\right], \tag{35}$$

and the corresponding (7×5) matrix is

$$F_2 = \left[\begin{array}{ccccc} 0 & 0 & 0 & 0 & 0 \\ 0 & 0 & 0 & 0 & 0 \\ 0 & 0 & 0 & 0 & -1 \\ 0 & 0 & 0 & -1 & 0 \\ 1 & 0 & 0 & 0 & 0 \\ 0 & 1 & 0 & 0 & 0 \\ 0 & 0 & 1 & 0 & 0 \end{array}\right]. \tag{36}$$

The final forms with constant parameter values as entries in F_1 are provided in Section 5.3.3 for the generic LASERNAV II. The above linear system is driven by process noise $u(t)$. The corresponding continuous-time process noise covariance intensity matrix is depicted in Section 5.3.4 for the generic LASERNAV II.

4.2 The Linearized Observation Matrix H

Similarly, differentiating the observation equation $h(x)$ of Eq. 27 (i.e., forming the Jacobian matrix) yields the following simple linearized observation matrix:

$$H = \begin{bmatrix} 1 & 0 & 0 & 0 & 0 & 0 & 0 & 0 & 0 & 0 & 0 & 0 \\ 0 & 1 & 0 & 0 & 0 & 0 & 0 & 0 & 0 & 0 & 0 & 0 \end{bmatrix} . \tag{37}$$

The measurement covariances corresponding to each different measurement type are depicted in Section 5.3.5 and Fig. 7 depicts how quantified values were arrived at for the visual update case (assuming an aircraft altitude of from 500 to 750 ft.).

The down-looking GaAs line-scanner has a Field-of-View (FOV) of $\pm$ 45°, which at a nominal altitude, h, of 500 ft corresponds to a sweepwidth of $\pm$ 500 ft perpendicular to the direction of flight. As measured from the G-1 aircraft (with a spherical coordinate system established along the aircraft body frame, with origin at the center of the sensor aperature, but with two axes parallel to an assumed locally flat earth), the range, R, to the pre-surveyed retroreflector location (when present within the down-looking line-scanner's FOV) is

$$R = h \ \csc(\phi) , \tag{38}$$

where the depression angle ϕ is measured at the aircraft from the horizontal down. This same simple expression is obtained even after considering this navaid position fix application in 3-dimensions (with two angles, ϕ and θ, being accounted for and not merely viewed in a planar analysis as a simplification) since

$$R = \sqrt{x^2 + y^2 + z^2} , \tag{39}$$

when using the following obvious substitutions (where θ is measured in the horizontal plane):

$$x = R \ \sin(\frac{\pi}{2} - \phi)\cos(\theta) , \tag{40}$$

$$y = R \ \sin(\frac{\pi}{2} - \phi)\sin(\theta) , \tag{41}$$

$$z \;=\; -R\,\cos(\frac{\pi}{2}-\phi) = -h\,, \tag{42}$$

and simplifying the above via use of standard trigonometric identities corresponds to:

$$\begin{aligned} R &= \sqrt{\left[\frac{h}{\cos(\frac{\pi}{2}-\phi)}\cos(\phi)\cos(\theta)\right]^2 + \left[\frac{h}{\cos(\frac{\pi}{2}-\phi)}\cos(\phi)\sin(\theta)\right]^2 + \left[\frac{h}{\cos(\frac{\pi}{2}-\phi)}\sin(\phi)\right]^2} \\ &= h\sqrt{\left[\frac{\cos(\phi)\cos(\theta)}{\sin(\phi)}\right]^2 + \left[\frac{\cos(\phi)\sin(\theta)}{\sin(\phi)}\right]^2 + \left[\frac{\sin(\phi)}{\sin(\phi)}\right]^2} \\ &= h\sqrt{1+(\cot(\phi))^2\left[(\cos(\theta))^2+(\sin(\theta))^2\right]} \\ &= h\sqrt{1+(\cot(\phi))^2} = h\sqrt{(\csc(\phi))^2} = h\;\csc(\phi) \end{aligned} \tag{43}$$

again yielding the original expression, as a minor excursion to get back to what was claimed to be our starting point in Eq. 38. From Papoulis's textbook [133, p. 212, Eq. 7-77], for any random variable (i.e., random component of) R that is a function $f(\cdot,\cdot,\cdot)$, of several other independent random variables (having random components) h, θ, and ϕ as

$$R \;=\; f(h,\theta,\phi)\,, \tag{44}$$

the consequential associated variance is reasonably approximated by

$$\sigma_R^2 \;\approx\; |\frac{\partial f(\cdot)}{\partial h}|^2\,\sigma_h^2 + |\frac{\partial f(\cdot)}{\partial \theta}|^2\,\sigma_\theta^2 + |\frac{\partial f(\cdot)}{\partial \phi}|^2\,\sigma_\phi^2\,; \tag{45}$$

which, for the present application, becomes

$$\begin{aligned} \sigma_R^2 &= |\frac{\partial f(\cdot)}{\partial h}|^2\,\sigma_h^2 + |\frac{\partial f(\cdot)}{\partial \phi}|^2\,\sigma_\phi^2 \\ &= |\csc(\phi)|^2\,\sigma_h^2 + h^2|-\csc(\phi)\cot(\phi)|^2\,\sigma_\phi^2 \\ &= (\csc(\phi))^2\left[\sigma_h^2 + h^2(\cot(\phi))^2\,\sigma_\phi^2\right]\,, \end{aligned} \tag{46}$$

where, as availed from a typical baro-altimeter with uncertainty $\sigma_h = 72$ ft [23, p. 463], this ETB data collection application involves use of a nominal altitude $h = 500$ ft, and the angular uncertainty (associated with the resolution of the down-looking GaAs line-scanner) is $\sigma_\phi = 1$ milliradian. From expression in Eq. 46, it can be deduced that the resulting position uncertainty is worst case for $\phi \sim 0^o$ but this is not a realistically likely extreme to occur in practice. From Fig. 7, a more reasonable choice in this ETB data collection application is to take

$$\begin{aligned}\tan(\phi_o) &= \frac{h}{\text{velocity} \times (\text{time required for scanner to move one resolution element})} \\ &= \frac{h}{\text{velocity} \times t_d} = \frac{500 \text{ ft}}{(72 \text{ meters/sec})\ (39.37 \text{ in/meter}) \times (\frac{1 \text{ ft}}{12 \text{ in}})(0.00000067 \text{ sec})} \\ &= 3141592.650\ ,\end{aligned} \tag{47}$$

since the value t_d, used above in Eq. 47, is defined in [55, p. 85, Eq. 7.4] as

$$\begin{aligned}t_d &= \frac{\phi_b}{\dot{\phi}} = \frac{(\phi_b)^2 \epsilon_s h}{\Phi\ v} \\ &= \frac{(10^{-3})^2 \frac{1}{2}(500 \text{ ft})}{\frac{\pi}{2}\ (72 \text{ meters/sec})\ (39.37 \text{ in/meter}) \times (\frac{1 \text{ ft}}{12 \text{ in}})} \\ &= 0.00000067 \text{ sec}\ ,\end{aligned} \tag{48}$$

consistent with $\phi_o \sim 1$ milliradian, which implies that $\csc(\phi_o) \sim 1$ and $\cot(\phi_o) \sim 0$, hence from Eq. 46

$$\sigma_R^2 \approx \sigma_h^2\ , \tag{49}$$

as used in the computation of the nominal measurement noise covariance intensity matrix of Eqs. 55, 63.

Slight navigator delay or missynchronization in time [16] (senescence) between actually flying over a landmark and the navigator's successfully entering into INS the presence of the visual landmark (retroreflector's registration for the laser radar) of known surveyed location (within view as the G-1 aircraft flies over the landmark because of the existence of our down-looking GaAs line scanning sensor (or possibly our CO_2 laser radar instead), with their real-time displays, as are mandatory for being able to enter updates into the LASERNAV II *in real-time*, as likely needed) can be converted to an effective position error incurred. According to the INSTALLATION MANUAL [28], LASERNAV II can accommodate visual or radio-based NAV updates, as manually inserted in the *Freeze Frame* mode. A representative functional processing flow for accommodating visual NAV updates is offered in Fig. 8.

[16] According to [1, p. 432, 1^{st} col., 2^{nd} par.], known time-delays can easily be incorporated into the observation by considering the measurements to behave as a first-order system with an identically specified time-constant. Such additional realism in the model can be achieved by the addition of another state variable with the penalty that the order of the underlying model is increased.

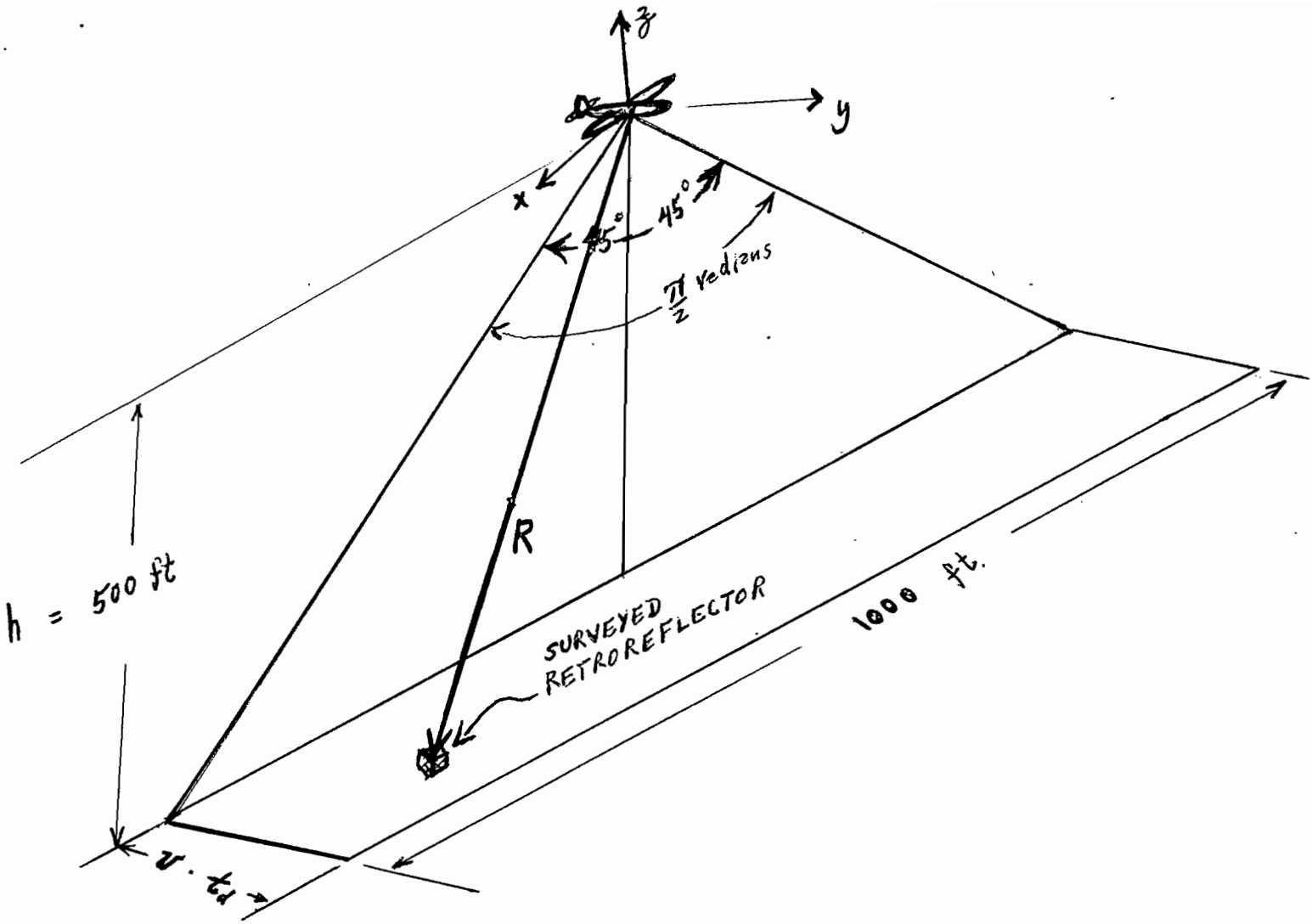

Figure 7. Visual NAV Update: Altitude of aircraft above ground test/measurement area establishes intensity of measurement error as a function of leverarm (500 ft altitude minimum/750 ft maximum), angle, in radians (segment of sensors Field-of-View (FOV)=$\pm$ 45°), and aircraft speed (nominally 140 kts≈72 m/sec≈4321 m/min) (Resolution: 1 millirad (min. 15 cm, max. 21 cm))

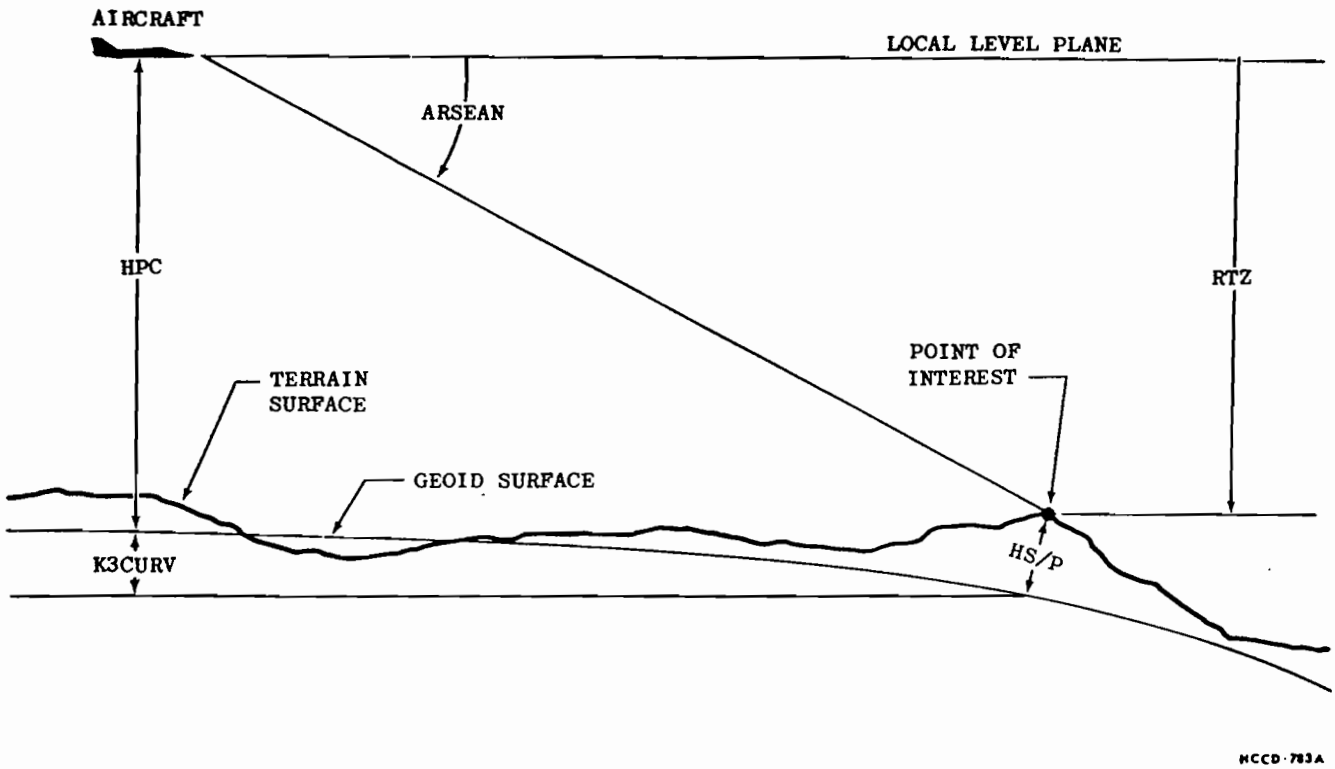

Figure 8. From [57], Functional Processing Flow for Use of a Visual NAV Update from a Point of Known Surveyed Location

5. EXTRACTING NECESSARY MODELING INFORMATION FROM HONEYWELL's PARAMETERIZATION OF A GENERIC LASERNAV II SYSTEM

We were availed with the following historical numbers, representing 1-σ ensemble values of a "typical" generic LASERNAV II system, consistent with what is minimally needed to characterize a Ring Laser Gyro (RLG) based navigation system [51], [52], [113, pp. 1161-1163], [115] by HONEYWELL. We are using these numbers of Section 5 corresponding to residual uncompensated drifts and biases in order to proceed in our investigation here at Lincoln by having representative numbers with units provided so that we know how to appropriately scale the parameters of our program to provide the output in the proper units (that we seek). These numbers of Section 5 are being treated as HONEYWELL proprietary and reflect how a nominal LASERNAV II performs if its accelerometer and gyro suppliers meet their intermediate specs and which enables Honeywell to guarantee that as a consequence the completed LASERNAV II system meets spec (as only coarsely quantified at the aggregate level of the final systems characteristics in the INSTALLATION MANUAL [28]).

5.1 The Generic LASERNAV II Gyro Parameters

GYRO ERROR SOURCES 1-σ values:

- Bias Instability:
  - x- and y-, 0.004°/hr, SPECIFIES KF INITIAL CONDITIONS
  - z-, 0.0088°/hr, SPECIFIES KF INITIAL CONDITIONS
- Gyro angle random walk:
  - x- and y- 0.00214°/$\sqrt{\text{hr}}$, SPECIFIES KF PROCESS NOISE COVARIANCE
  - z-, 0.005°/$\sqrt{\text{hr}}$, SPECIFIES KF PROCESS NOISE COVARIANCE
- Gyro scale factor error:
  - x-, y-, and z-, 5 parts per million (ppm),
- Gyro orthogonality error:
  - x-, y-, and z-, 56 micro-radians, SPECIFIES KF INITIAL CONDITIONS

- Gyro misalignment error:
  - x-, y-, and z-, 20 micro-radians. SPECIFIES KF INITIAL CONDITIONS

5.2 The Generic LASERNAV II Accelerometer Parameters (Spec Values Imposed on Two Different Suppliers)

ACCELEROMETER ERROR SOURCES 1-σ values [17]:

- Bias Instability:
  - x- and y-, 56 micro-g's, SPECIFIES KF INITIAL CONDITIONS
  - z-, 840 micro-g's, SPECIFIES KF INITIAL CONDITIONS
- Accelerometer nonlinearity:
  - x- and y-, 13.3 micro-g's,
  - z-, 200 micro-g's,
- Accelerometer scale factor error:
  - x- and y-, 300 parts per million (ppm),
  - z-, 1500 ppm,
- Accelerometer orthogonality error (i.e., non-orthogonalities in mounting):
  - x-, y-, 56 micro-radians,
  - z-, 840 micro-radians,
- Accelerometer bias trending during alignment:
  - x-, y-, 0.011 micro-g's/sec,
  - z-, 0.25 micro-g's/sec.

[17] These are from specs imposed by HONEYWELL on accelerometers, supplied by subcontractors SUNSTRAN and SYSTAR-DONNER, and on suppliers of the gyro subsystems.

The statements enclosed within the boxes in the above Sections 5.1 and 5.2 serve as forward pointers to where and how these necessary parameters are subsequently used in Sections 5.3.2 to 5.3.5 as a convenient means of providing traceability of parameters (that later appear in the Kalman filter(KF)/covariance analysis) back to where it originally arose in the ETB data collection application.

5.3 Finishing the Modeling for the Known Parameter Values

5.3.1 Conversion factors

While 1 arcmin=1 nautical mile for segments of a great circle of the earth (such as occur for all circles of longitude), and a reasonable conversion from arcmin to nautical miles for latitude involves multiplying by the reciprocal of cos(latitude), the proper conversion factors [26, p. 124, Table 6] from angular measure to linear measure for both latitude and longitude as a function of the latitude (for latitude=42^o 20 arcmin) are:

$$111{,}073\ \frac{\text{meters}}{\text{degrees of latitude}} = \frac{111{,}073}{60}\ \frac{\text{meters}}{\text{arcmin of latitude}} = 1851.22\ \frac{\text{meters}}{\text{arcmin of latitude}},$$

$$82{,}851\ \frac{\text{meters}}{\text{degrees of longitude}} = \frac{82{,}851}{60}\ \frac{\text{meters}}{\text{arcmin of longitude}} = 1380.85\ \frac{\text{meters}}{\text{arcmin of longitude}}.$$

For converting the plot and print output time scale from hours (that will be naturally occurring if velocities are expressed in miles/hour or kilometers/hour) to minutes that appear to be more appropriate for this present application, where the time step between navigation fixes varies from $\Delta = \frac{45}{60}$ minutes to $\Delta = 30$ minutes, the obvious scale factor to use is $\frac{1}{60}\ \frac{\text{hr}}{\text{min}}$.

5.3.2 Initial condition covariance $P_{0|0}$

A dimensional analysis was performed on the equations describing the INS errors and the following indicated convention to use in the software was selected to be consistent and compatible with our application. The phase one expression for $P_{0|0}$, obtained from the generic LASERNAV II parameters provided earlier in Section 5, is:

$$\text{diag}\{P_{0|0}\} = \begin{bmatrix} (.4 \text{ nmi})^2 \\ (.4 \text{ nmi})^2 \\ (6 \textit{ knots})^2 \\ (6 \textit{ knots})^2 \\ (59.464 \text{ micro} - \text{radians})^2 \\ (59.464 \text{ micro} - \text{radians})^2 \\ (59.464 \text{ micro} - \text{radians})^2 \\ (0.004^o/\text{hr})^2 \\ (0.004^o/\text{hr})^2 \\ (0.0088^o/\text{hr})^2 \\ (56 \text{ micro} - \text{g's})^2 \\ (56 \text{ micro} - \text{g's})^2 \end{bmatrix} = \begin{bmatrix} (740.8 \text{ meters})^2 = 548,784 \text{ (meters)}^2 \\ (740.8 \text{ meters})^2 = 548,784 \text{ (meters)}^2 \\ (185.2 \frac{\text{meters}}{\text{min}})^2 = 34,299.04 (\frac{\text{meters}}{\text{min}})^2 \\ (185.2 \frac{\text{meters}}{\text{min}})^2 = 34,299.04 (\frac{\text{meters}}{\text{min}})^2 \\ (0.20442 \text{ arcmin})^2 = 0.0418 \text{ (arcmin)}^2 \\ (0.20442 \text{ arcmin})^2 = 0.0418 \text{ (arcmin)}^2 \\ (0.20442 \text{ arcmin})^2 = 0.0418 \text{ (arcmin)}^2 \\ (0.004 \frac{\text{arcmin}}{\text{min}})^2 = 0.000016 (\frac{\text{arcmin}}{\text{min}})^2 \\ (0.004 \frac{\text{arcmin}}{\text{min}})^2 = 0.000016 (\frac{\text{arcmin}}{\text{min}})^2 \\ (0.0088 \frac{\text{arcmin}}{\text{min}})^2 = 0.000077 (\frac{\text{arcmin}}{\text{min}})^2 \\ (1.9717 \frac{\text{meter}}{\text{min}^2})^2 = 3.887 (\frac{\text{meter}}{\text{min}^2})^2 \\ (1.9717 \frac{\text{meter}}{\text{min}^2})^2 = 3.887 (\frac{\text{meter}}{\text{min}^2})^2 \end{bmatrix} \quad ,(50)$$

where in the above the Root Summed Squared (RSS) result: $\sqrt{(56)^2 + (20)^2} = 59.464$ was used along with the 1-σ uncertainties on position and velocity from [28, Table 501]. A finalized, non-diagonal, phase two version of $P_{0|0}$ to be used in the production run simulations is offered in Section 6.1. It is obtained by starting with this diagonal initial condition $P_{0|0}$ to start the covariance simulation software, then proceeding to run the software for a few (i.e., 30) iterations until a type of steady-state is reached possessing, in general, both diagonal and off-diagonal terms for $P_{0|0}$.

5.3.3 Explicit parameters for the linearized system matrix F_1

Finishing the generic LASERNAV II model for system matrix F_1 using explicit parameters in the expression for the matrix F_1 of Eq. 35, when linearized about the latitude of the Boston area (λ_o=Latitude=42° 20 arcmin = $42.33\overline{3}$) simplifies (since $\tan(\lambda_o) = 0.910994$, $\sec(\lambda_o) = 1.352741$, $\cos(\lambda_o) = 0.739239$, $\sin(\lambda_o) = 0.673442$, aircraft altitude=$h$ = 500 ft = 0.1524 km, $\Omega = \frac{2\,\pi \text{ radians}}{24 \text{ hr}} = 0.261$ radians/hr = 0.00436 radians/min, R_o = 6378.145 km = 2.092567257×10^7 ft)

to become [12]:

$$
F_1 = \begin{bmatrix}
0 & 0 & \frac{1}{(R_o+h)} & 0 & 0 & 0 & 0 \\
\frac{1}{(R_o+h)} V_{GE} \tan(\lambda) \sec(\lambda) & 0 & 0 & \frac{1}{(R_o+h)} \sec(\lambda) & 0 & 0 & 0 \\
-(2\Omega \cos(\lambda) + \frac{1}{(R_o+h)} (\sec(\lambda))^2) V_{GE} & 0 & 0 & -2\omega_A & -g & 0 & A_E \\
(2\Omega \cos(\lambda) + \frac{1}{(R_o+h)} (\sec(\lambda))^2) V_N & 0 & \omega_A + \Omega \sin(\lambda) & -\omega_E \tan(\lambda) & 0 & g & -A_N \\
\Omega(\psi_A \sin(\lambda) + \psi_N \cos(\lambda)) + \frac{1}{(R_o+h)} V_{GE} \psi_N (\sec(\lambda))^2 & 0 & \frac{1}{(R_o+h)} & \frac{1}{(R_o+h)} (\psi_N \tan(\lambda) - \psi_A) & 0 & \omega_A & -\omega_N \\
-\psi_E(\Omega \cos(\lambda) + \frac{1}{(R_o+h)} V_{GE} (\sec(\lambda))^2) + \Omega \sin(\lambda) & 0 & \frac{-1}{(R_o+h)} \psi_A & \frac{-1}{(R_o+h)} (\psi_E \tan(\lambda) + 1) & -\omega_A & 0 & \omega_E \\
-\psi_E \Omega \sin(\lambda) - \Omega \cos(\lambda) - \frac{1}{(R_o+h)} V_{GE} (\sec(\lambda))^2 & 0 & \frac{1}{(R_o+h)} \psi_N & \frac{1}{(R_o+h)} (\psi_E - \tan(\lambda)) & \omega_A & -\omega_E & 0
\end{bmatrix}
$$

$$
= \begin{bmatrix}
0 & 0 & \frac{1}{(6378145+152.4)} \\
\frac{1}{(6378297.4)} (3055.6)(0.910994)(1.352741) & 0 & 0 \\
-(2(0.00436)(0.739239) + \frac{1}{(6378297.4)} (1.352741)^2)(3055.6) & 0 & 0 \\
(2(0.00436)(0.739239) + \frac{1}{(6378297.4)} (1.352741)^2)(3055.6) & 0 & -0.00326 + (0.00436)(0.673442) \\
(0.00436)((0.20442)(0.673442) + (0.20442)(0.739239)) + \frac{1}{(6378297.4)} (3055.6)(0.20442)(1.352741)^2 & 0 & \frac{1}{(6378297.4)} \\
-(0.20442)((0.00436)(0.673442) + \frac{1}{(6378297.4)} (3055.6)(1.352741)^2) + (0.00436)(0.673442) & 0 & \frac{-1}{(6378297.4)} (0.20442) \\
-(0.20442)(0.00436)(0.673442) - (0.00436)(0.739239) - \frac{1}{(6378297.4)} (3055.6)(1.352741)^2 & 0 & \frac{1}{(6378297.4)} (0.20442)
\end{bmatrix}
$$

$$
\begin{bmatrix}
0 & 0 & 0 & 0 \\
\frac{1}{(6378297.4)} (1.352741) & 0 & 0 & 0 \\
2(0.00326) & -(35209.8) & 0 & 3520.98 \\
(0.00047)(0.910994) & 0 & (35209.8) & -3520.98 \\
\frac{1}{(6378297.4)} ((0.20442)(0.910994) - (0.20442)) & 0 & -0.00326 & -0.003577 \\
\frac{-1}{(6378297.4)} ((0.20442)(0.910994) + 1) & 0.00326 & 0 & -0.00047 \\
\frac{1}{(6378297.4)} ((0.20442) - (0.910994)) & -0.00326 & 0.00047 & 0
\end{bmatrix}
$$

$$
= \begin{bmatrix}
0.0000 & 0.0000 & 0.000000157 & 0.0000 & 0.0000 & 0.0000 & 0.0000 \\
0.0005904 & 0.0000 & 0.0000 & 0.0000002 & 0.0000 & 0.0000 & 0.0000 \\
-19.6978 & 0.0000 & 0.0000 & 0.00652 & -35209.8 & 0.0000 & 3520.98 \\
19.6978 & 0.0000 & -0.0003238 & 0.00042817 & 0.0000 & 35209.8 & -3520.98 \\
0.00144 & 0.0000 & 0.000000157 & -0.000000003 & 0.0000 & -0.00326 & -0.003577 \\
0.0021568 & 0.0000 & -0.000000032 & -0.000000186 & 0.00326 & 0.0000 & 0.00047 \\
-0.004700 & 0.0000 & 0.000000032 & -0.000000108 & -0.00326 & 0.00047 & 0.0000
\end{bmatrix}, \tag{51}
$$

where in the above via Eqs. 2, 3, 4:

$$
\begin{bmatrix} \omega_N \\ \omega_E \\ \omega_D \end{bmatrix} = \begin{bmatrix} (0.00436)(0.739239) \\ 0 \\ -(0.00436)(0.673442) \end{bmatrix} + \begin{bmatrix} \frac{4321}{\sqrt{2}(6378145)} (0.739239) \\ -\frac{4321}{\sqrt{2}(6378145)} \\ -\frac{4321}{\sqrt{2}(6378145)} (0.673442) \end{bmatrix} = \begin{bmatrix} 0.003577 \\ -0.00047 \\ -0.00326 \end{bmatrix}, \tag{52}
$$

[18] Rather than assume aircraft velocity components to be in one or the other channel exclusively and consequently risk zeroing out some terms in the linearized system matrix, we instead assume that the aircraft velocity components are equal in magnitude in both North-South and East-West directions, as 45° North by Northeast, where $V_{GE} = 3055.6$ meters/min, $V_N = 3055.6$ meters/min, and therefore $V = \sqrt{V_{GE}^2 + V_N^2} = 4321$ meters/min(=72 meters/sec=140 kts).

and assumption also is that the relatively benign aircraft accelerations are $A_E = 0.1g = 3520.98$ ft/min^2 and $A_N = 0.1g = 3520.98$ ft/min^2; but for straight and level flight at constant velocity, these accelerations are zeroed out in our simulations.

5.3.4 Process noise covariance Q

The expression for the process noise covariance intensity matrix Q is:

$$Q = \text{diag}\{0,0,0,0,0,0,0, \overbrace{(0.016576\ \tfrac{\text{arcmin}}{\sqrt{\text{min}}})^2}^{(0.00214\ \frac{^\circ}{\sqrt{\text{hr}}})^2}, \overbrace{(0.016576\ \tfrac{\text{arcmin}}{\sqrt{\text{min}}})^2}^{(0.00214\ \frac{^\circ}{\sqrt{\text{hr}}})^2}, \overbrace{(0.03872\ \tfrac{\text{arcmin}}{\sqrt{\text{min}}})^2}^{(0.005\ \frac{^\circ}{\sqrt{\text{hr}}})^2}, 0, 0\} \tag{53}$$

$$= \text{diag}\{0,0,0,0,0,0,0,0.00027478\,(\tfrac{\text{arcmin}}{\sqrt{\text{min}}})^2, 0.00027478\,(\tfrac{\text{arcmin}}{\sqrt{\text{min}}})^2, 0.0015\,(\tfrac{\text{arcmin}}{\sqrt{\text{min}}})^2, 0, 0\}\,,$$

and corresponds to the presence of random components of gyro drift-rates that serve as drivers or as an ultimate primal source of system errors.

5.3.5 Measurement noise covariance R

The expression for the measurement noise covariance intensity matrix R_1, corresponding to use of VOR/DME [23], [33] as a navaid fix source, is [42, p. 3, paragraph 1]:

$$\begin{aligned} R_1 &= \text{diag}\{(\tfrac{0.2}{\sqrt{2}}\ \text{nmi})^2, (\tfrac{0.2}{\sqrt{2}}\ \text{nmi})^2\} \\ &= \text{diag}\{(261.9\ \text{meters})^2, (261.9\ \text{meters})^2\} \\ &= \text{diag}\{68598\ (\text{meters})^2, 68598\ (\text{meters})^2\}\,. \end{aligned} \tag{54}$$

The principles of operation for VOR/DME, as an external navaid fix source, are provided in Section A.2 of the Appendix. Other candidate external navaid fix sources to be considered for use in the future (like GPS and differential GPS) are also described in the Appendix.

The down-looking GaAs laser line-scanner of near-infrared/visible wavelength (NIRV) active/passive subsystem, a component of the entire multispectral active/passive line scanner (MAPLS), is currently perceived as the likely candidate to be used to obtain the retroreflector information for image orientation purposes for ETB. Both the forward-looking CO_2 laser and the *GaAs* laser line-scanner currently have real-time displays so necessary for making real-time visual Nav updates to LASERNAV II from sightings of retroreflectors located at known, previously surveyed locations. The detailed characteristics of both the CO_2 laser and the GaAs laser line-scanner are provided, respectively, in Section 1.3 and Section 7.5.4 of [55]. The *GaAs* laser line-scanner has a resolution of 1 millirad $\times$ 1 millirad at the nominal aircraft surveillance altitude of from 500 to 750 ft (corresponding explicitly to 15 cm and 21 cm resolutions, respectively). Group 47's 35 MHz microwave Synthetic Aperture Radar (SAR), used for post process imaging with 1 ft $\times$ 1 ft resolutions, uses

arrays of dihedral (double bounce) and trihedral (triple bounce) corner cubes (of 3 different sizes for 3 orders of magnitude dB_{sm} polarimetric calibrations) that civil engineers in Gr. 46 had to survey, cross-align, and orient accurately en masse (in maintaining the original polarizations within the reflections) to simultaneously exhibit their "sweet spot" registration flashes in order to stick up above the considerable ground clutter floor to enable successful removal of anomalous speckle [56]. However, the reflector usage problem for Group 53's ETB data collection appears to be less demanding than the application of [56] with regard to retroreflector orientation in order to receive successful sensor indications of their presence since the requisite angle sensitivity is more easily achievable between reflector and sensor and less clutter/speckle should be present in the laser radar bands. Likewise, from Section 4.2, the expression for the measurement noise covariance intensity matrix [19] R_2, corresponding to use of visual updates as a navaid fix source, is:

$$\begin{aligned} R_2 &= \text{diag}\{(\csc(\phi_o))^2\left[\sigma_L^2 + L^2(\cot(\phi_o))^2\sigma_\phi^2\right],\ (\csc(\phi_o))^2\left[\sigma_L^2 + L^2(\cot(\phi_o))^2\sigma_\phi^2\right]\} \\ &= \text{diag}\{(72 \text{ ft} \times 0.3048 \text{ meters/ft})^2, (72 \text{ ft} \times 0.3048 \text{ meters/ft})^2\} \\ &= \text{diag}\{(21.94 \text{ meters})^2, (21.94 \text{ meters})^2\} \\ &= \text{diag}\{481.609 \text{ (meters)}^2, 481.609 \text{ (meters)}^2\}\ , \end{aligned} \tag{55}$$

where notation in the above was defined in Section 4.2.

One option for modeling synchronized simultaneous navaid usage: For both the above mentioned navaid sensors to avail measurements simultaneously to the LASERNAV II at a specified measurement fix/reset sample time, the situation apparently is

$$z(k) = z_1(k) = Hx(k) + v_1(k) \tag{56}$$

and

$$z(k) = z_2(k) = Hx(k) + v_2(k) \tag{57}$$

so combining the two simultaneous measurements yields

$$2z(k) = z_1(k) + z_2(k) = 2Hx(k) + v_1(k) + v_2(k) \tag{58}$$

---

[19] Use of retroreflector in this manner as a navaid fix source is predicated on the assumption that nominal navigation accuracy is sufficient to guarantee that retroreflector will fall within $\pm$ 45° FOV of aircraft's down-looking GaAs line-scanner.

or (as similarly obtained in [134, p. 94]) rearranging to be

$$z(k) = Hx(k) + \frac{1}{2}[v_1(k) + v_2(k)] \tag{59}$$

so the effective measurement noise covariance intensity matrix for combined simultaneous VOR/DME and retroreflector usage (as obtained using this methodology) is provided from the following expectation

$$E\{\frac{1}{2}[v_1(k) + v_2(k)]\frac{1}{2}[v_1(j) + v_2(j)]^T\} = \frac{1}{4}\{R_1 + R_2\}\delta_{j,k} = R_{3'}\,\delta_{j,k} \tag{60}$$

as

$$\begin{aligned} R_{3'} &= \frac{1}{4}[R_1 + R_2] \\ &= \text{diag}\{(131.42 \text{ meters})^2, (131.42 \text{ meters})^2\} \\ &= \text{diag}\{17269 \text{ (meters)}^2, 17269 \text{ (meters)}^2\}\,. \end{aligned} \tag{61}$$

However, we object to using this result for our ETB situation since this result would indicate that (contrary to the tenents of Kalman filtering) use of both navaid measurements simultaneously is worse than using the best measurement by itself; yet we know that for Kalman filtering with all statistics known (as in the present situation) additional measurements, no matter how coarse, should never hurt or diminish the resulting navigation accuracy. This apparent dilemma is resolved in the next section, where a satisfactory model is developed for this ETB situation that we *do* use as the final modeling solution that is consistent with the well known tenents of Kalman filtering.

Preferred option for modeling synchronized simultaneous navaid usage: The approach that we currently employ for modeling synchronized simultaneous use of both VOR/DME and pre-surveyed retroreflector fixes is now described. We interprete the simultaneous measurements from two different navaids, as also done in the investigation of [135, Section 3], to be of the form of a (4×1)-vector:

$$z(k) = \begin{bmatrix} z_1 \\ \cdots \\ z_2 \end{bmatrix} = \begin{bmatrix} H \\ \cdots \\ H \end{bmatrix} x(k) + \begin{bmatrix} v_1 \\ \cdots \\ v_2 \end{bmatrix}$$

$$= \begin{bmatrix} 1 & 0 & 0 & 0 & 0 & 0 & 0 & 0 & 0 & 0 & 0 & 0 \\ 0 & 1 & 0 & 0 & 0 & 0 & 0 & 0 & 0 & 0 & 0 & 0 \\ \cdots & \cdots & \cdots & \cdots & \cdots & \cdots & \cdots & \cdots & \cdots & \cdots & \cdots & \cdots \\ 1 & 0 & 0 & 0 & 0 & 0 & 0 & 0 & 0 & 0 & 0 & 0 \\ 0 & 1 & 0 & 0 & 0 & 0 & 0 & 0 & 0 & 0 & 0 & 0 \end{bmatrix} x(k) + \begin{bmatrix} v_1 \\ \cdots \\ v_2 \end{bmatrix}, \tag{62}$$

where the effective measurement noise covariance intensity matrix is

$$R_3 = \begin{bmatrix} R_1 & \vdots & 0_{(2\times 2)} \\ \cdots & \cdots & \cdots \\ 0_{(2\times 2)} & \vdots & R_2 \end{bmatrix}$$

$$= \begin{bmatrix} (261.9 \text{ meters})^2 & 0 & \vdots & 0 & 0 \\ 0 & (261.9 \text{ meters})^2 & \vdots & 0 & 0 \\ \cdots & \cdots & \cdots & \cdots & \cdots \\ 0 & 0 & \vdots & (21.94 \text{ meters})^2 & 0 \\ 0 & 0 & \vdots & 0 & (21.94 \text{ meters})^2 \end{bmatrix}$$

$$= \begin{bmatrix} 68598 \text{ (meters)}^2 & 0 & \vdots & 0 & 0 \\ 0 & 68598 \text{ (meters)}^2 & \vdots & 0 & 0 \\ \cdots & \cdots & \cdots & \cdots & \cdots \\ 0 & 0 & \vdots & 481.609 \text{ (meters)}^2 & 0 \\ 0 & 0 & \vdots & 0 & 481.609 \text{ (meters)}^2, \end{bmatrix}. \tag{63}$$

Throughout, an underlying dimensional analysis was performed and software program output units have been uniformly selected to be meters for length (L) and minutes for time (T) and shown to correspond to the software program input units provided here in Section 5 in final form. The appropriate matrices that are used as input to the Kalman filter software were obtained by numerically scaling the 49 entries of interest, as found in Eqs. 50-55, 62, and 63, as performed here for the LASERNAV II application.

6. CONSIDERATIONS OF INITIAL ALIGNMENT AND ITS EFFECTS

6.1 A Two-Phased Approach for Specifying the Non-Diagonal Covariance Initial Condition Ultimately Used in This Investigation

As mentioned in the concluding paragraph of Section 3.4, the theory of linear Kalman filtering (as applies for most linearized navigation problems) states that the *a priori* covariance of estimation error $P_{k|k} = E[(x_k - \hat{x}_{k|k})(x_k - \hat{x}_{k|k})^T]$ is identical to the *a posteriori* covariance of estimation error $P_{k|k} = E[(x_k - \hat{x}_{k|k})(x_k - \hat{x}_{k|k})^T | \mathcal{Y}_k]$, given all the measurements, $y(k)$, up to time k (i.e., conditioned on the associated "underlying sigma-algebra generated by the measurements"). Because of the above fact, the actual values of the measurements received can be ignored (but attention must be paid to the frequency and quality (variance) of the associated measurements) and mere off-line covariance analysis can be used to predict just how well one can expect an optimal linear filter to do in tracking the states of the navigation system error model. This covariance satisfies a Riccati equation which is already implemented in our software along with the associated Kalman filter.

Another property of linear Kalman filters that we seek to exploit here to our advantage is the "robustness of the Riccati equation solution to incorrect initial conditions" [18]. This means that although we don't initially know all the possible off-diagonal entries that should be specified in a positive definite initial condition $P_{0|0}$ (that we initially take to be a diagonal matrix for convenience and which exhibits its proper σ^2 values for all these known entries along the main diagonal of Eq. 50 (with the source of this information specified in Sections 5.1, 5.2, and 5.3.2 for ease of traceback justification), the remaining off-diagonal terms were obtained using the Kalman filter covariance calculation software [20] to solve the Riccati Equation for its unique steady-state solution (which now reflects inherent system interconnection structure embodied in the system matrix F (and in its associated transition matrix $\Phi(k+1,k)$) as well as being the result of the presence of the driver or forcing term white noises [21] $u(t)$ and $v(t)$). From the steady-state solution (confirmed by its stable effect in position error, as depicted in Fig. 9 after the transient has died out, and in the tilt or attitude errors [22], as depicted in Fig. 10) to the Riccati equation (under 30 consecutive VOR/DME

---

[20]Not using the riskier special purpose version in [85] that achieves the Riccati solution by iteration, but by the standard general purpose built-in approach that was personalized here with initial breakpoints (later removed) that allowed us to step through and view the calculated contents of the covariance on each of 30 consecutive time steps.

[21]Of known process noise and measurement noise covariance intensity levels, Q and R, respectively, as exhibited in Eqs. 53 and 54 (and 55, 63) (which are, respectively, positive semidefinite with zeros in specified slots on the diagonal of the matrix and positive definite; but, otherwise, with known specified values along the main diagonal).

[22]While the East and North tilt error are benign and exhibit the characteristic low magnitude undamped oscillation at the expected 84 minute Schuler period, the Azimuth tilt depicted here in

position fixes, one every 3 minutes), we can pluck each of the final diagonal and off-diagonal terms resulting (after the initial transient has died out) from the above mentioned first phase of the two phase solution approach to be the reasonable, consistent answer to be used for Phase 2 $P(0)$ as

$$P(0) = \begin{bmatrix}
1.73E+03 & 2.26E+02 & -3.00E+07 & 3.18E+06 & 4.47E+00 & 3.91E+01 & -1.10E+03 & -6.02E-01 & -2.45E-02 & 4.39E-01 & 6.21E-05 & 8.07E-05 \\
2.23E+02 & 2.35E+03 & -7.00E+06 & 4.60E+06 & 1.36E+00 & 1.87E+00 & -1.95E+02 & 1.76E-01 & 7.71E-01 & -2.48E-02 & 2.60E-05 & -1.08E-04 \\
-3.00E+07 & -7.00E+06 & 2.43E+12 & -3.17E+11 & -1.62E+05 & -8.74E+05 & 3.64E+07 & -1.48E+05 & -1.57E+04 & 1.32E+05 & -1.53E+01 & -2.42E+01 \\
3.18E+06 & 4.60E+06 & -3.17E+11 & 1.01E+12 & 1.52E+05 & 1.64E+05 & -5.95E+06 & 1.84E+04 & 1.18E+05 & -6.47E+03 & -4.24E+01 & -1.31E+01 \\
4.47289E+00 & 1.36E+00 & -1.62E+05 & 1.52E+05 & 2.33E+00 & 1.15E-01 & -3.46E+00 & 8.99E-03 & 4.88E-02 & -7.97E-02 & 4.18E-05 & -2.34E-05 \\
3.91E+01 & 1.86E+00 & -8.74E+05 & 1.64E+05 & 1.15E-01 & 2.93E+00 & -2.26E+01 & -2.62E-02 & 2.07E-02 & -2.49E-03 & 6.76E-05 & 6.83E-05 \\
-1.10E+03 & -1.95E+02 & 3.64E+07 & -5.95E+06 & -3.46E+00 & -2.26E+00 & 1.19E+03 & -3.80E-01 & -5.88E-01 & 6.02E+00 & 6.94E-05 & 7.62E-05 \\
-6.02E-01 & 1.76E-01 & -1.48+05 & 1.84E+04 & 8.99E-03 & -2.62E-02 & -3.80E-01 & 2.48E-02 & -1.26E-05 & 2.59E-05 & 5.23E-09 & 6.40E-09 \\
-2.45E-02 & 7.71E-01 & -1.568E+04 & 1.18E+05 & 4.88E-02 & 2.07E-02 & -5.88E-01 & -1.26E-05 & 2.48E-02 & 1.09E-06 & -5.89E-09 & 4.52E-09 \\
4.398E-01 & -2.48E-02 & 1.32E+05 & -6.47E+03 & -7.97E-02 & -2.49E-03 & 6.02E+00 & 2.59E-05 & 1.09E-06 & 1.348E-01 & -2.74E-09 & -2.95E-09 \\
6.21E-05 & 2.60E-05 & -1.53E+01 & -4.24E+01 & 4.18E-05 & 6.76E-05 & 6.94E-05 & 5.23E-09 & -5.89E-09 & -2.74E-09 & 3.89E+00 & 1.76E-13 \\
8.07E-05 & -1.08E-04 & -2.42E+01 & -1.31E+01 & -2.34E-05 & 6.83E-05 & 7.62E-05 & 6.40E-09 & 4.52E-09 & -2.95E-09 & 1.76E-13 & 3.89E+00
\end{bmatrix} \tag{64}$$

and then start anew in the computer evaluations of Section 7.2, using these results as the new proper initial conditions to be used in again solving the Riccati equation for $P_{k|k}$ as it evolves in time as a consequence of our navaid source selection and navaid fix rate policy (as depicted in Section 7.2). In plucking out and using all of the steady-state terms in this manner for the second phase (final) solution approach of Section 7.2, all inherent cross-correlation present is now accounted for and included or incorporated in the analysis/evaluation (while now avoiding the presence of an initial transient and its attendant settling time) and consequently no significant adverse structural ramifications occur since we don't ignore effects of cross-correlation or off-diagonal terms. The parameter input files used for the simulations of Section 7.2 correspond exactly to what is offered in this report, as reported in Sections 3 to 6.

Fig. 10 exhibits unbounded growth only because we are constrained in this investigation to use merely a 12 state model that does not include explicit damping of the effective vertical channel and so the corresponding Azimuth tilt is taking off also. Inclusion of additional states in the model corresponding to standard baro-damping [112], or laser altimeter-damping, or GPS-damping [116] of the vertical channel *would* stabilize the Azimuth tilt response but would adversely impact and violate all other design decisions we have already made regarding ease-of-use of low order models in our simulations. Our easy alternative here is to subsequently depict only the East and North tilts in Section 7.2 and to delete or overlook Azimuth tilt in what follows so as to not unnecessarily alarm the reader with an apparently anomalous response that for more computational expense in simulation (but with no beneficial informative impact) wouldn't really appear. It is asserted here that once standard reference sensor-damping of the vertical occurs or is introduced, then Azimuth tilt will also be as benign and exhibit a behavior similar to that of the East and North Tilts already displayed.

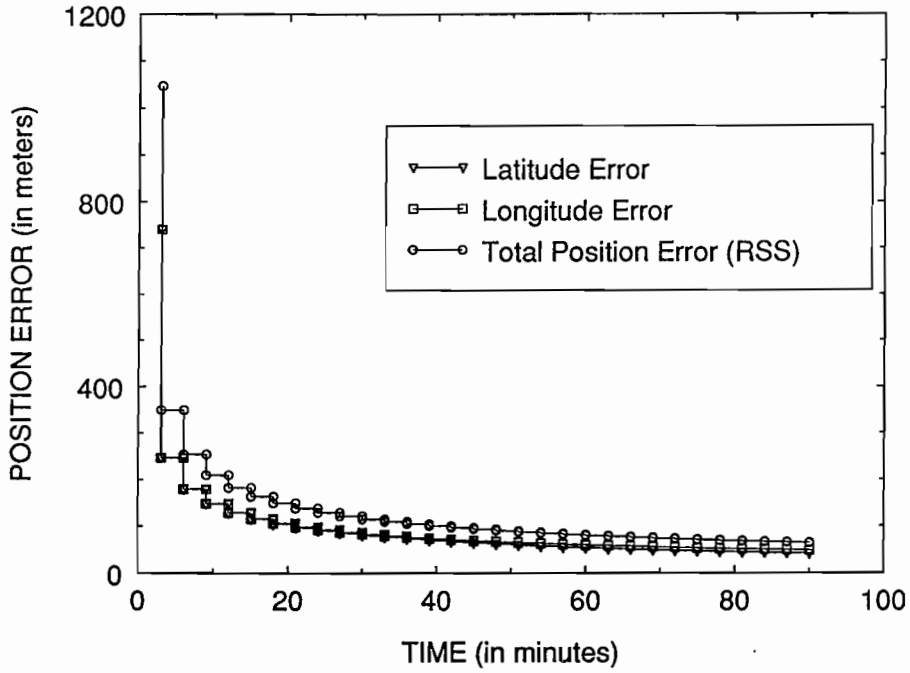

Figure 9. Simulated Covariance Analysis Computations: ENSEMBLE STD. DEV. OF POSITION ERROR VS. TIME (3 min VOR/DME fixes)

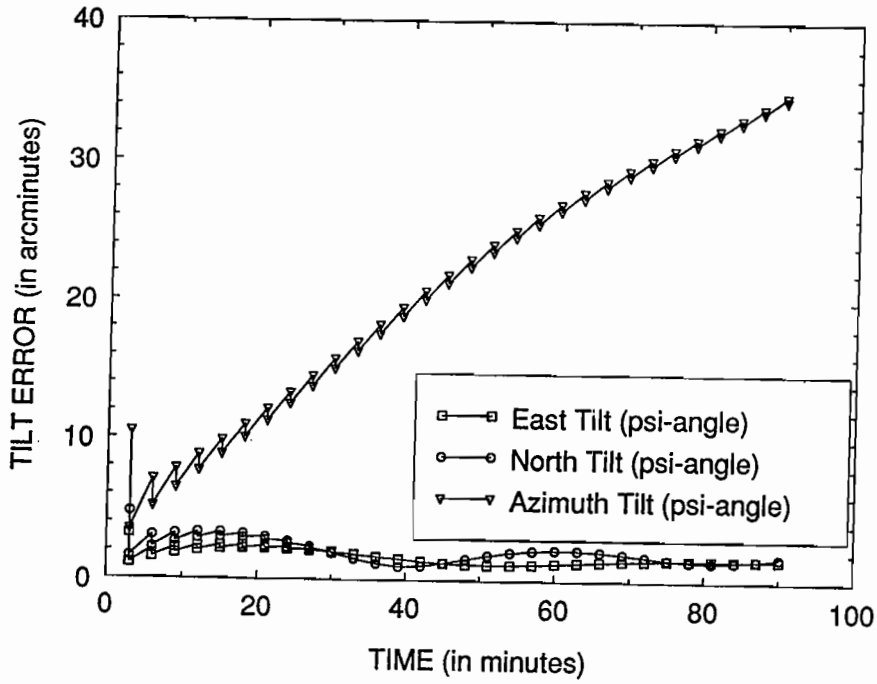

Figure 10. Simulated Covariance Analysis Computations: ENSEMBLE STD. DEV. OF TILT ERROR VS. TIME (3 min VOR/DME fixes)

6.2 INS Calibration/Alignment

Physically, Inertial Navigation System (INS) alignment is the process of expediently determining appropriate initial conditions for the integration of the differential equations describing inertial navigation [103], [117]. Six coupled second order differential equations for the attitude and position of the "platform" are involved, thus establishing the need to specify 12 initial conditions as, nominally, being 3 position, 3 velocity, 3 "platform" orientation angles, and 3 "platform" rate coordinates.

Since the INS (in the normal mode) is inherently a *dead-reckoner*, which integrates open-loop sensed acceleration into, first, velocity, then into position; it is incapable of fully self-contained initialization (within a short time frame to be practical) so the INS must usually depend on inferring the necessary information for initialization as supplied from an externally sensed position (and/or velocity) reference. The INS alignment process is thus normally defined as the estimation and/or control of "platform" attitude and its rates through the observation of their effects as errors in the measured position and/or velocity states.

This description of the essence of the alignment process is universally applicable to all of the available alternative INS (nonlinear) mechanizations, the sole distinction being how gyros in a *Local Level* mechanization are torqued to bring the platform into physical alignment with the desired frame, versus the computational "torquing" involved in establishing the rotation representation in strapdown systems. Strapdown system alignment is actually simpler, since it avoids complications otherwise introduced in implementing conventional gyro torquers with their nonlinear constraints (or stops) on the practical limits that can be achieved by the torquer in seeking the goal of perfectly leveling the stable platform (see [91] for alignment details in handling a strapdown laser gyro INS as well as [104], [106], [109], [122]).

The concept of alignment basically reduces to efficiently and expediently tracking a pair of known reference vectors which can be directly sensed by the inertial instruments and which contain enough information to suffice in completely defining a reference frame. The obvious choice to be reference vectors for terrestrial navigators are the gravity vector (for "levelling") and either the earth angular velocity vector (for "earth-rate gyro-compassing" for ground-based alignment) or the vehicle angular velocity vector with respect to inertial space (for "space-rate gyro-compassing" for quick reaction (but in general coarser) in-air alignment). Both of these approaches encounters singularities if the two vectors selected become collinear or if one of the vectors vanish (due to inadvertent sensor failure). An additional option for performing an in-air alignment ([121], [124]) is to create externally trackable (by cooperating external tracking radar) specific force vector(s) by executing dynamic maneuvers in-flight to provide information that is fed back to the aircraft via a communications link. There is an apparent advantage of potentially reducing the time required for alignment by using dynamic alignment since an acceleration stimulus operating through "platform" attitude errors produces a more immediate effect (i.e., is one integration less removed) in its effect in the observable states than an angular velocity stimulus would be. However, the mechanism is nonlinear and may take longer to converge to the answer. A final aspect of the alignment process

involves the "transfer alignment" from a Primary *Master* INS to a Secondary *Slave* INS. If the Primary INS system data is utilized solely as a position/velocity reference for the Secondary INS, then the process constitutes a so-designated *standard alignment.* However, more rapid response can be obtained in this final alignment phase by exploiting the analogous inertial nature in common to both Primary and Secondary INS as expedited by employing either accelerometer matching (of sensed gravity) or attitude matching (being the two most common examples of using this technique). For alignment on aircraft carriers, velocity matching is typically used between the Primary shipboard INS and the Secondary aircraft INS while on the flight deck (and similarly for aligning missile gyros from the shipboard INS on submarines). Non-ideal alignment disturbances (which interfere with the normal alignment process) are usually also present as unknown Master INS errors, local vibrations, and uncompensated bending and/or flexure between the locations of the Primary and Secondary INS.

INS alignment by the slaving of observable states to an external reference is well suited for Kalman filter-based optimal estimation ([103], [110], [118], [119]) unless the initial estimates are not within the region of close linear approximation. If this happens, convergence time may suffer unless one uses Extended Kalman filter ([124], [128]) or parameter identification techniques ([105]) in a practical "coarse alignment phase" prior to the "fine alignment phase". One coarse alignment procedure is to use the accelerometer outputs in conjunction with external measurement of aircraft velocity to directly torque the gyros (or the rotational representation in strapdown mechanizations). After the initial transients have died out, the difference between the indicated and measured aircraft velocities are proportional to the components of earth rate along the level axes and can be utilized to derive an estimate of the initial alignment of the "platform" frame relative to North (assuming that excessive aircraft sideslip is not being experienced). Normally, Local Level systems will cage to aircraft axes on power-up, while strapdown algorithms can be *a priori* initialized assuming zero pitch and roll.

The fine alignment phase usually utilizes Kalman filter estimation of residual attitude errors by processing the available external observations. The filter settling time for this is about $\frac{1}{4}^{th}$ a Schuler period, as exhibited in Section 6.1, but is an order of magnitude faster (about 2-3 minutes) if dynamic alignment is utilized by having the aircraft perform horizontal planar maneuvers (S-shaped turns).

A known difficulty with gyro-compassing procedures (see [113, pp. 1161-1163]) is the non-separability of azimuth error from effective East gyro drift-rate and the non-separability of "platform" tilts from effective East and North accelerometer biases under conditions of quasi-constant alignment of instrument and geographic axes. Observability resolution enhancement techniques ([108], [109], [123], [125], [126], [137]) involve changing the relative orientation of the axes (through aircraft motion for strapdown mechanizations or by azimuth slews for Local Level mechanizations).

For the covariance analysis of this present investigation, all that was really needed here was to obtain the initial condition covariance $P(0)$ in the manner indicated in Section 6.1 as the

straight forward approach (where settling time was not an issue). This approach was taken here [23] since our simulated INS is in fact a Local Level mechanization (while the actual LASERNAV II is a strapdown system, where its own particulars of strapdown calibration/alignment ([106], [107], [108], [109], [110]) must be explicitly observed and adhered to in *actual* implementation even though we are not similarly constrained here). A fundamental understanding of what constitutes the calibration/alignment process in mechanizing an Inertial Navigation System, as conveyed in Section 6.2, is also necessary as part of the explanation of what we did in Section 6.1 (and why) in performing the simulations and in explaining what we observed as outputs.

[23] As justified on pages 1 and 2 in the first footnote in Section 1.

7. REPRESENTATIVE NAV PERFORMANCE EVALUATION RESULTS

7.1 Similar Airborne Navigation Accuracy Evaluations being Viewed as a Constructive Preliminary Guide

Representative flight situations for a typical 0.1 nmi/hr gyro drift-rate airborne Inertial Navigation System (INS) in the (Kalman filter) aided inertial mode (and its associated Kalman filter response, used to characterize the INS's mission accuracy) in mission situations of:

- No position fixes being taken;
- Use of 1 position fix per hour;
- Use of 2 position fixes per hour;

are respectively depicted in Figs. 11 to 13 for Flightpath No. 1 (with no turns); in Figs. 14 to 16 for Flightpath No. 2 (with one turn per hour); and in Figs. 17 to 19 for Flightpath No. 3 (with two turns per hour). In addition to 2-D flight path and groundtrack as a reference, the following four curves depicting:

- Position error in nautical miles vs. time;
- Corresponding Kalman gains that would be used to process a position fix vs. time for the following:
  - Velocity: in ft/sec of velocity correction per 1000 ft of position error observable;
  - Position: as a fraction of the position observables which would be applied as possible correction;
  - Wander angle: in terms of arc-sec of heading corrections per 1000 ft of position observable (yielding two gain curves, one for each axis of available position observable);

were simulated (by others; our simulations are in Section 7.2) and are presented below for each situation of flight path (3 representative examples) and three options of sensor fix usage. More ETB mission specific trajectories and scenarios follow in Section 7.2 for detailed planning of the data collection missions.

The main thing to notice for the three different Flightpaths is that for the case of no external navaid position fixes being used, the INS position error exhibits unbounded growth to unacceptable levels with the passing of time; while for the case of using one navaid fix per hour, the INS error is well-behaved and contained, and is even better when two fixes per hour are used. Since the LASERNAV II gyro drift-rate indicated in Section 5.1, being

$$\sqrt{(0.004^\circ/\text{hr})^2 + (0.004^\circ/\text{hr})^2 + (0.0088^\circ/\text{hr})^2} = 0.01046^\circ/\text{hr} = 0.59 \text{ nmi/hr}$$

is coarser (worse) than the assumed 0.1 nmi/hr drift-rate of the above application (cf., confirming CEP simulation results following a 6 hr flight for projected high accuracy strapdown laser gyros reported in [113, p. 1168, Table IV], where after RSSing all the individual participating constituents in the overall system the total effective CEP rate is 0.12 nmi/hr), it is anticipated that more frequent fixes will be needed to tame the LASERNAV II INS position error and keep it within an acceptable range for the ETB data collection application.

The simulations depicted in Figs. 11 to 19 are for a General Dynamics F-111D, which travels considerably faster than the Grumman G-1 Gulfstream, at the 140 kts of our ETB data collection application. The F-111D's indicated mission time is longer, its INS drift-rate is lower, its flight dynamics are more severe, and its flight environment is more challenging. The simulations that follow are specialized to the relatively benign situation of ETB data collection using the parameters characterizing the LASERNAV II navigation system.

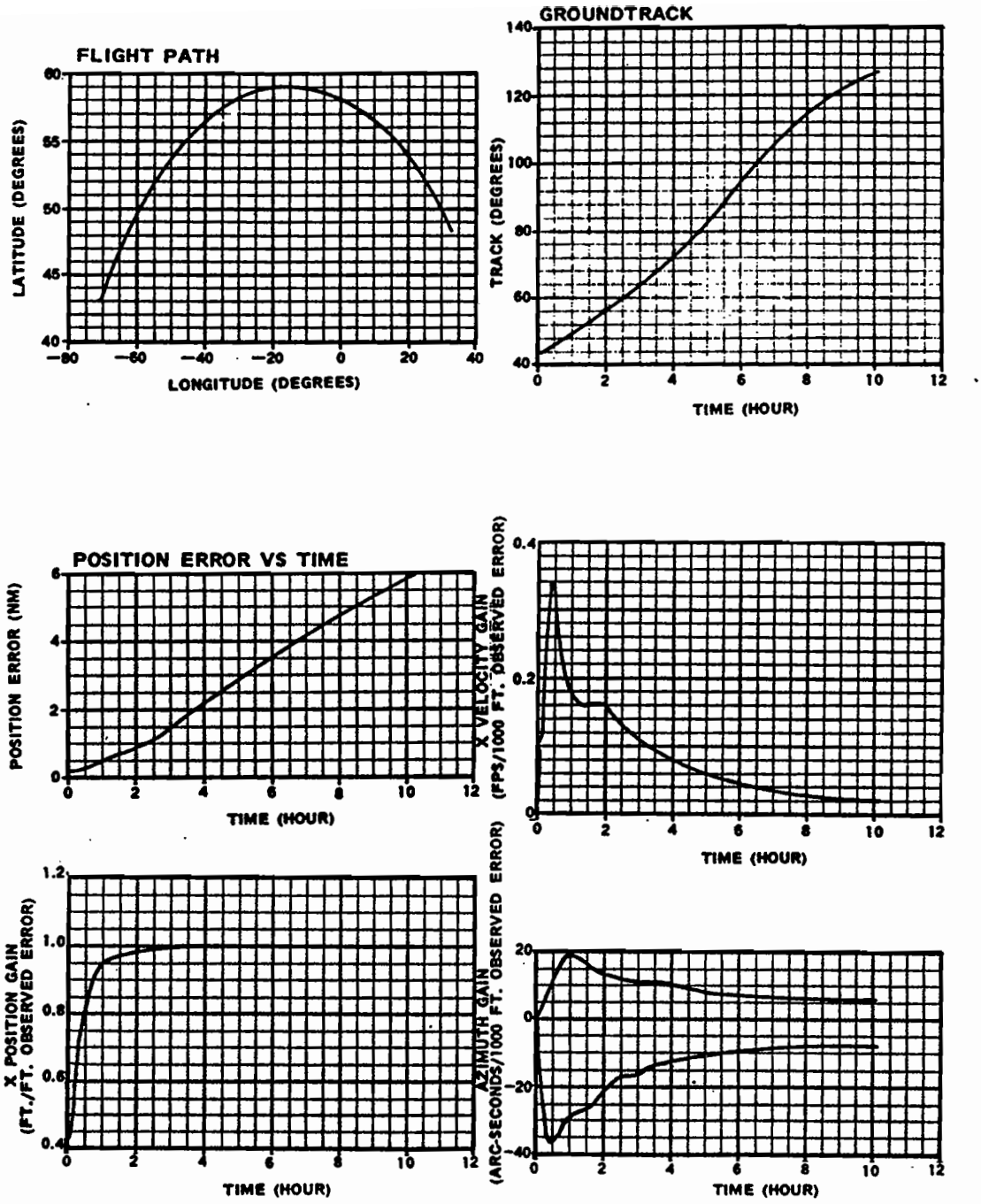

Figure 11. From [57], Simulated Kalman Computations: Flight Path No. 1 (No Turns, No Position Fixes)

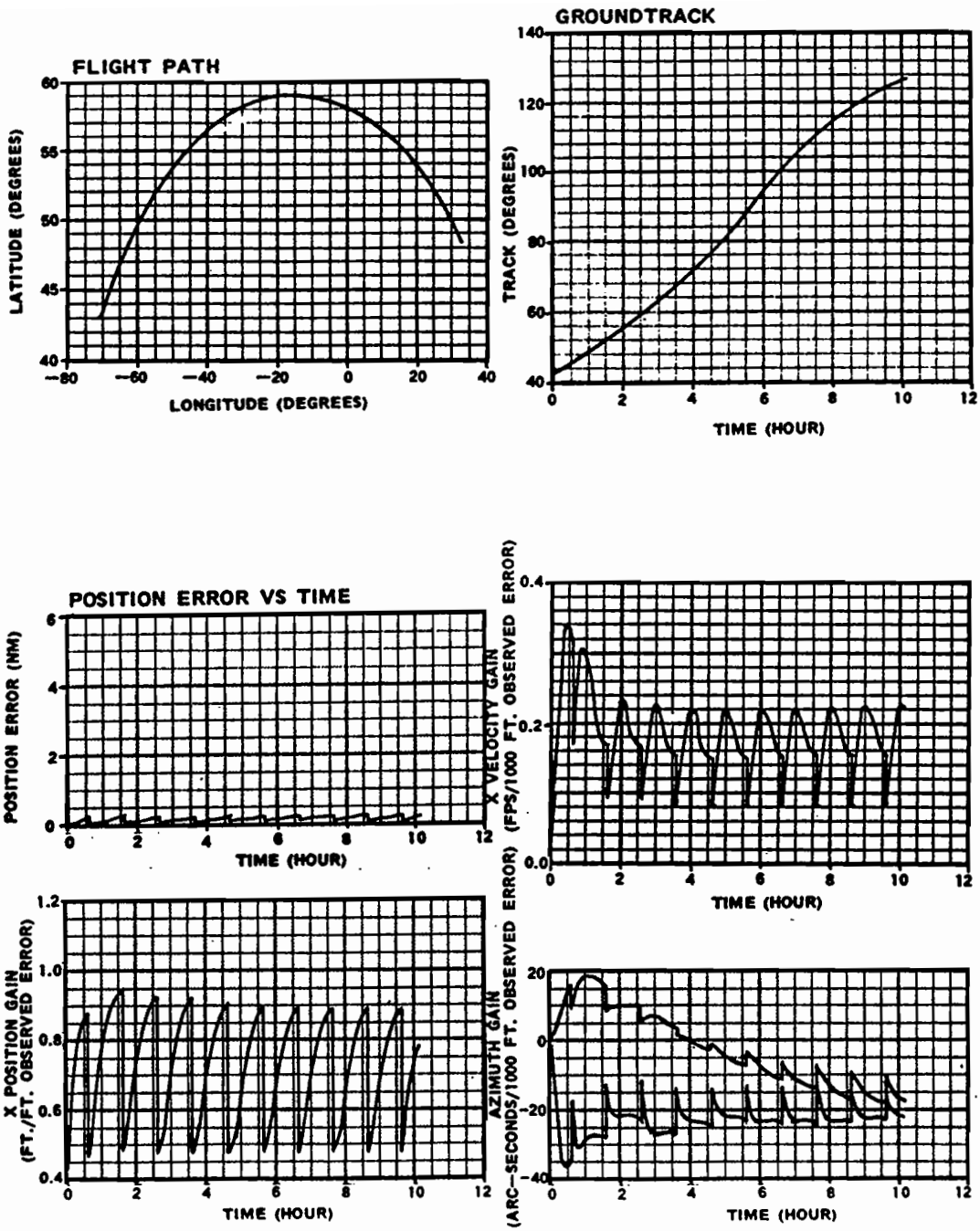

Figure 12. From [57], Simulated Kalman Computations: Flight Path No. 1 (No Turns, 1 Position Fix Per Hour)

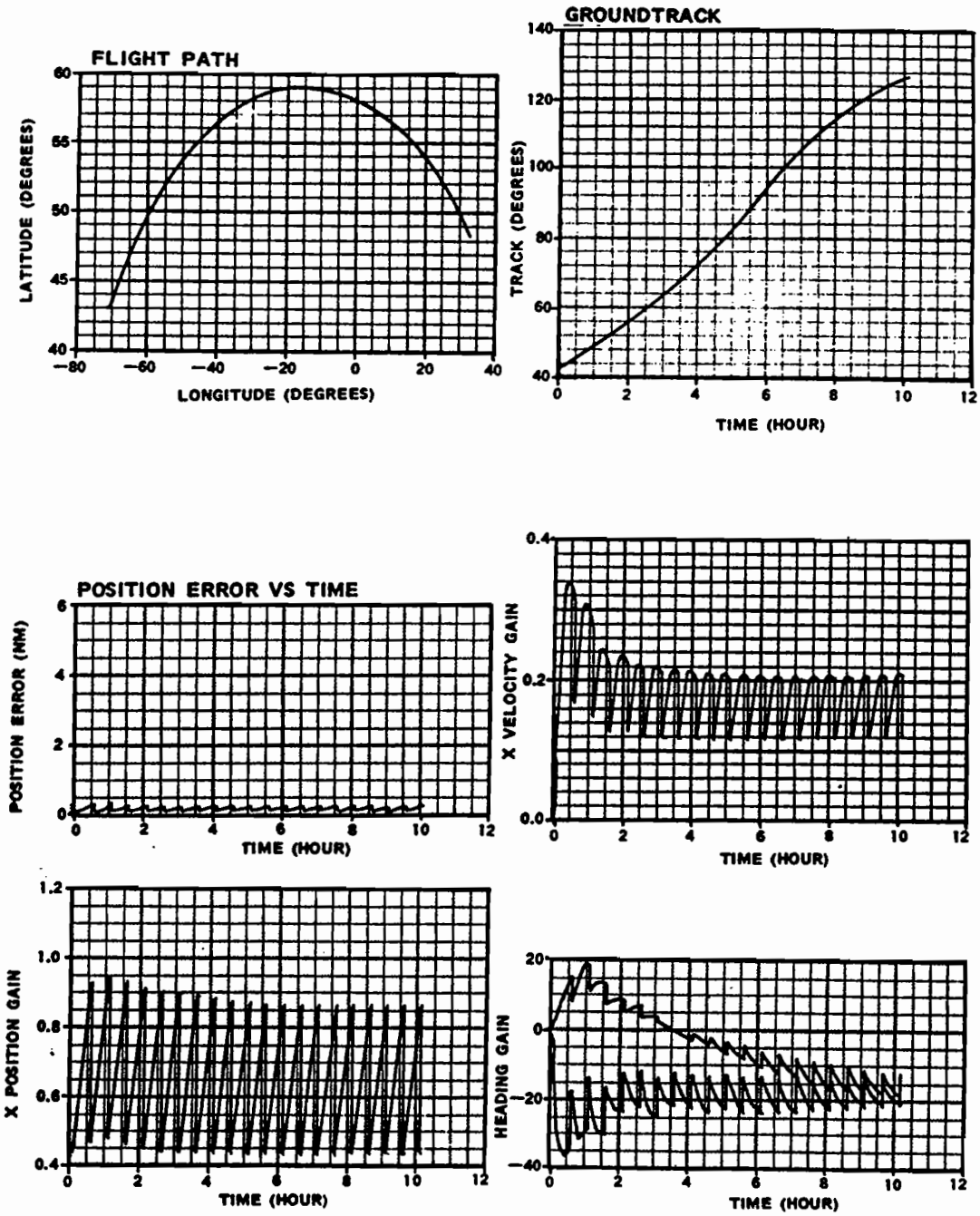

Figure 13. From [57], Simulated Kalman Computations: Flight Path No. 1 (No Turns, Two Position Fixes Per Hour)

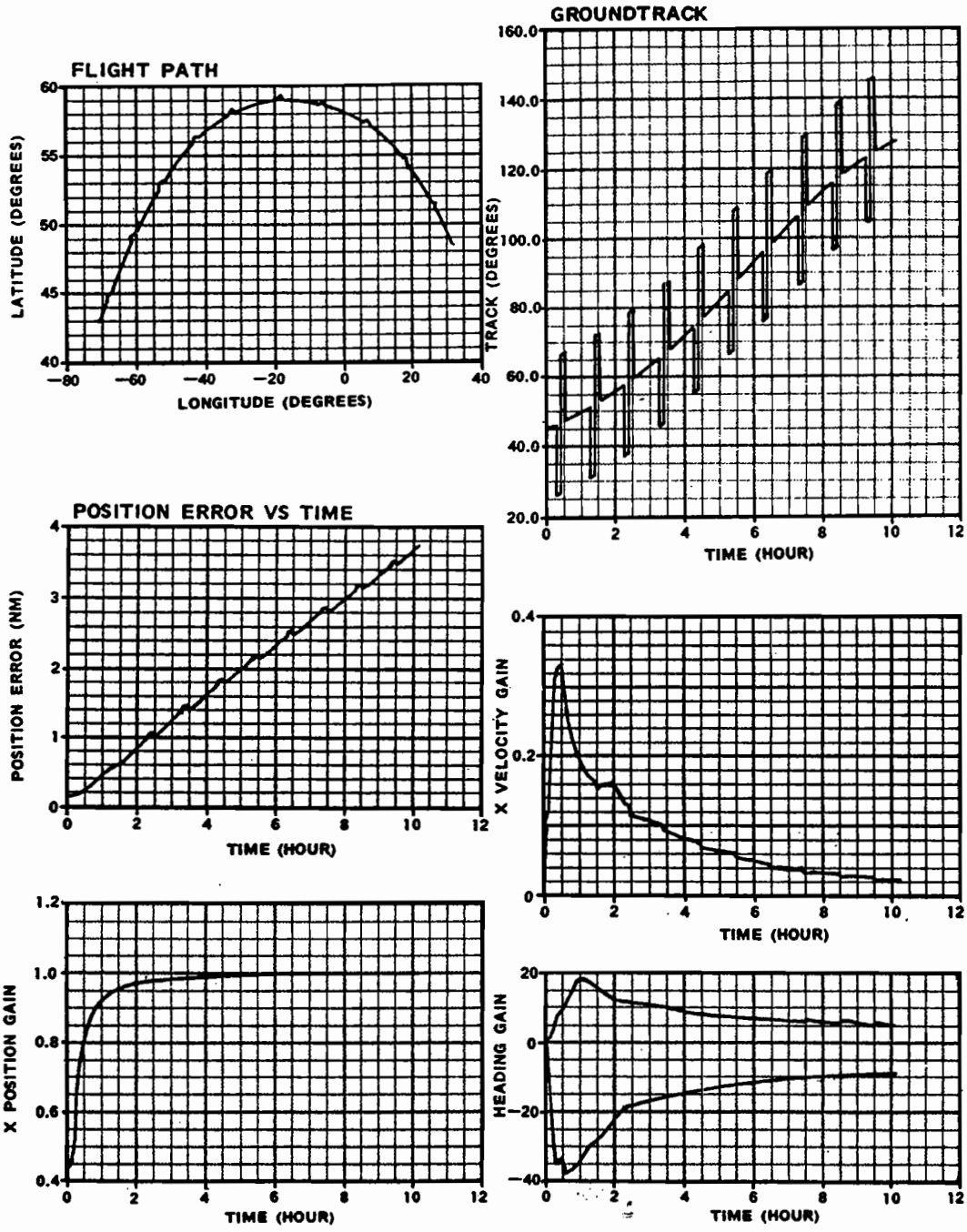

Figure 14. From [57], Simulated Kalman Computations: Flight Path No. 2 (1 Turn per hr, No Position Fixes)

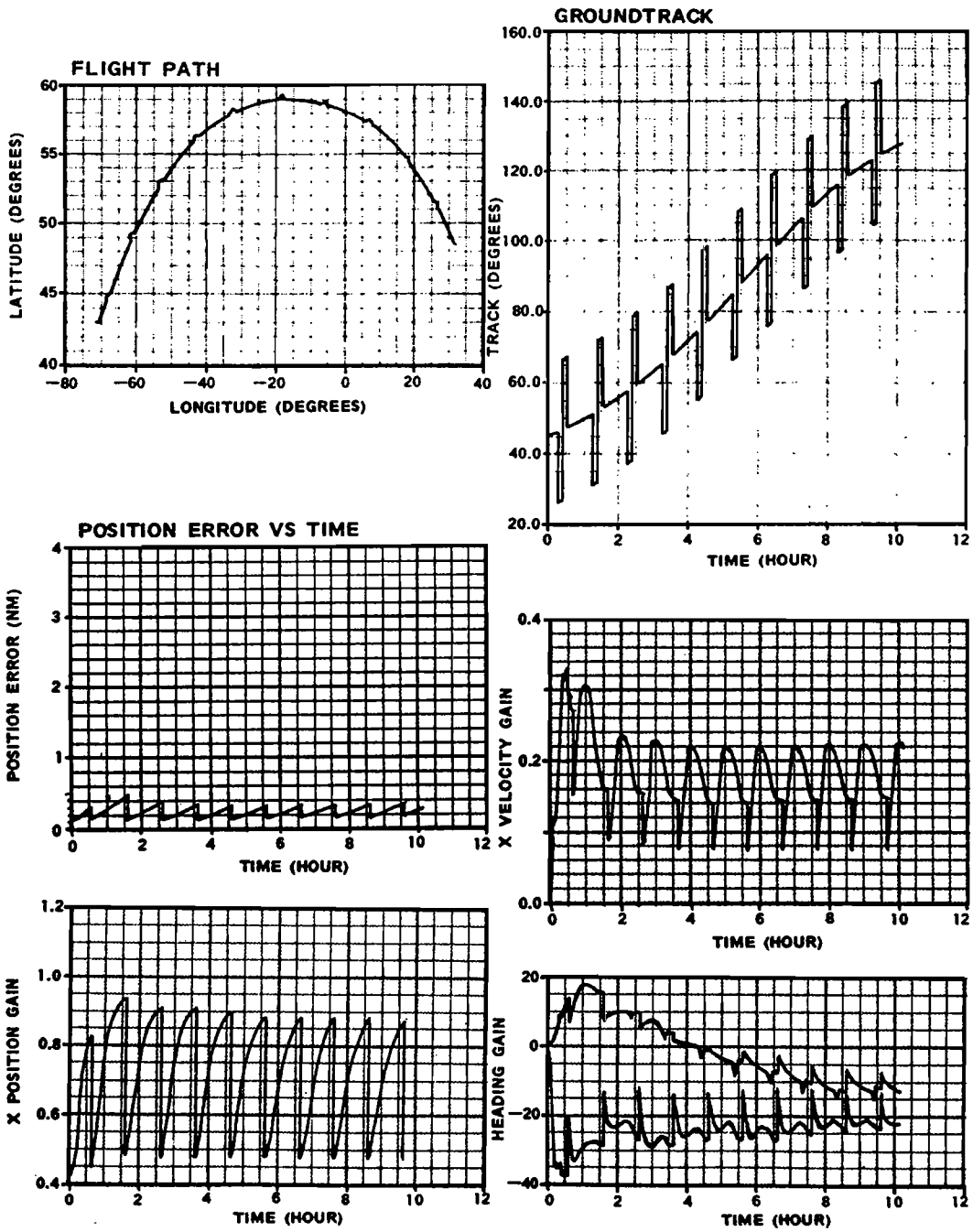

Figure 15. From [57], Simulated Kalman Computations: Flight Path No. 2 (1 Turn per hr, 1 Position Fix Per Hour)

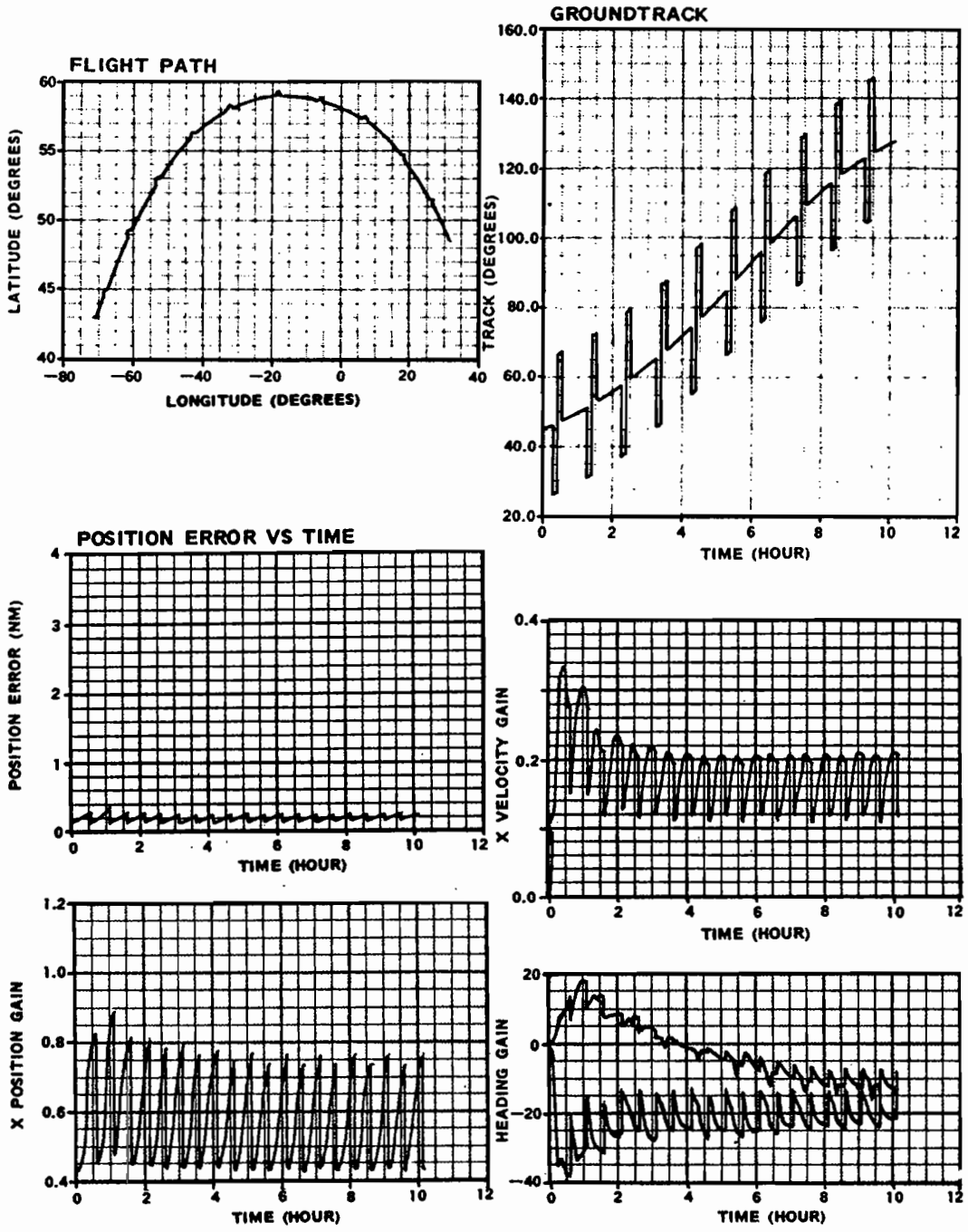

Figure 16. From [57], Simulated Kalman Computations: Flight Path No. 2 (1 Turn per hr, Two Position Fixes Per Hour)

7.2 Evaluation of G-1 Navigation Accuracy with LASERNAV II as will be Used for ETB Data Collection Missions

7.2.1 Exclusive use of VOR/DME navaid fixes

As depicted, respectively, in Figs. 9 and 10 for LASERNAV II with periodic 3 minute VOR/DME fixes, both the collection of constituent position errors and the associated collection of significant tilts exhibit an initial transient [24] that eventually dies out completely over a Schuler period of 84 minutes. Fig. 20 depicts tilts identical to those exhibited in Fig. 10 except that the Azimuth tilt is now absent (deleted as promised and for the reason explained in Section 6.1). Again at this finer vertical scale, the underlying sinusoidal oscillations exhibited are Schuler oscillations and correspond to an angular frequency of $\omega = \sqrt{g/R}$, where g is the acceleration of gravity and R is the mean radius of the earth at the particular geographic location of concern.

Notice the initially jagged saw toothed curves in Fig. 20 at the start of the simulated East and North tilts (psi-angle, ϕ, instantaneous misalignments) depicting how these tilts evolve as a function of time, where the saw teeth here represent the behavior of the error (or accuracy present) in the Kalman estimate before and after each 3 minute time sample that avails measurement information constituting another VOR/DME fix reset/update (corresponding to the predictor/corrector $\sqrt{P_{k|k-1}}$ and $\sqrt{P_{k|k}}$, respectively, in the parlance of Kalman filtering, as defined in Table 1 of Section 3). As initially expected from the discussion of Section 6.1, the results of Figs. 9, 10, and 20 still contain a component due to the Phase 1 transient (as it is dying out and the sawtooth is no longer as distinct after $\frac{1}{2}(84)$ minutes); however, Figs. 21 and 22 depict, respectively, Phase 2 position error and tilt error evolution *after* the transient is no longer present (recall that the initial condition covariance, used in obtaining all the subsequent Phase 2 runs offered in Section 7.2, is the final covariance value obtained from the particular Phase 1 runs depicted in Figs. 9 and 10, a procedure that is justified in Section 6.1). As confirmation of this asserted "ending/beginning" correspondence, notice that the initial segment of the curves depicted in Figs. 21 and 22 (with this same 3 minute VOR/DME fix rate) exactly mesh with the final values exhibited in Figs. 9 and 20, respectively, as a perfect fit (the vertical scales of Figs. 20 and 22 were forced to be identical to facilitate such a cross-comparison). In steady-state Phase 2 operation with periodic VOR/DME fixes every 3 minutes, Fig. 21 demonstrates 1-σ total position error (or navigation accuracy with LASERNAV II) to be no better than $\approx$ 50 meters (in real-time operation). Fig. 22 demonstrates 1-σ tilt error (with LASERNAV II at 3 minute VOR/DME fixes) to be in the vicinity of 2 to 3 arcminutes (in real-time operation). These results of Figs. 21 and 22 are in the best case situation of VOR/DME fixes being available every 3 minutes. More practical fix schedules of less frequent availability will be considered next.

---

[24] This transient is present for so long due to the simplified manner in which calibration/alignment is done here for our simulations since cal/align algorithm expediency for real-time use is not our concern in this investigation, as explained in Section 6.

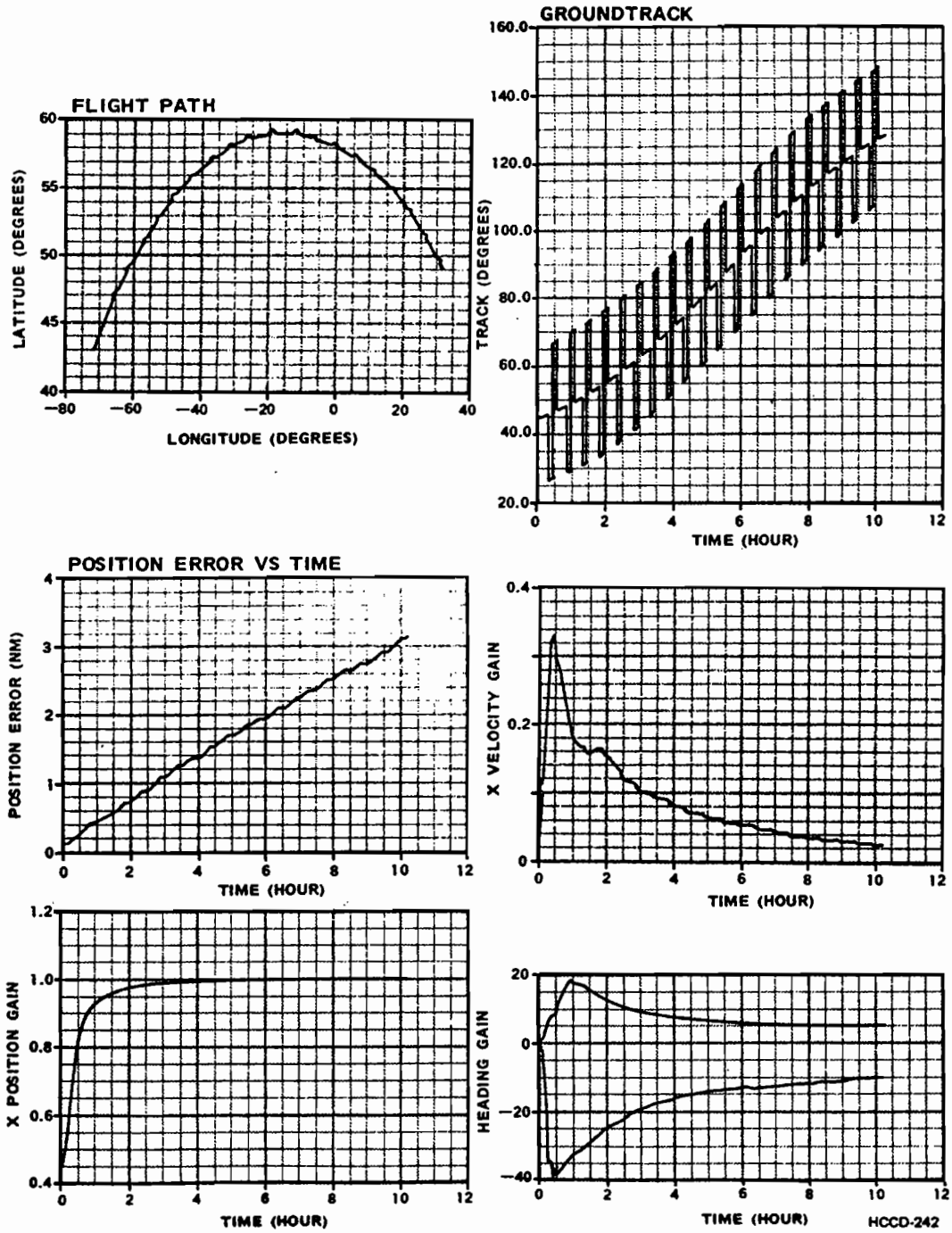

Figure 17. From [57], Simulated Kalman Computations: Flight Path No. 3 (Two Turns per hr, No Position Fixes)

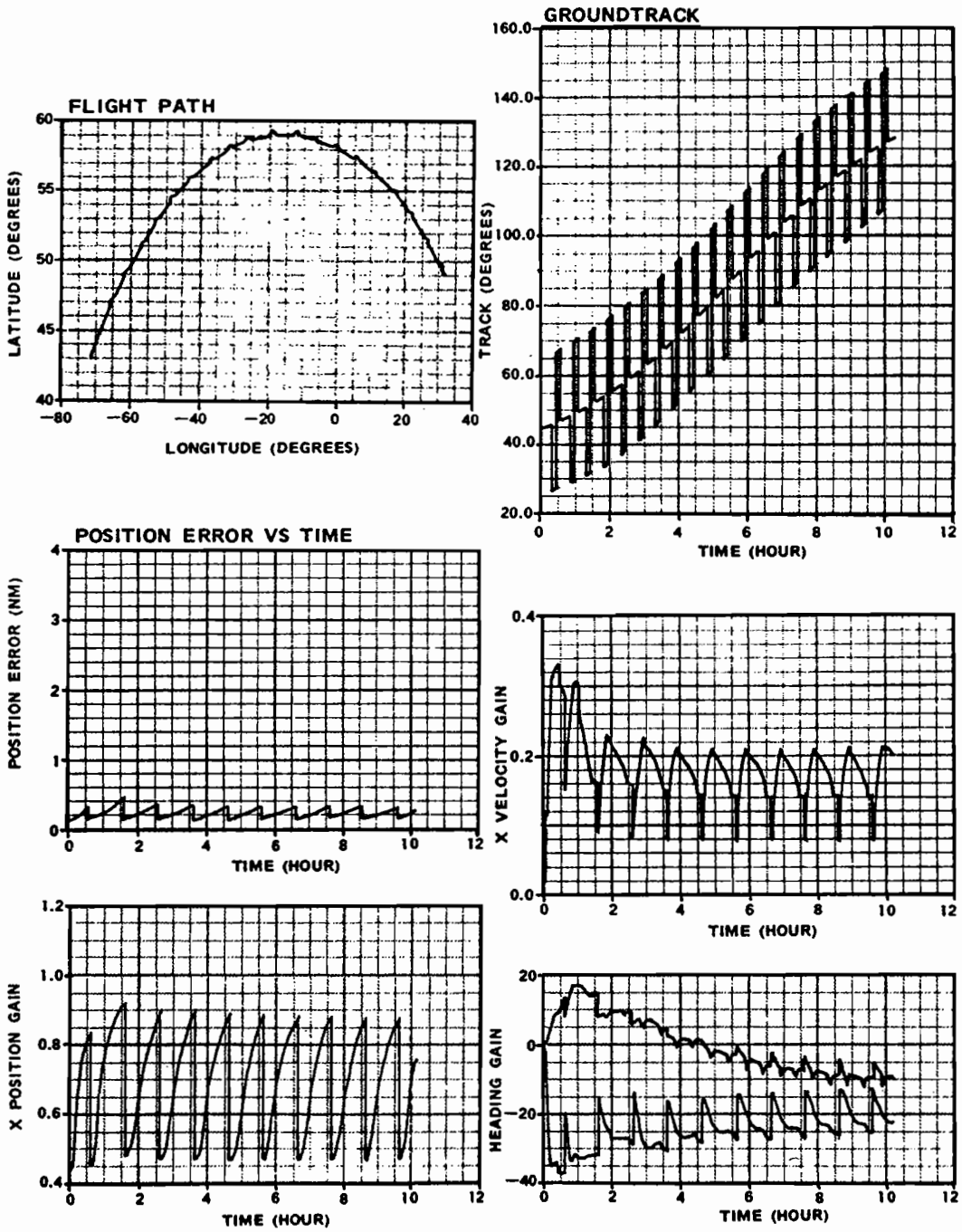

Figure 18. From [57], Simulated Kalman Computations: Flight Path No. 3 (Two Turns per hr, 1 Position Fix Per Hour)

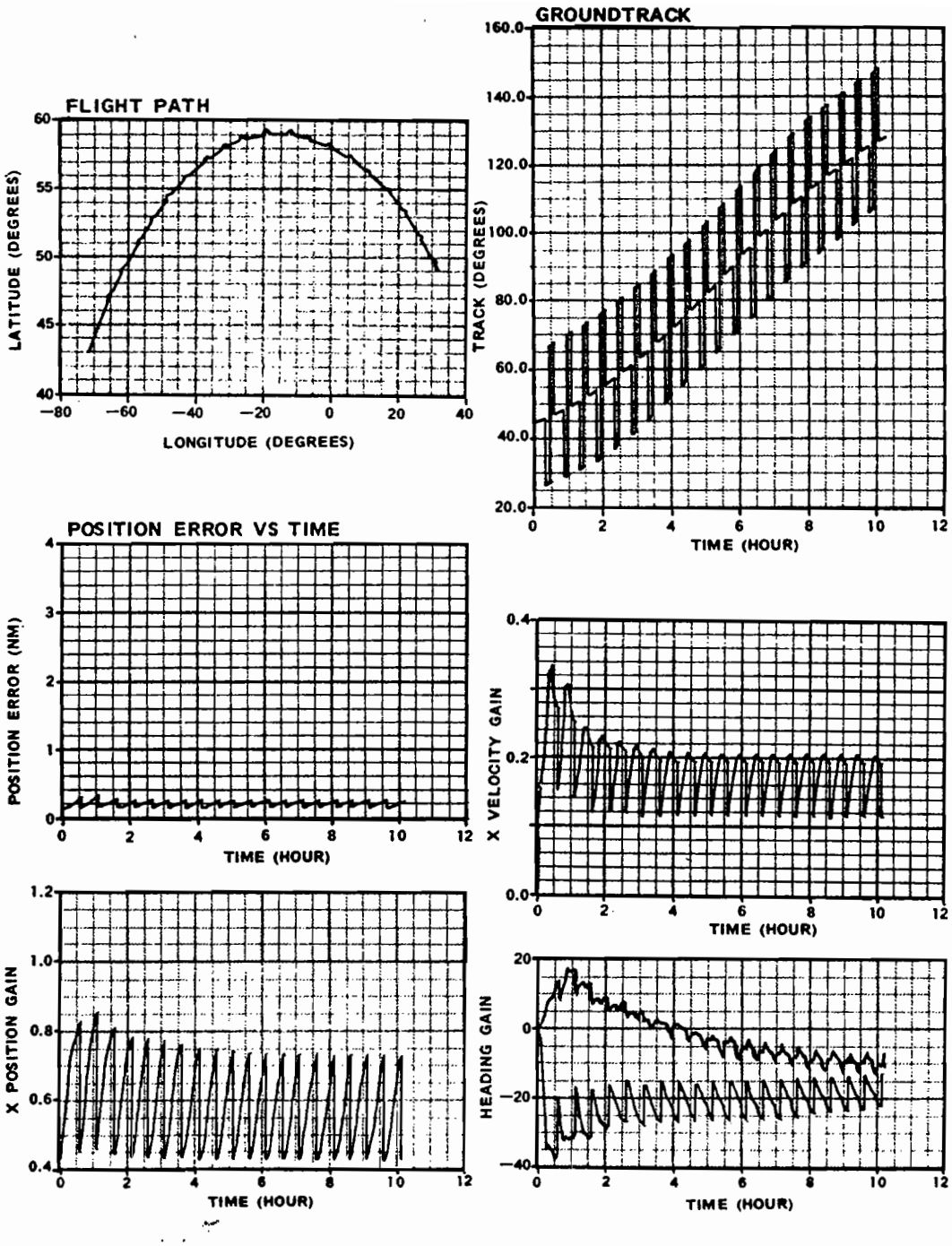

Figure 19. From [57], Simulated Kalman Computations: Flight Path No. 3 (Two Turns per hr, Two Position Fixes Per Hour)

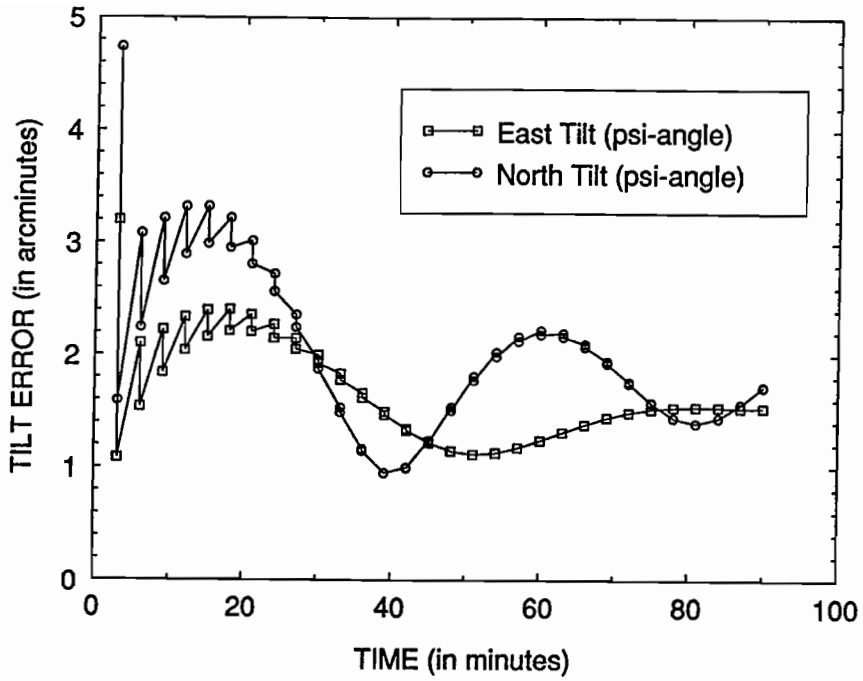

Figure 20. Simulated Covariance Analysis Computations: ENSEMBLE STD. DEV. OF TILT ERROR VS. TIME (3 min VOR/DME fixes)-initial transient still present but allowed to die out

Figs. 23 and 24 depict the time evolution of position and tilt error, respectively, for the longer time step of 15 minute VOR/DME fixes. Notice from Fig. 23 that total position error slopes up into the vicinity of 80 to 90 meters after 4 hours. Notice also from Fig. 24 that tilts appear to rise more rapidly than one would normally feel comfortable with and enter into the range of almost 6 arcminutes after 4 hours have elapsed.

Figs. 25 and 26 depict the time evolution of position and tilt error, respectively, for the even longer time step of 30 minute VOR/DME fixes. Notice from Fig. 25 that total position error slopes up into the vicinity of 80 to 95 meters after 4 hours. Notice also from Fig. 26 that tilts again appear to rise more rapidly than one would normally feel comfortable with and enter into the range of close to 6 arcminutes after 4 hours have elapsed.

Figs. 27 and 28 depict the time evolution of position and tilt error, respectively, for the longest time step (considered in this investigation) of 45 minute VOR/DME fixes. Notice from Fig. 27 that total position error slopes up into the vicinity of 108 meters after 4 hours. Notice also from Fig. 28 that tilts again appear to rise more rapidly than one would feel comfortable with and enter into the range of 6 arcminutes after 4 hours have elapsed.

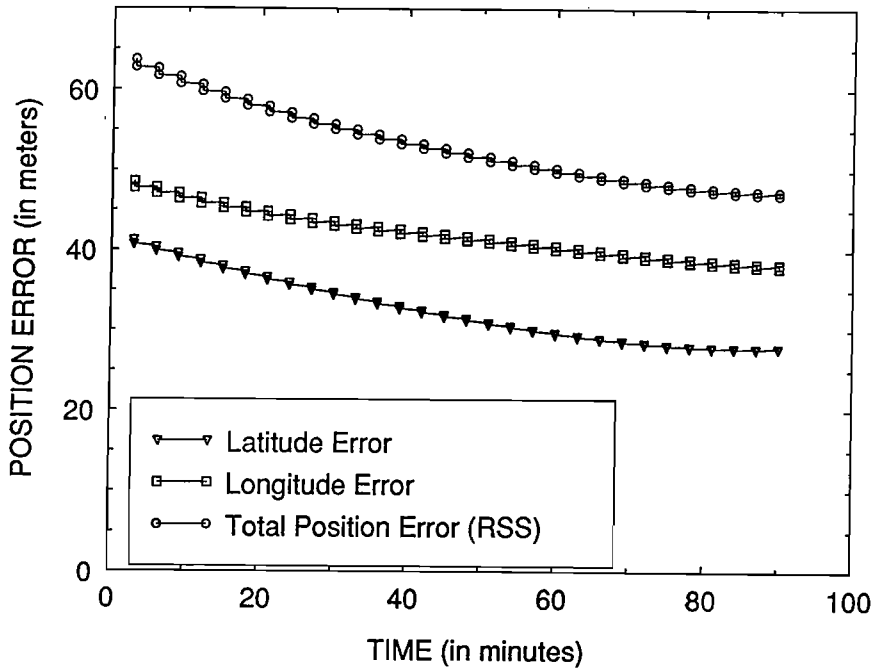

Figure 21. Simulated Covariance Analysis Computations: ENSEMBLE STD. DEV. OF POSITION ERROR VS. TIME (3 min VOR/DME fixes)

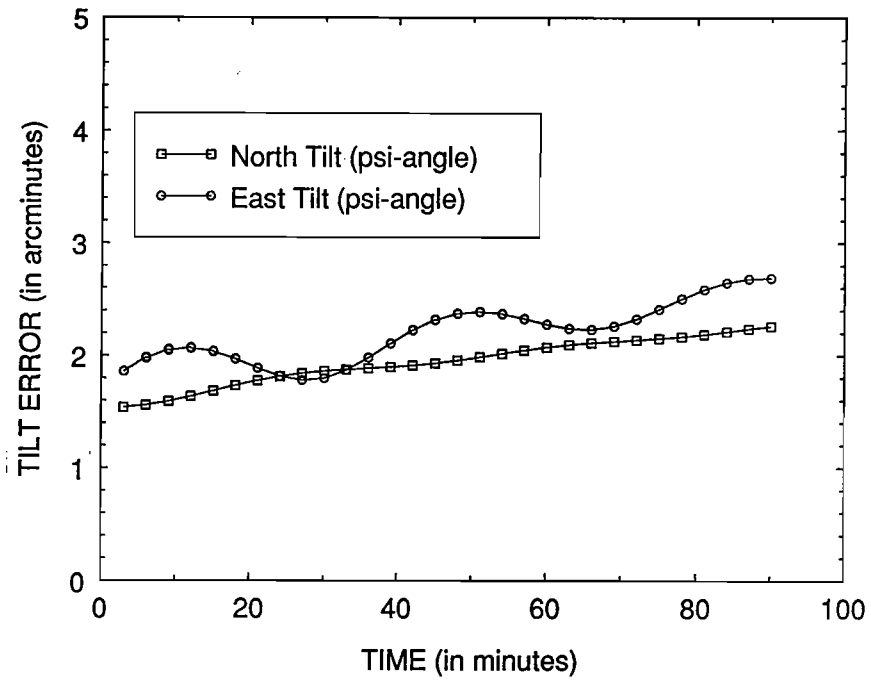

Figure 22. Simulated Covariance Analysis Computations: ENSEMBLE STD. DEV. OF TILT ERROR VS. TIME (3 min VOR/DME fixes)

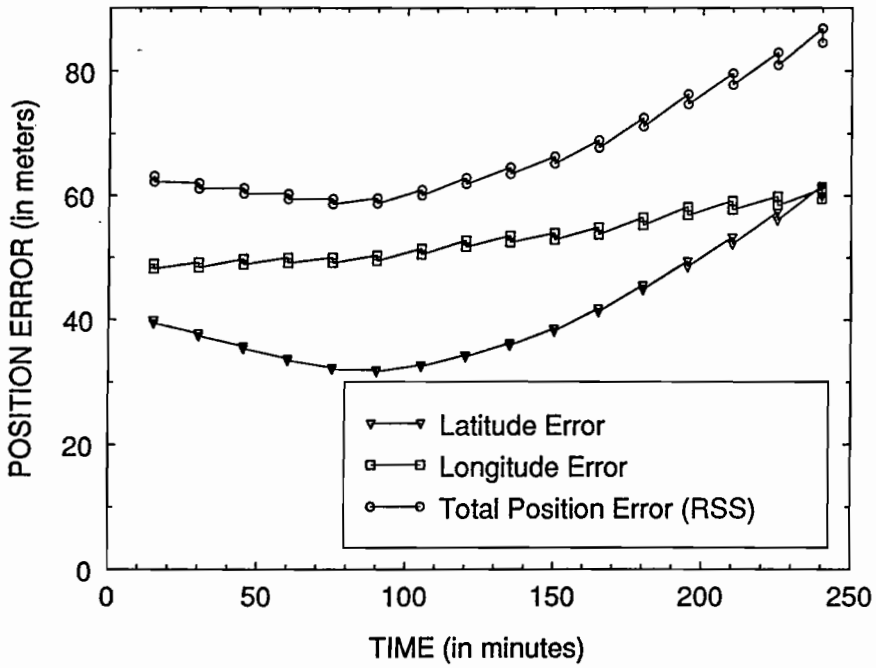

Figure 23. Simulated Covariance Analysis Computations: ENSEMBLE STD. DEV. OF POSITION ERROR VS. TIME (15 min VOR/DME fixes)

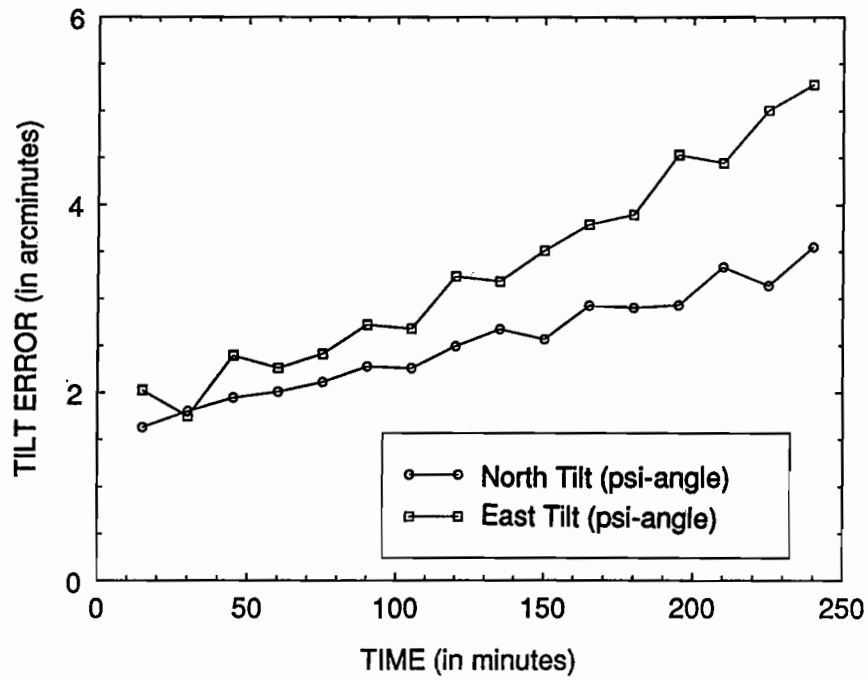

Figure 24. Simulated Covariance Analysis Computations: ENSEMBLE STD. DEV. OF TILT ERROR VS. TIME (15 min VOR/DME fixes)

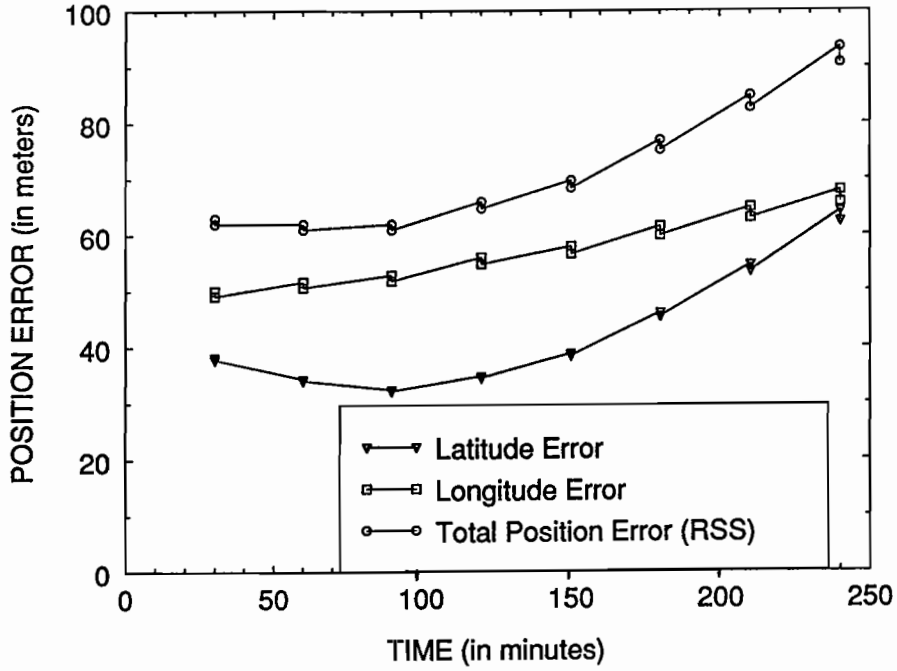

Figure 25. Simulated Covariance Analysis Computations: ENSEMBLE STD. DEV. OF POSITION ERROR VS. TIME (30 min VOR/DME fixes)

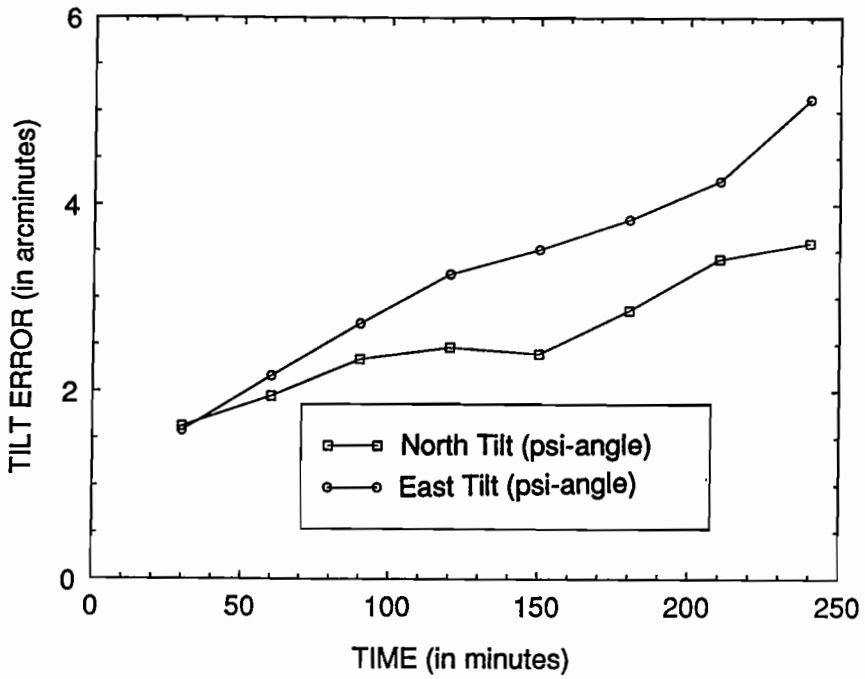

Figure 26. Simulated Covariance Analysis Computations: ENSEMBLE STD. DEV. OF TILT ERROR VS. TIME (30 min VOR/DME fixes)

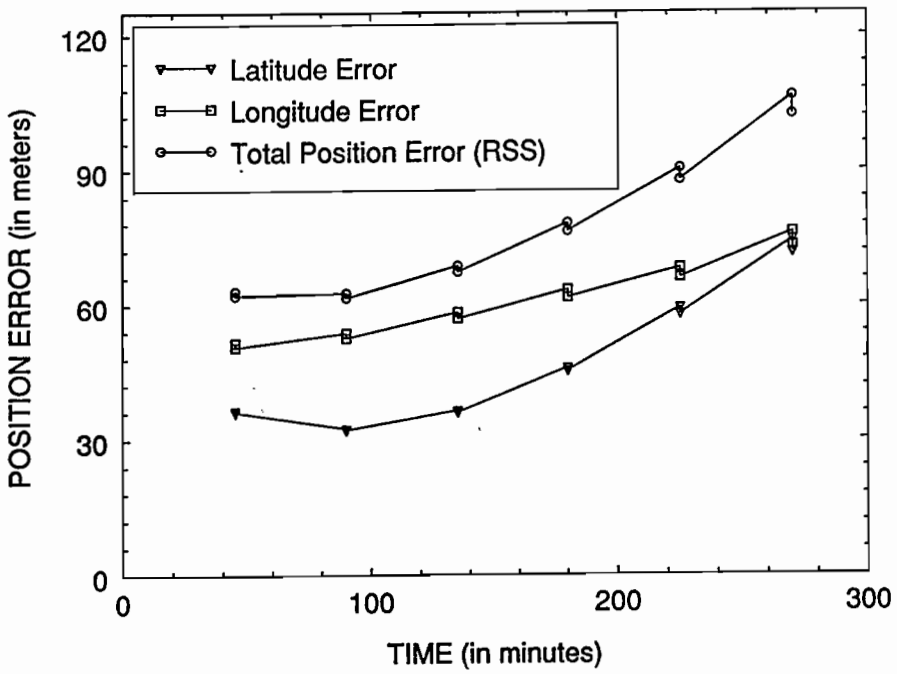

Figure 27. Simulated Covariance Analysis Computations: ENSEMBLE STD. DEV. OF POSITION ERROR VS. TIME (45 min VOR/DME fixes)

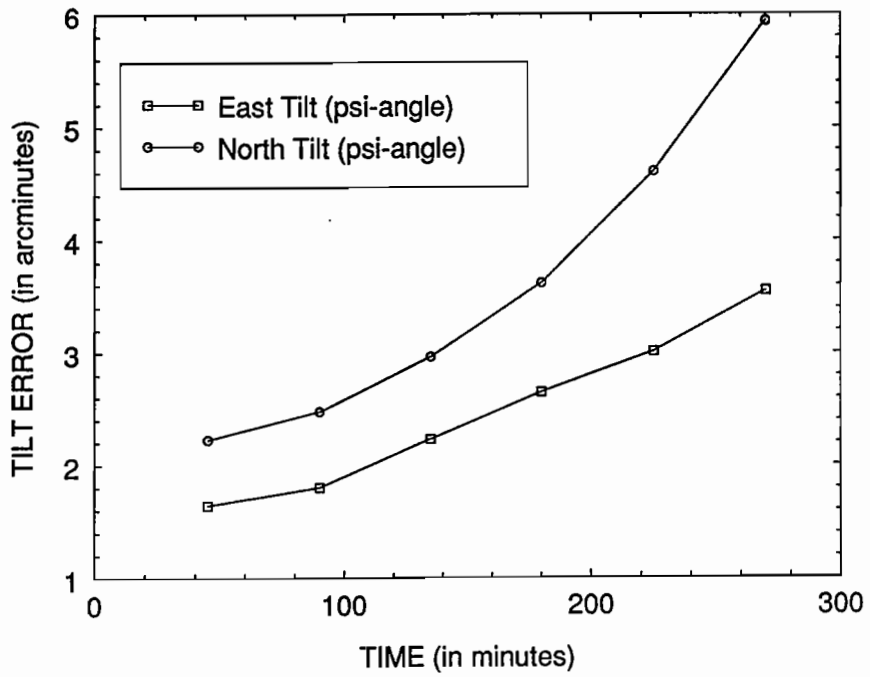

Figure 28. Simulated Covariance Analysis Computations: ENSEMBLE STD. DEV. OF TILT ERROR VS. TIME (45 min VOR/DME fixes)

7.2.2 Exclusive use of navaid fixes from surveyed retroreflector sites

Fig. 29 depicts tilts using 3 minute periodic time samples where each sample avails measurement information constituting another Retro/Pos fix reset/update. Figs. 29 and 30 depict, respectively, Phase 2 position error and tilt error evolution *after* the transient is no longer present. In steady-state Phase 2 operation with periodic Retro/Pos fixes every 3 minutes, Fig. 29 demonstrates 1-σ total position error (or navigation accuracy with LASERNAV II) to be no better than $\approx$ 12 meters (in real-time operation). Fig. 30 demonstrates 1-σ tilt error (with LASERNAV II at 3 minute Retro/Pos fixes) to be in the vicinity of 2 to 2.5 arcminutes (in real-time operation). These results of Figs. 29 and 30 are in the best case of Retro/Pos fixes being available every 3 minutes. More practical fix schedules of less frequent availability will be considered next.

Figs. 31 and 32 depict the time evolution of position and tilt error, respectively, for the longer time step of 15 minute Retro/Pos fixes. Notice from Fig. 31 that total position error levels off and stays in the vicinity of 20 to 22 meters after 4 hours. Notice also from Fig. 32 that tilts appear to rise more rapidly than one would normally feel comfortable with and enter into the range of almost 5 arcminutes after 4 hours have elapsed.

Figs. 33 and 34 depict the time evolution of position and tilt error, respectively, for the even longer time step of 30 minute Retro/Pos fixes. Notice from Fig. 33 that total position error levels off and stays in the vicinity of 27 to 30 meters after 4 hours. Notice also from Fig. 34 that tilts again appear to rise more rapidly than one would normally feel comfortable with and enter into the range of close to 5 arcminutes after 4 hours have elapsed.

Figs. 35 and 36 depict the time evolution of position and tilt error, respectively, for the longest time step (considered in this investigation) of 45 minute Retro/Pos fixes. Notice from Fig. 35 that total position error levels off and stays in the vicinity of 36 meters after 4 hours. Notice also from Fig. 36 that tilts again appear to rise more rapidly than one would feel comfortable with and enter into the range of 5 to 6 arcminutes after 4 hours have elapsed.

7.2.3 Use of both VOR/DME and surveyed retroreflector site fixes simultaneously

Fig. 37 depicts tilts using 3 minute periodic time samples where each sample avails measurement information constituting another combined VOR/DME and Retro/Pos fix reset/update. Figs. 37 and 38 depict, respectively, Phase 2 position error and tilt error evolution *after* the transient is no longer present. In steady-state Phase 2 operation with periodic combined VOR/DME and Retro/Pos fixes every 3 minutes, Fig. 37 demonstrates 1-σ total position error (or navigation accuracy with LASERNAV II) to be no better than $\approx$ 12 meters (in real-time operation). Fig. 38 demonstrates 1-σ tilt error (with LASERNAV II at 3 minute combined VOR/DME and Retro/Pos fixes) to be in the vicinity of 2 to 2.5 arcminutes (in real-time operation). These results of Figs. 37 and 38 are in the best case of combined VOR/DME and Retro/Pos fixes being available every 3 minutes. More practical fix schedules of less frequent availability will be considered next.

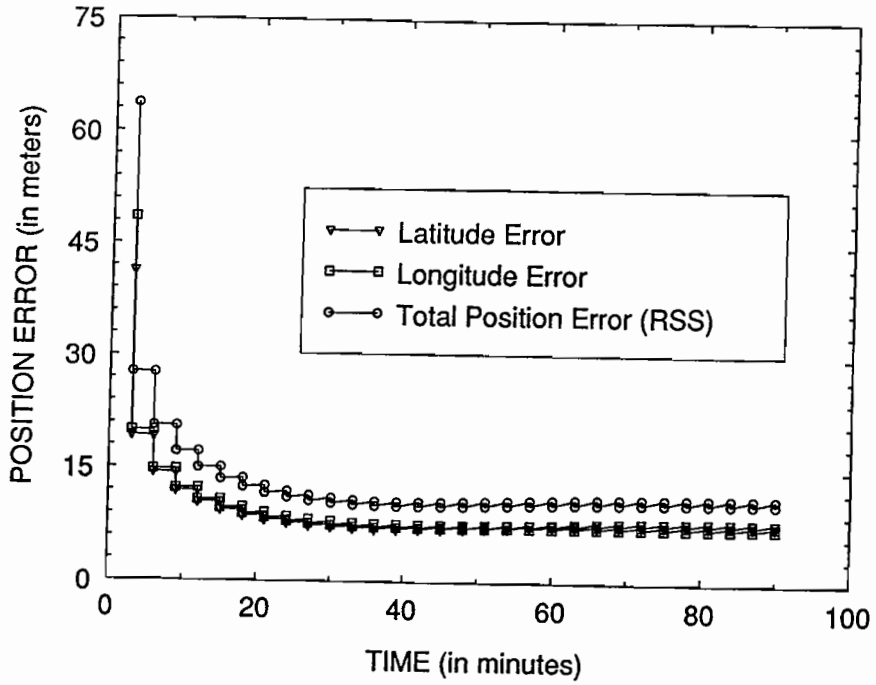

Figure 29. Simulated Covariance Analysis Computations: ENSEMBLE STD. DEV. OF POSITION ERROR VS. TIME (3 min Retro/Pos fixes)

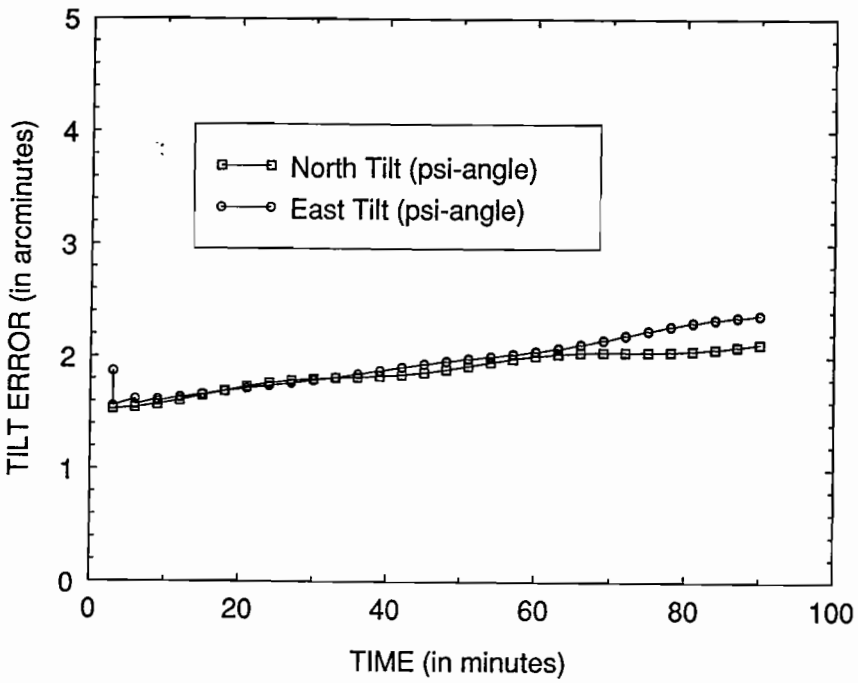

Figure 30. Simulated Covariance Analysis Computations: ENSEMBLE STD. DEV. OF TILT ERROR VS. TIME (3 min Retro/Pos fixes)

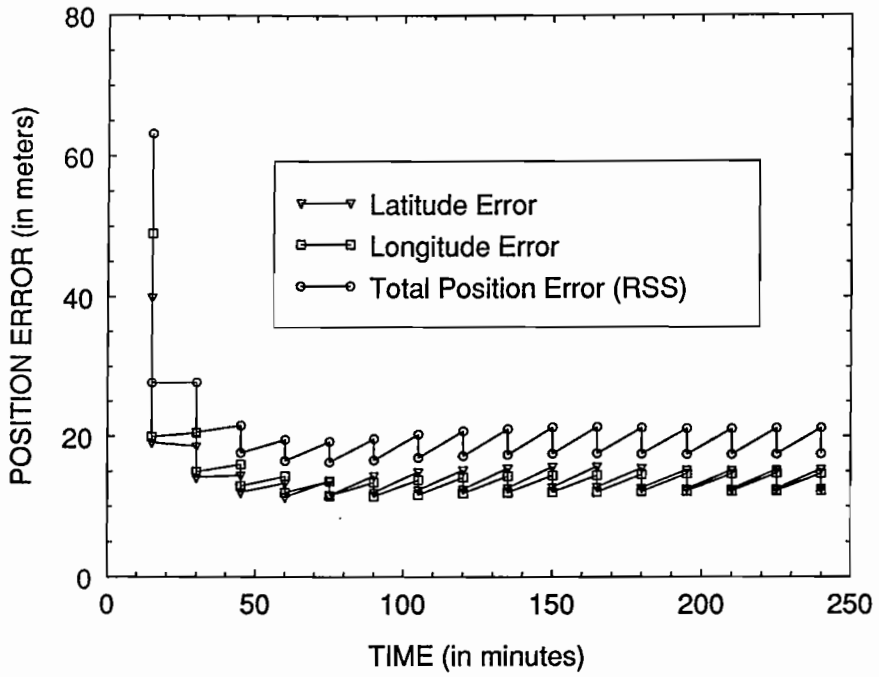

Figure 31. Simulated Covariance Analysis Computations: ENSEMBLE STD. DEV. OF POSITION ERROR VS. TIME (15 min Retro/Pos fixes)

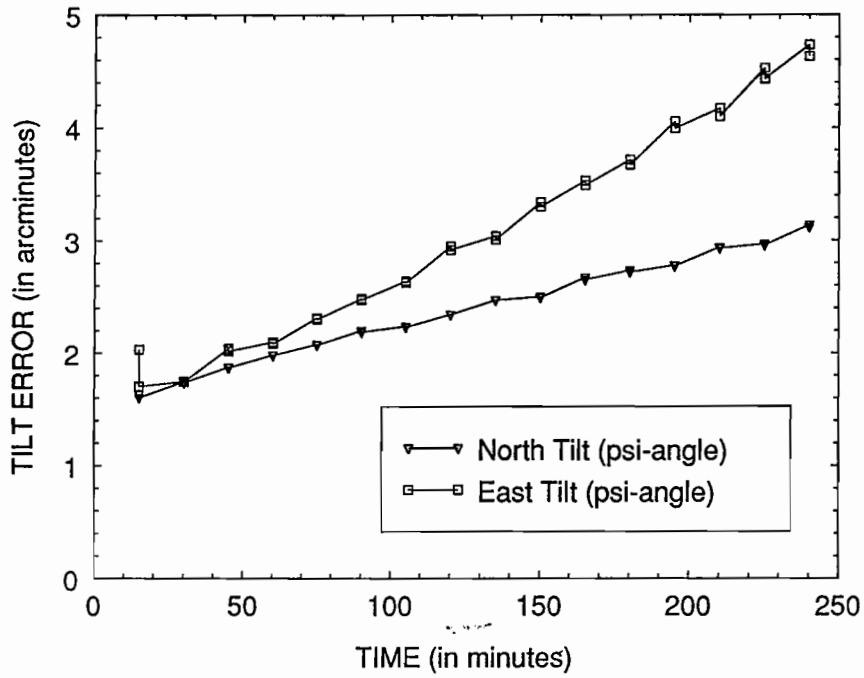

Figure 32. Simulated Covariance Analysis Computations: ENSEMBLE STD. DEV. OF TILT ERROR VS. TIME (15 min Retro/Pos fixes)

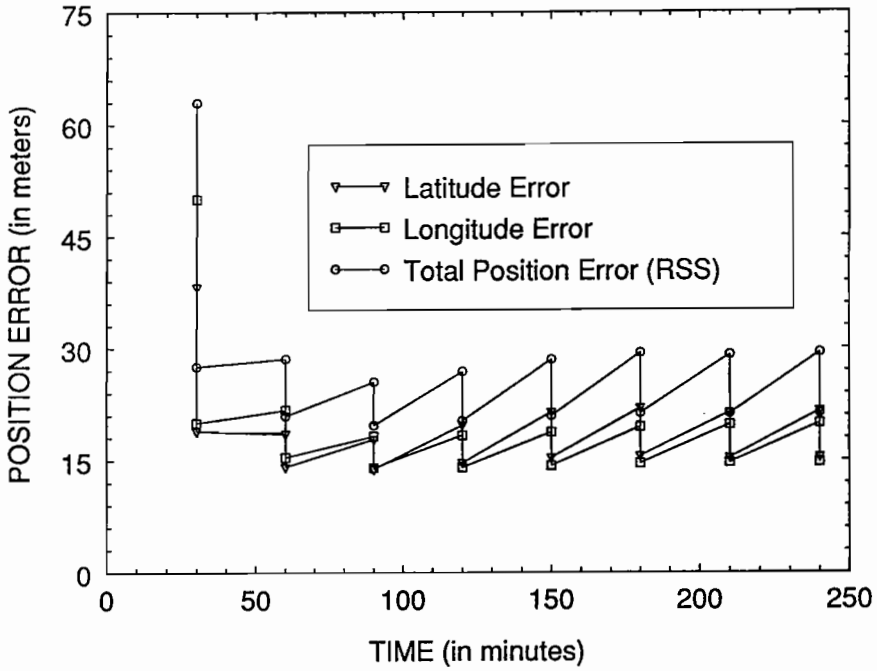

Figure 33. Simulated Covariance Analysis Computations: ENSEMBLE STD. DEV. OF POSITION ERROR VS. TIME (30 min Retro/Pos fixes)

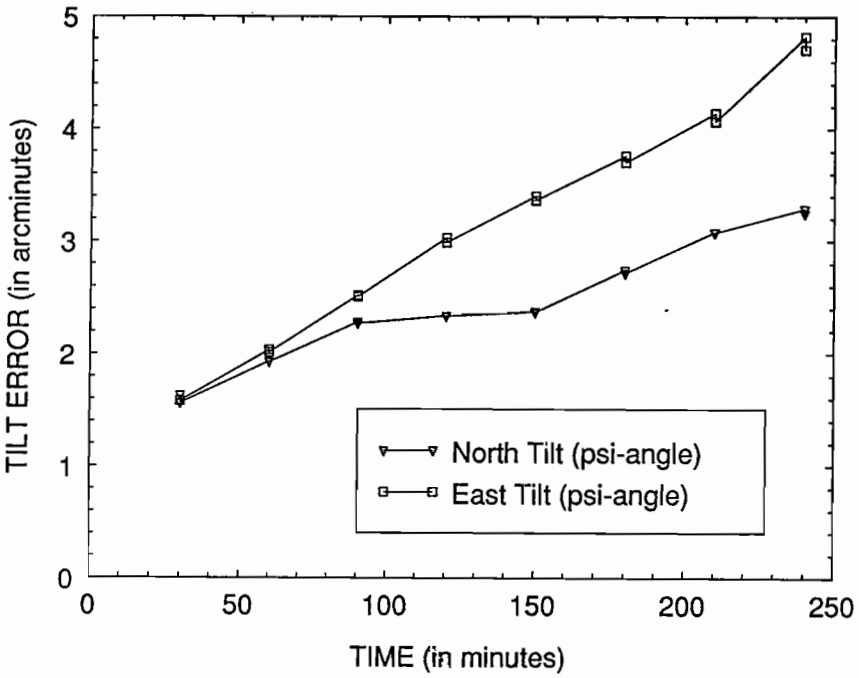

Figure 34. Simulated Covariance Analysis Computations: ENSEMBLE STD. DEV. OF TILT ERROR VS. TIME (30 min Retro/Pos fixes)

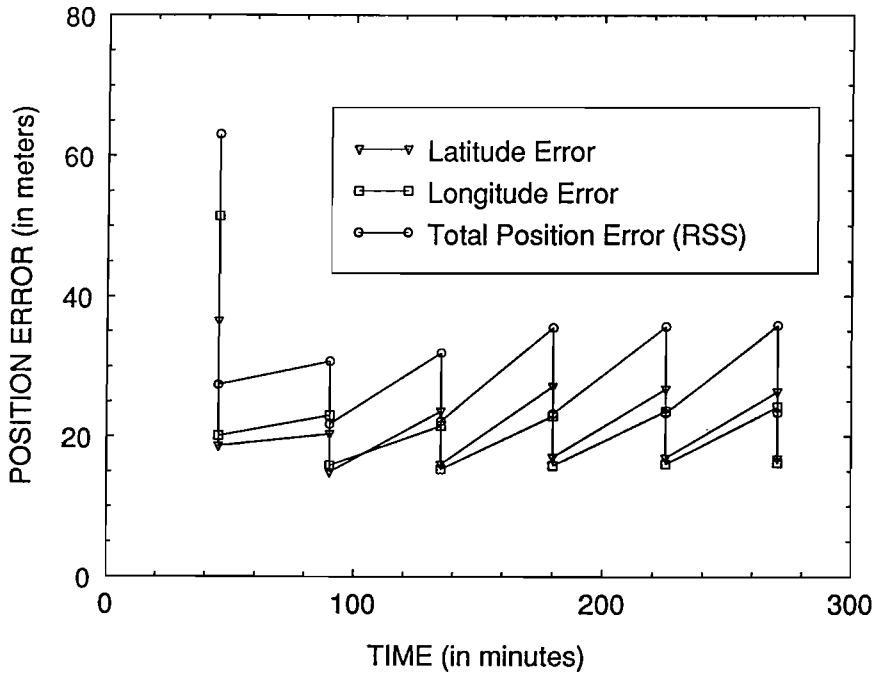

Figure 35. Simulated Covariance Analysis Computations: ENSEMBLE STD. DEV. OF POSITION ERROR VS. TIME (45 min Retro/Pos fixes)

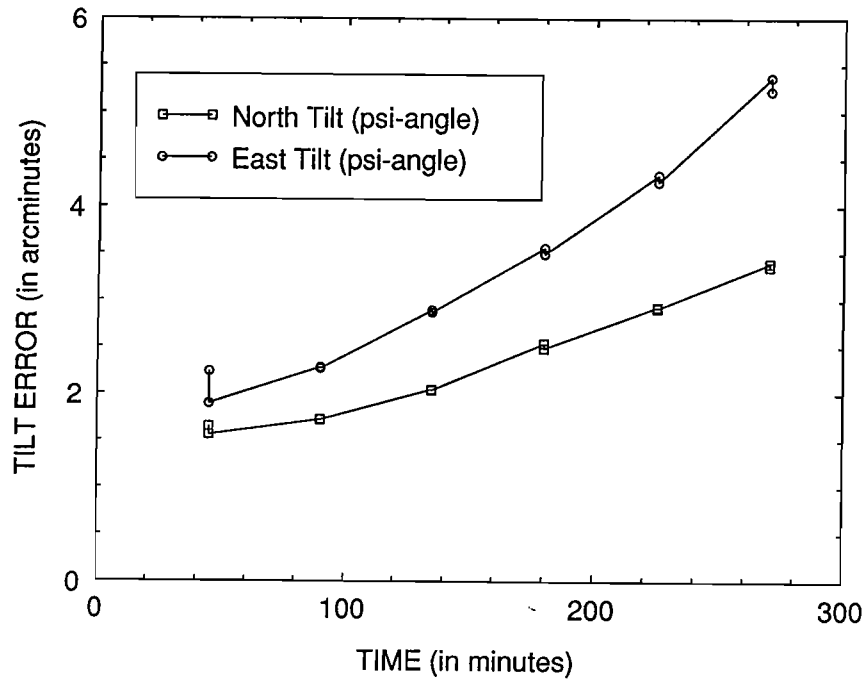

Figure 36. Simulated Covariance Analysis Computations: ENSEMBLE STD. DEV. OF TILT ERROR VS. TIME (45 min Retro/Pos fixes)

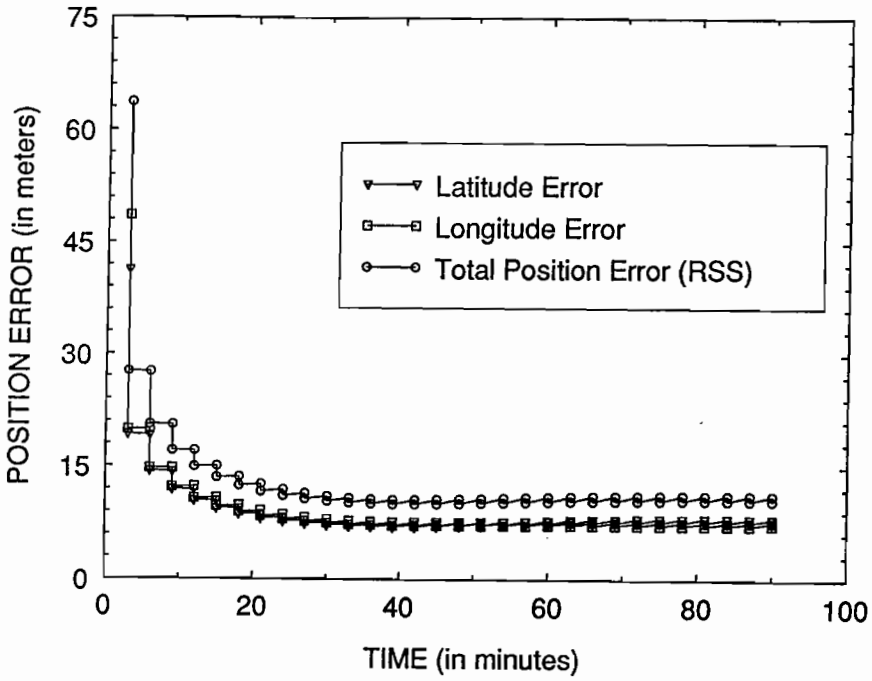

Figure 37. Simulated Covariance Analysis Computations: ENSEMBLE STD. DEV. OF POSITION ERROR VS. TIME (3 min combined VOR/DME and Retro/Pos fixes)

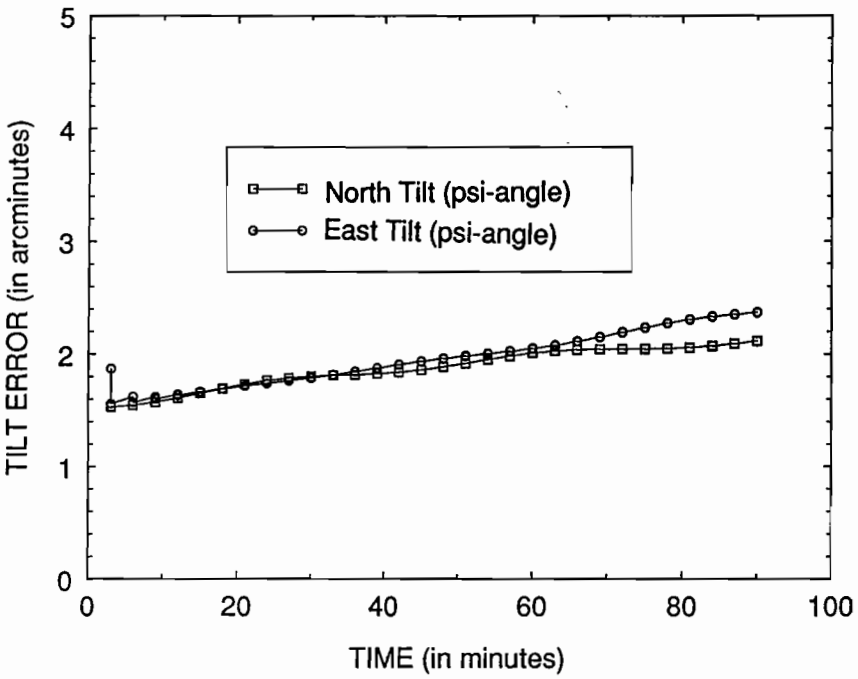

Figure 38. Simulated Covariance Analysis Computations: ENSEMBLE STD. DEV. OF TILT ERROR VS. TIME (3 min combined VOR/DME and Retro/Pos fixes)

Figs. 39 and 40 depict the time evolution of position and tilt error, respectively, for the longer time step of 15 minute combined VOR/DME and Retro/Pos fixes. Notice from Fig. 39 that total position error levels off and stays in the vicinity of 20 to 22 meters after 4 hours. Notice also from Fig. 40 that tilts appear to rise more rapidly than one would normally feel comfortable with and enter into the range of almost 5 arcminutes after 4 hours have elapsed.

Figs. 41 and 42 depict the time evolution of position and tilt error, respectively, for the even longer time step of 30 minute combined VOR/DME and Retro/Pos fixes. Notice from Fig. 41 that total position error levels off and stays in the vicinity of 25 to 30 meters after 4 hours. Notice also from Fig. 42 that tilts again appear to rise more rapidly than one would normally feel comfortable with and enter into the range of close to 5 arcminutes after 4 hours have elapsed.

Figs. 43 and 44 depict the time evolution of position and tilt error, respectively, for the longest time step (considered in this investigation) of 45 minute combined VOR/DME and Retro/Pos fixes. Notice from Fig. 43 that total position error levels off and stays in the vicinity of 35 meters after 4 hours. Notice also from Fig. 44 that tilts again appear to rise more rapidly than one would feel comfortable with and enter into the range of 5 arcminutes after 4 hours have elapsed. This completes our coverage of the simulation results that were have performed to date in support of ETB data collection missions.

7.2.4 LASERNAV II inherent inertial drift with NO navaid fixes

For perspective, in order to better appreciate the resulting navigation accuracy provided by LASERNAV II when utilizing the external navaids as sources of occassional periodic position fixes as treated above, we shall now briefly consider the extreme situation when no navaid fixes are used at all. In order to use the structure of the existing software of [85] for this degenerate situation of no navaid fixes being taken, the effective 2×12 observation matrix is taken to be $H = [0]$ and the associated 2×2 positive definite effective measurement noise covariance intensity matrix is taken to be so large that it is essentially infinite in single precision as $R = \lim_{\sigma \to \infty} \sigma \, I_{2\times 2}$, where it is actually sufficient to just numerically fix σ to be very large as, say, $1.00E{+}30$. As a consequence, the Kalman gain of Table 1 will be essentially zeroed because of the dominating effect of the matrix inversion of an extremely large positive definite matrix resulting in an extremely small answer, hence the effect of fictitious measurements being present will be wiped out and the resulting covariance solution that evolves with time will be as though it emanates from a pure Lyapunov equation (corresponding to no sensor measurements being available). The resulting growth in position and tilt error for this no measurement situation is as depicted in Figs. 45 and 46, respectively, for purposes of comparison with the results of Sections 7.2.1 to 7.2.3. As in the earlier cases treated above, the steady-state initial condition for $P(0)$ is from Eq. 64 and corresponds to an initial calibration/alignment having been initially performed (to perhaps be interpreted as occurring before take-off).

Two conclusions become apparent from Figs. 45 and 46. It is apparent that, as compared to the use of exclusive VOR/DME position fixes as depicted in Section 7.2.1 (at the sample rates lower than every 3 minutes), (1) it is better to not use these relatively coarse fixes (coarse as compared to

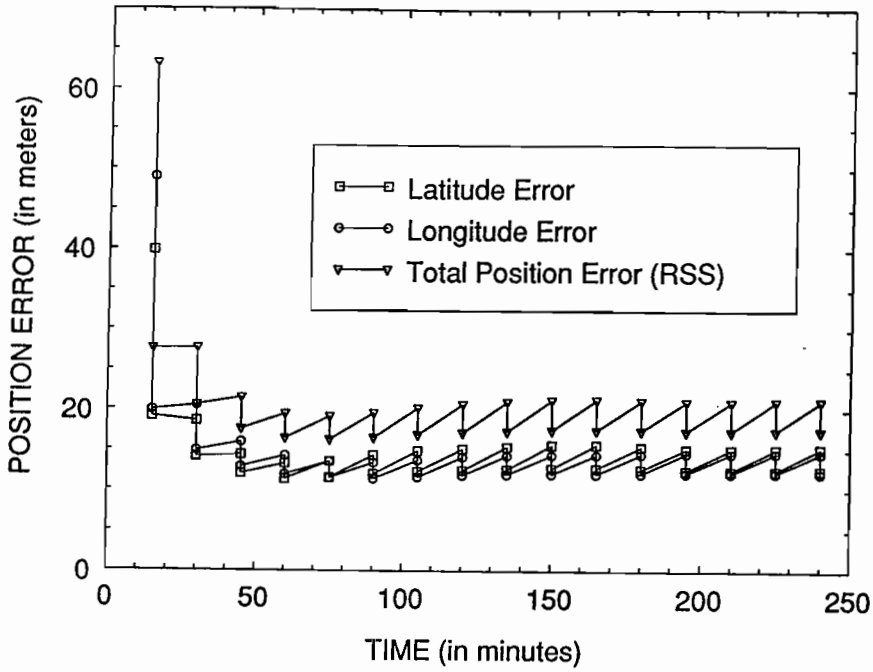

Figure 39. Simulated Covariance Analysis Computations: ENSEMBLE STD. DEV. OF POSITION ERROR VS. TIME (15 min combined VOR/DME and Retro/Pos fixes)

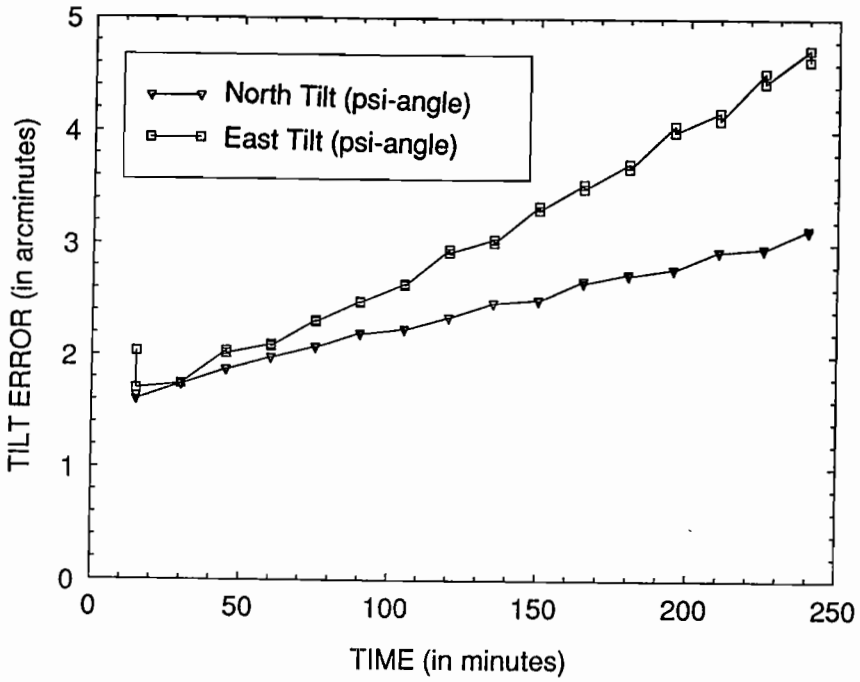

Figure 40. Simulated Covariance Analysis Computations: ENSEMBLE STD. DEV. OF TILT ERROR VS. TIME (15 min combined VOR/DME and Retro/Pos fixes)

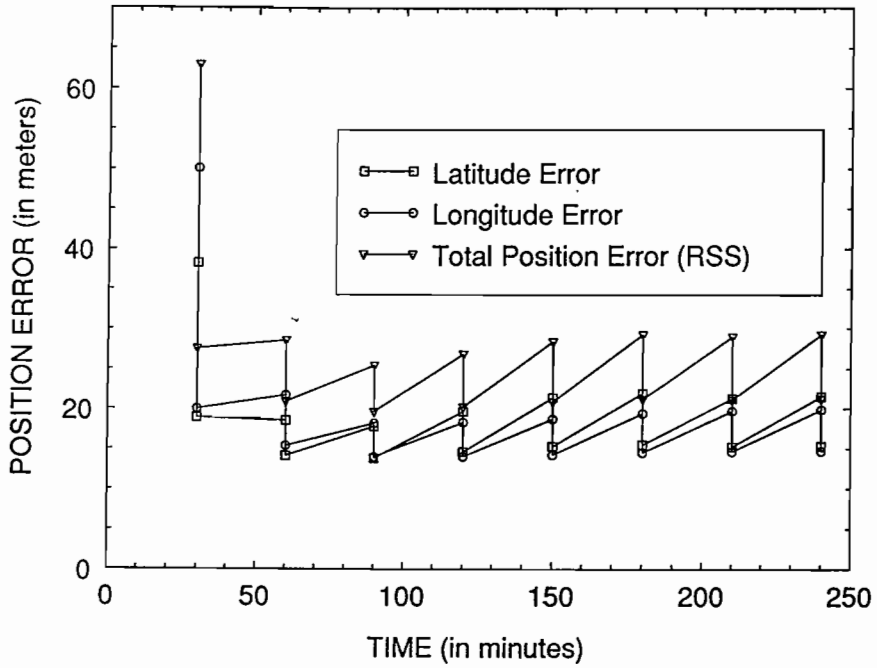

Figure 41. Simulated Covariance Analysis Computations: ENSEMBLE STD. DEV. OF POSITION ERROR VS. TIME (30 min combined VOR/DME and Retro/Pos fixes)

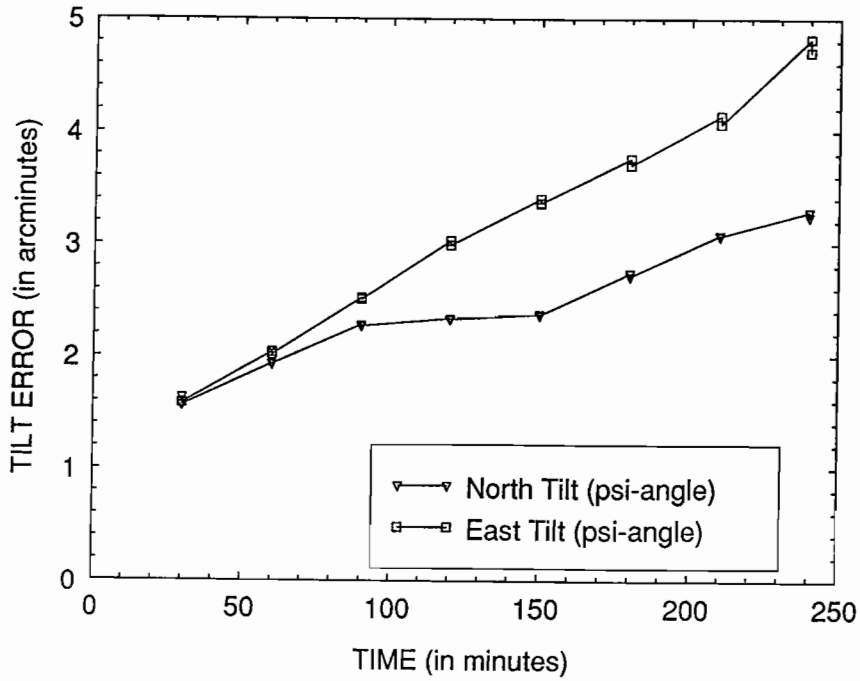

Figure 42. Simulated Covariance Analysis Computations: ENSEMBLE STD. DEV. OF TILT ERROR VS. TIME (30 min combined VOR/DME and Retro/Pos fixes)

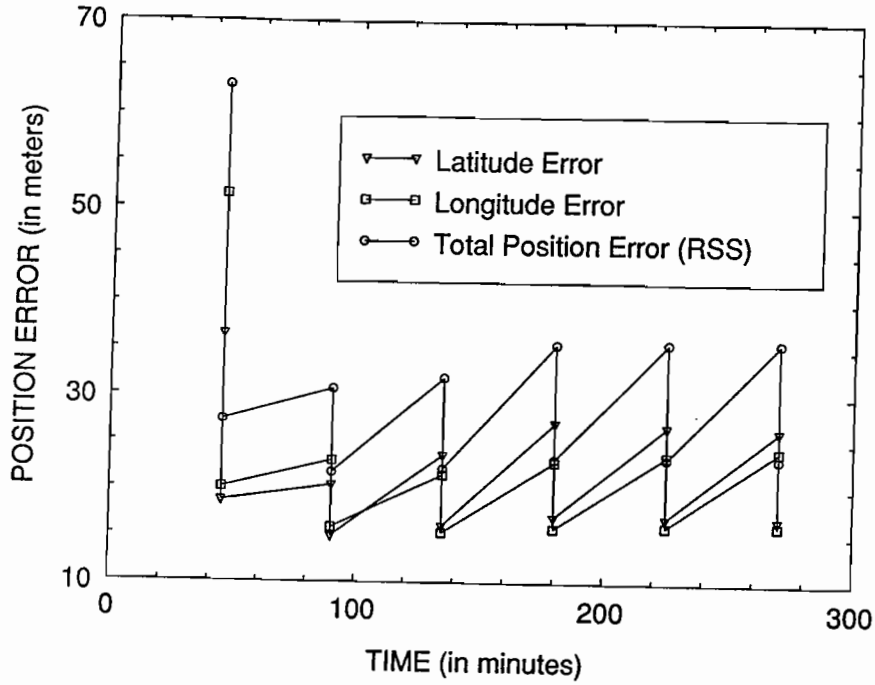

Figure 43. Simulated Covariance Analysis Computations: ENSEMBLE STD. DEV. OF POSITION ERROR VS. TIME (45 min combined VOR/DME and Retro/Pos fixes)

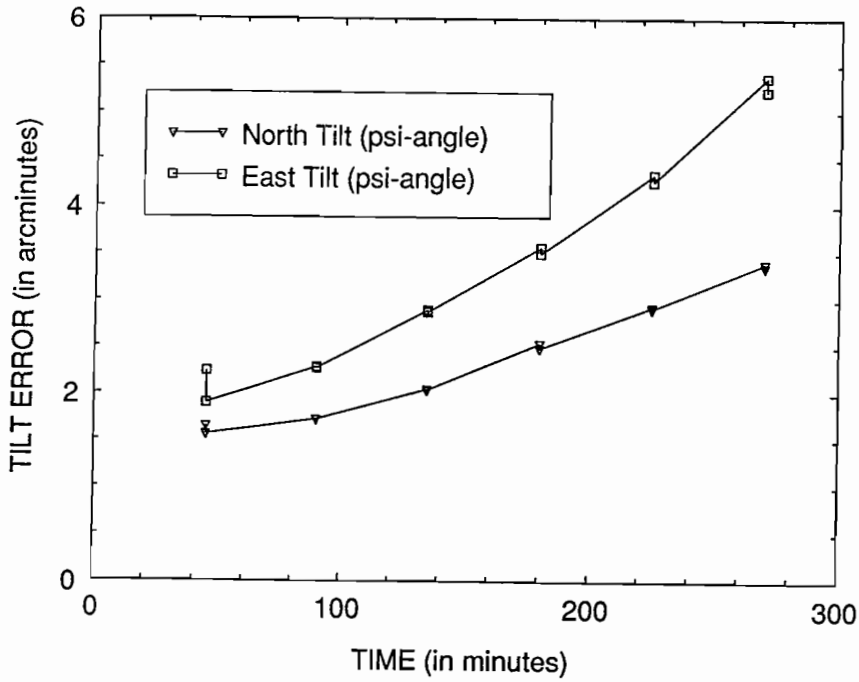

Figure 44. Simulated Covariance Analysis Computations: ENSEMBLE STD. DEV. OF TILT ERROR VS. TIME (45 min combined VOR/DME and Retro/Pos fixes)

the inherent accuracy embodied within the LASERNAV II itself and only slowly degraded by the drift rates that are also inherent) since, except for using VOR/DME every 3 minutes, the use of VOR/DME fixes at the slower rate tends to hasten the corruption of navigation position accuracy. In all cases of using external position fixes (even when using the high accuracy GaAs line scanner position fixes from surveyed retroreflector locations), (2) the tilt errors are more degraded when position fixes are used than they would be without position fixes being used to improve the accuracy of position determination. Therefore, we are in a compromise situation were external position fixes are needed to improve the net navigation position accuracy yet use of these very position fixes aggrevates the psi-angle tilts and causes them to be larger than would otherwise be the case.

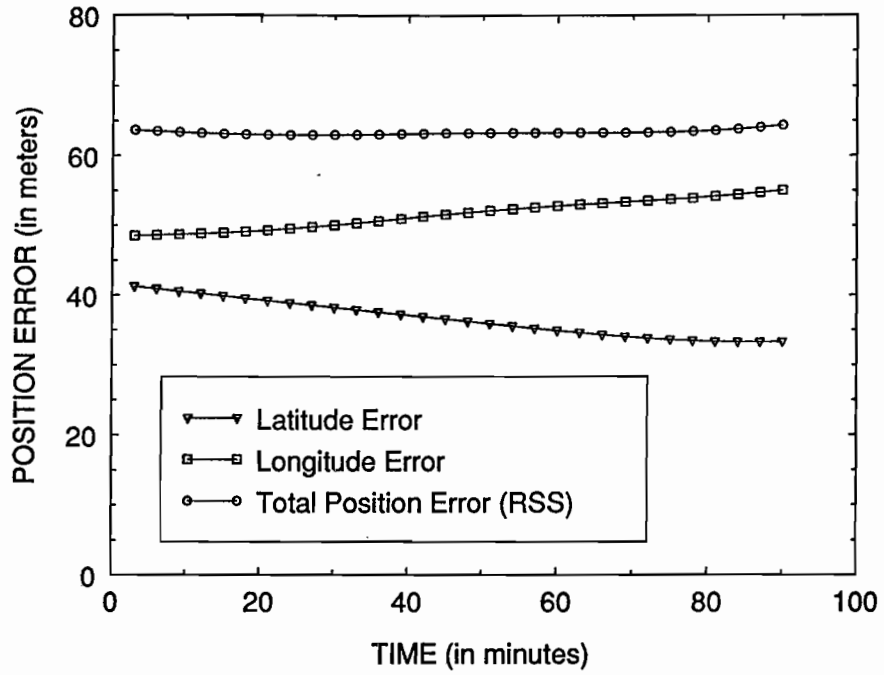

Figure 45. Simulated Covariance Analysis Computations: ENSEMBLE STD. DEV. OF POSITION ERROR VS. TIME (NO navaid fixes used at all following initial Cal/Align)

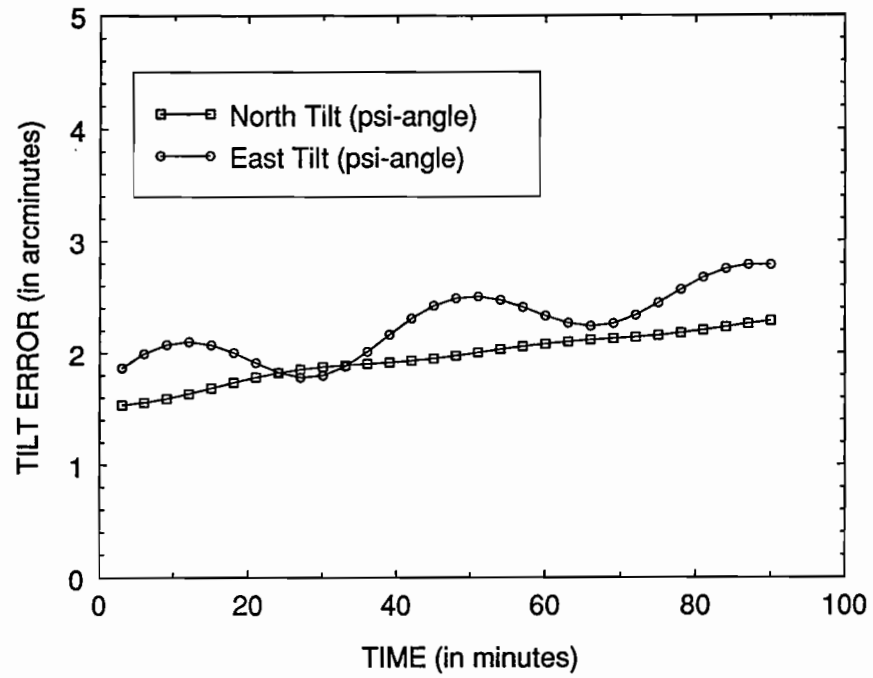

Figure 46. Simulated Covariance Analysis Computations: ENSEMBLE STD. DEV. OF TILT ERROR VS. TIME (NO navaid fixes used at all following initial Cal/Align)

8. KNOWN DEPARTURES FROM THE IDEAL, AS INHERITED IN OUR EVALUATION TOOLS (AND CORRECTED)

8.1 Assessment of Original Status of Commercially Procured Kalman Filter Code

There are several departures from the ideal involving use of expedient (but universally accepted) approximations and simplifying assumptions that were invoked (i.e., footnote 1 on pp. 1, 2; footnotes 9 and 10 on p. 18; footnote 14 on p. 21; footnote 18 on p. 35; footnote 19 on p. 37; and all rectilinear accelerations being assumed to be zero in Eqs. 35 and 51, as mentioned at the end of Section 5.3.3) in performing our Kalman filter/covariance-based navigation accuracy assessments. To serve as a gauge of what remains to be done and where improvements in realism can be further achieved, consider the following acknowledged shortcomings of our working tools:

1. Kalman filter/covariance analysis software available from *Optimization Software, Inc.* doesn't use the discrete-time equivalent Q_d to continuous-time white process noise covariance intensity matrix, Q, to be:

$$Q_d = e^{F\Delta}\left[\int_0^{\Delta} e^{-F\tau}\, G\, Q\, G^T\, e^{-F^T\tau}\, d\tau\right] e^{F^T\Delta}\ \delta_{kj}\ , \tag{65}$$

where the above Kronecker delta is defined as

$$\delta_{kj} = \begin{cases} 1 & \text{if k=j} \\ 0, & \text{otherwise.} \end{cases} \tag{66}$$

but instead uses the Kalman approximation:

$$Q_d' = \Delta\, Q \tag{67}$$

that we claim is an *uncalibrated* approximation in [15] and, for implementation, Q_d' or Q_d is to be further factored (via a Choleski decomposition if necessary) as $Q_d = FF^T$, where here F is used as the process noise gain matrix according to the notation of [85]. Maybe the use of Q_d' here is not so bad (not as bad as it was in the previous application of the author's experience, where it was demonstrated just how bad it could be in [15, following Eq. 42]) but we suspect that this approximation of Eq. 67 may suffice here (but haven't yet looked into this issue in this first cut analysis to find out or ventured to modify this software to be exactly to our liking along this line).

2. Graphical display generated by the *Optimization Software, Inc.* Kalman filter software program is responsive and automatic but deficient in that:

   - it has no mechanism for the user to specify axis labels and units; however, it shows grid ticks (but not scales);

- it has no mechanism for labeling axes and no manual over-ride of the max/min scale option so idiosyncratic behavior can sometimes occur (e.g., a quantity vacillating close to zero in a benign fashion was automatically given an output scale to emphasize its extremes and even though its excursions were of no consequence, its depiction in this way made it look to be much worse than it was) as it selects its own max/min scale.

3. While one version of our software (issued in 1984 and procured by Lincoln in July 1987) is in BASIC (and *is* available as source code [25]) and runs (slowly) as an interpreter version, another version of our software (modified via MICROSOFT proprietary participation using a file entitled *BRUN3087* and released a few months later than Lincoln's first version and procured by Lincoln in Oct. 1987) runs as a load module only (and has no source code available for us to modify). However, these two alternate unmodified versions of our software have provided identical output results during the extensive low-dimensional simulation test cases that were run. The only difference noted is that the load module version executes a proper exit from the menu back to DOS when processing is complete (and EXIT is requested as a valid item on the menu); while the BASIC source code version, upon request from the menu, first exits from the Kalman filter program back to the BASIC prompt, and can then exit from BASIC back to DOS by typing SYSTEM (as a two step procedure versus the one step procedure for the later version). A recent version of BASIC, called QuickBASIC Version 4.50 has been obtained and allows the available source code to be run as object code exclusively (without the need for an interpreter or an interpret step once the current extensive use of MERGE and DELETE commands (legal in BASIC and GWBASIC but illegal in QuickBASIC) are purged from the source code and replaced by commands that *are legal* in QuickBASIC) and should enable this and *all* BASIC programs to run faster. QuickBASIC is in fact what the above mentioned new load module version of the Kalman filter software was implemented in.

4. The following minor idiosyncracies are also present in how we use this available optimization software to get first cut answers:

---

[25] While we can't modify the write-protected version on the disk supplied with the user manual, we did modify (in a controlled manner) the version of it that we transferred to the hard C-disk in order to enhance running time and to accommodate larger output files for larger dimensioned problems and longer problem run times that our application demands. Our original selection of this particular approach to computational evaluation (rather than use a mainframe or workstation) was motivated by the portability of this PC code and its ease of use as a menu-driven user-friendly package (with conveniently defined special purpose file structure for input/output) and its appealing accommodation of interruptions.

- Time step being constant in this OPTIMIZATION SOFTWARE, INC software corresponds to external position fixes being obtained periodically (while theory and real world practicalities don't necessarily strictly adhere to this constraint);
- The *transition matrix* used throughout the computer run is calculated once, up front as a preprocessing step, then retained as being constant (while a variation more appropriate for our purposes but not possible with this simplistic software version is to relinearize $f(x)$ at each new time point and either recalculate the matrix exponential to provide the new *transition matrix* at each relinearization or else just use the first few Taylor series terms of the matrix exponential to approximate the *transition matrix* at this new time point, as is done in many real-time applications);
- Because we can't change cases within the same run in this software used for first cut computer evaluation of navigation system accuracy, we can only handle exclusive use of one navaid at a time instead of in mixed combinations. Runs will correspond first to exclusive periodic use of VOR/DME and then to exclusive periodic use of visual updates from retroreflectors; however, we can handle synchronized simultaneous periodic fixes from both update sources at once;
- Subsequent runs will incorporate realism of coordinated turns in flight trajectory profile [26] (handled as being a known specified deterministic input file that the software can accommodate). Current runs are merely to establish baseline steady-state accuracy achievable under ideal conditions assuming that truth model of INS is identical to filter model instead of using a more involved reduced-order filter evaluation methodology (of which none of the several existing theoretical approaches is entirely satisfactory anyway [87, pp. 79-82]);
- In lieu of our current software not being able to be as accommodating as indicated above to offer a perfect fit, we will assume that the single linearization that we do perform (as reported in the second bullet above of Item 5) is close enough to our ideal and proceed with this simplification in our first cut computer evaluation. Later use of CONTROL-C, MATLIB, or MATRIX-X on a PC (as a refinement) should offer the additional flexibility of being exacting and being able to easily accept the subsequent modifications that we may desire to program in FORTRAN for ease in later porting to Gr. 53's VAX or SUN (instead of in BASIC, as we use here for the PC).

---

[26] A simplified coarse model of the effect on an INS due to aircraft maneuvers (modeling the aircraft maneuvers as just three states) is offered in [34]. This simplistic model is too coarse for our needs.

8.2 Modifications that We Made to Better Accommodate the ETB Application Evaluations

In order to perform the evaluations provided in Section 7, we made the following modifications/corrections to Optimization Software, Inc.'s Kalman filter [27] source code (in BASIC):

- Undeclared array XINIT, which defaulted (under BASIC) to a value of 10 (preventing use of the code on systems higher than 10) has now been declared as XINIT(N) (and now allows software to be used for systems with dimensions higher than 10).
- Performed minor re-adjustment (in several subroutines) of row and column spacing in echo of matrix input so that the VDT can now accommodate a 12-dimensional state variable model.
- Double occurrence of XINIT for specification of initial conditions in both AVBSIM.BAS and in AVBFILTR.BAS now distinguished by renaming one version to be XINITT.
- Inputting and outputting of application related system matrices, covariances, etc., converted from previous format of "XXX.XXXX" to current scientific notation "+X.XXE+XX".
- Miserable graphics originally supplied with the Kalman filter software package now augmented using EASYPLOT^{TM} via creation of auxiliary output files as a bridge. Now also tap off covariances from internal computations within the Kalman filter to be plotted for covariance analysis depicting characteristic sawtooth for navigation accuracy (corresponding to before and after each measurement fix/update).

---

[27] While this commercially available software code initially gave the correct answers for three low-dimensional test cases (from Table 3-1, p. 28 of [82]) of known analytic closed-form solution (also see [15]), the need to run a 12-state model for our ETB application motivated and necessitated these modifications. We later also used a 12-state test case of known solution as well to verify and validate our numerous modifications (and again ran low-dimensional test cases to be certain that previous correct performance had not been clobbered by the changes) in preparation to running our actual ETB application. Sought to coordinate software changes with Prof. A. V. Balakrishnan of UCLA, author of several theoretical textbooks on estimation/control and editor of several series and related journals, who is evidently the father of this Kalman filter code implementation contributed to by many engineers/programmers passing through UCLA (so the code is worthwhile and has a now *known* pedigree). To facilitate cross-communication and in keeping with good programming practice, all changes that we make to the code as we proceed are documented and Prof. Balakrishnan has received a copy. Took this opportunity to encapsule my experience with this program by enhancing menu options to be more user friendly by clarifying both the considerable capabilities of this transportable software as well as elucidating its limitations and indicating how to get around them.

- The transition matrix calculation for converting continuous-time n-state model description to discrete-time, originally adaptively tailored the number of terms to be retained in the Taylor series by using a coarse norm. Now use tighter bound derived from column-sum and row-sum norms instead [83] and set a limit on total number of terms to use in calculation so it won't run away (otherwise incur numerous OVERFLOW's).
- Keyboard entry of all $12 \times 12 = 144$ elements of the initial covariance, previously required, is now avoided.
- Modified AVBFILTR.BAS to output a file for EASYPLOT that depicts the characteristic sawtooth covariance representation corresponding to $P^{(-)}$ and $P^{(+)}$ at each measurement time step, so familiar in navigation applications (instead of outputting just its best case lower envelop). As originally obtained, software of [85] did calculate covariances internally but didn't output them at all since it only advertised that it performs Kalman filtering estimation function.

The motivation for our using this PC-based software of [85]: it's menu-driven, easy-to-use, portable, well thought-out, validated with test problems of known closed-form solution, has now been corrected so that it can handle problems larger than just toy problems, and it can be personalized (with reasonable effort) from the source code version to offer additional features (as we have done).

The upshot assessment of the effect of all these idiosyncracies, approximations, and acknowledged errors, as they affect our simulated evaluation results, is that they are "no big deal" in a first cut evaluation [28]. The "big deals" were corrected to satisfy our immediate needs [29].

---

[28]A more complex 16-state representation of VOR/DME updating of an INS was found in [89] but we choose here to ignore the four additional states that distinguish this from our model of Sections 4 and 5.

[29]The author was initially somewhat apprehensive that the general trend toward rapid growth with time evidenced in our LASERNAV II navigation performance evaluation results of Section 7.2.1 for the time steps of 15, 30, and 45 minutes (but not exhibited for 3 minutes) may be merely a remnant of the technique used to compute the transition matrix (as incorporated within the software of [85]) if it incurred too much roundoff error during the calculations (as a distinct possibility). An alternate computational approach is available from [15, Fig. 1] but then needs to be run on the PC using our *available* RM/FORTRAN and its output then inserted into the Kalman filter as part of the discretized model (as can be conveniently edited in) along with exact calculation of the Q_d of Eq. 65, if so desired as a refinement of what currently exists in software (being Eq. 67). The author's initial fear was alleviated when the results of Sections 7.2.2 and 7.2.3 didn't register similar increases for the same step sizes (i.e., identical transition matrices).

Future plans to exploit the characteristics and outputs of the HONEYWELL LASERNAV II system to ultimately compensate optical/RF sensors to isolate them to a degree from aircraft motion during flight will likely appeal to recent results along these lines in [25], [27], [53] for combined optical and strapdown [30] INS application (see Fig. 47). In particular, [102] has new ideas (following up on ideas discovered to have been asserted earlier in [113]) on how to use strapdown laser gyros in a "hybrid" gimbal-strapdown mechanization to get better more stable behavior [31] than afforded by use of just strapdown alone. Other details for using a strapdown laser gyro INS are addressed in [91]. The explicit differential equations describing the error model of a strapdown system (that we avoided here for the sake of expediency in this investigation to circumvent a much larger computational burden, but which *would be needed* in an actual strapdown implementation) are derived in [115, pp. 845-846] and an overview functional flow block diagram for strapdown processing is provided in [115, p. 844, Fig. 11]. Considerations of the best way to represent angular pitch, roll, and yaw excursions of the aircraft, using information from the strapdown LASERNAV II INS (available at its 25 Hz rate) for compensating the cameras and scene sensors to isolate the deleterious effects of aircraft motion (cf., [111]) can be decided by reviewing [29]-[32, pp. 99-100], [35]-[40], [45, Appendices A, B, C]-[50] as well as current IEEE AES two-day-a-month Working Group results seeking to update references [51], [52] (which are currently tapped into by our being on the mailing list for minutes and recent results and to which we have already made an indirect contribution ourselves by catching an error and informing the chairman, and noticing that subsequent minutes have been appropriately modified to reflect our correction) in their endeavor to establish common standards for using the INS outputs (for purposes other than just navigation) in *Guide to the Characteristics and Application of Inertial Angular Sensors (Gyro, Accelerometer, and Other)* (under IEEE AES Project P-761 in process). The most up-to-date method for computing instantaneous aircraft attitude from the strapdown gyro measurements (for our purposes of ultimately leveling cameras or other airborne sensors) is offered in [138] as a highly readable overview of three alternative existing approaches (with benefits and drawbacks), which

---

[30]The distinguishing feature of the strapdown mechanized INS versus the conventionally gimballed INS is the absence of a gimbal-mounted reference table. In the strapdown system, the gyro and accelerometers are mounted directly to the vehicle frame. In the strapdown INS, the gyros provide angular rates to the B Matrix which converts them to direction cosines. These signals are used to specify vehicular attitude with respect to an inertial reference frame. The position computer accepts inertial accelerations and altitude information to develop cartesian coordinates representing the vehicle's position in inertial space. These vectors are then sent to the vector solver where they are summed to provide readouts of latitude and longitude. A methodology for generating strapdown specs for INS applications involving use of known external navaids is offered in [127].

[31]In 1962, J. R. Huddle, the author of [101] was one of the earliest Navigation practitioners to recognize the utility of the Kalman filter (a scant few years after its discovery in 1959-60) in this application arena.

provides enough insight to develop an original more computationally expedient fourth approach in [138] that is recommended for use in the ETB application. The potential utility of GPS or differential GPS in this present application offers further future options to be considered [40], [41], [43], [44], [48], [54], [122].

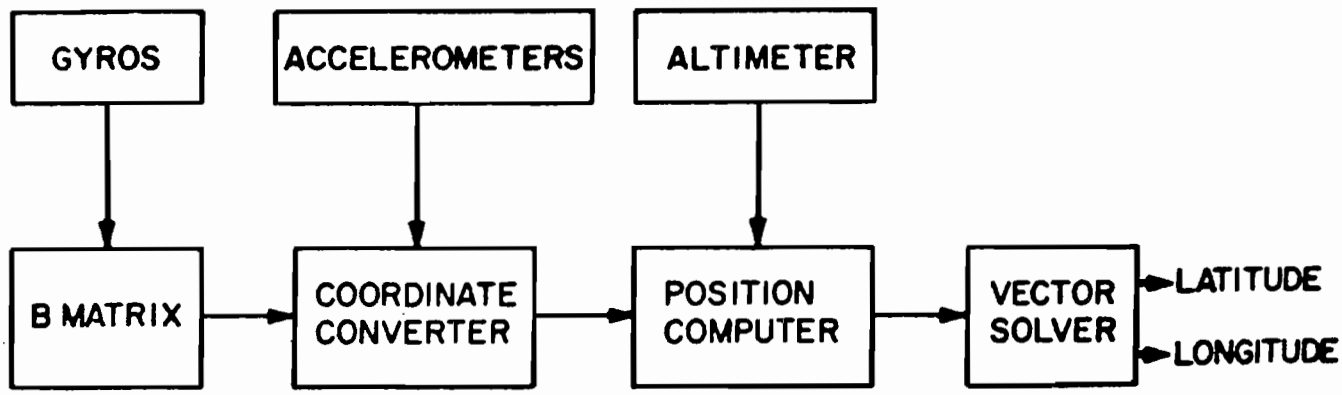

Figure 47. Simplified Overview of a Strap-Down INS

9. SUMMARY/CONCLUSIONS

9.1 Summary

PROBLEM STATEMENT: Investigate use of navigation information to expedite collection of test range data by allowing next row scan to dovetail to the last to avoid recording excessive overlap of redundant pixel data available from last pass. Explore use of INS WAYPOINTS for mission flight planning.

A bulletized summary of highlights of this study, associated constraints observed, and its results are offered below:

- INS (with its own internal Kalman filter) nominally provides 3-D position , velocity, and attitude, but accuracy drifts off with time unless compensated with external position fixes;
- PC-based Kalman filter software has been used to evaluate/predict expected accuracy provided by these different design options (with overall results summarized here in Tables 2 and 3 for position error and tilt error, respectively):
  - Use of INS only, with initialization before take-off (in Sec. 7.2.4);
  - Use of INS with some other radio navaid (e.g., VOR/DME) for periodic updates/resets in transit and on station (in Sec. 7.2.1);
  - Use of INS with periodic visual updates from retroreflectors of known surveyed location (in Sec. 7.2.2);
  - Use of INS with periodic simultaneous updates from both VOR/DME and retroreflector position fixes (in Sec. 7.2.3);
- To perform the above described evaluations, needed good models for each system and needed to use validated (trustworthy) software, as obtained by the following steps:
  - Validated software with low-dimensional test problems of known closed-form solution (as illustrated in [15] and more extensively in [82]);
  - Debugged and corrected a few oversights in the commercially provided software to allow a problem of the larger dimensions of our application to be run (as discussed in Section 8);
  - Procured parameters of LASERNAV II satisfying spec, i.e., errors no worse than ...(as discussed in Section 5);
  - Tying in to established 25+ year old tradition for properly handling such situations to expedite obtaining of evaluation/prediction results (as discussed in Secs. 2, 3, and 4).

- Obtained simplified linearized error model to represent Honeywell's LASERNAV II, as exercised in a Kalman filter/covariance analysis to predict expected navigation accuracy attainable during ETB data collection missions;
- The conventions and error models that account for the behavior of the gyros and accelerometers were developed by others and have been independently cross-checked and streamlined for this ETB application;
- *Pruned model of INS in aircraft*: Several $\sim$ 19 to 25 state error models exist for airborne INS [13]. Our model was whittled down to 12 states. Numbers in the matrices were checked and cross-checked. Numbers came from gyro and accelerometer specs and accuracies of fix source;
- Proper scaling and units to use were established as input to the software in order to obtain the output answers in the units that we want (in Secs. 5.3.1 and 5.3.3);
- Found accuracy of VOR/DME fix source;
- Developed *original* model for accuracy of visual NAV update (in Secs. 4.2 and 5.3.5) from limited precedent in F-111D manual [57];

- Performed the computer runs that provided the quantitative evaluations pertinent to the ETB data collection missions using evaluation precedents for the F-111D (in Sec. 7.1) as a useful guide;
- Identified natural subsidiary studies (relating to suggested review of alternative conventions for strapdown INS mechanizations, as discussed at end of Section 8) to support decisions on how the LASERNAV II can best be used to level the cameras or other sensors to compensate for aircraft motion and recommended use of the method of [138];
- Listed current shortfalls and approximations in Section 8.1 that were used as a guide for improvement in introducing more model realism and software convenience and refinements (Section 8.2) in both this and in possible subsequent (second cut) evaluations (see Sec. 9.4).

9.2 Conclusions

Based on the airborne navigation error models and LASERNAV II parameters used in this study, the output of this investigation is useful:

- In designating NUMBER of and LOCATIONS for navigation WAYPOINTS as part of mission TRAJECTORY PLANNING in covering a 10 km $\times$ 10 km patch area via row-wise overflights (row width reflecting the sweepwidth of the sensor used);

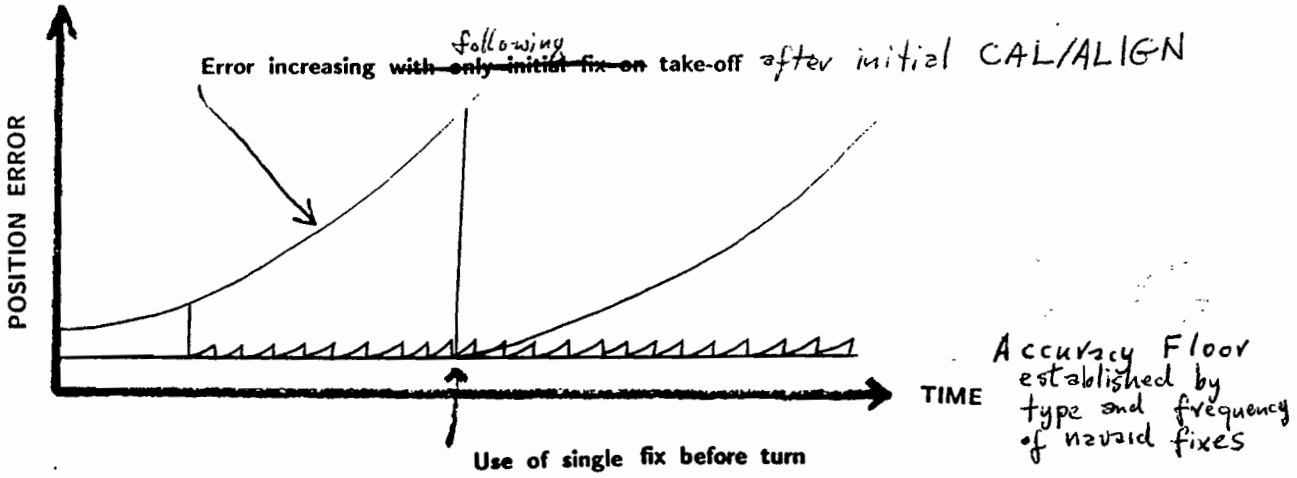

Effect of Gyro Drift-Rate on Accuracy Behaviour of INS

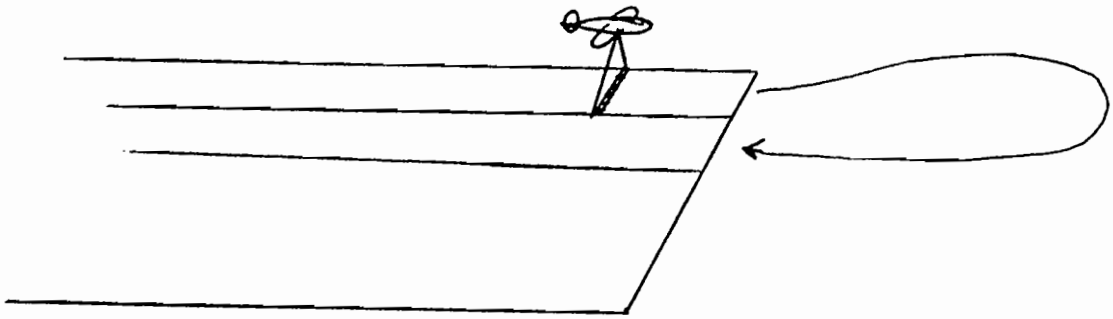

- **INS/Navaid fixes to support accuracy during coordinated turns at end of each pass to match-up measured strips and avoid unnecessary overlap or gaps**

Figure 48. Airborne Data Collection for Electronic Terrain Board (Data Base)

- Primary role of NAV is to allow DOVETAILING of sensor swath (avoid redundant data overlap with previous rows collected vs. avoid gaps between successive adjacent rows) during aircraft turn around;
- In specifying RATE of external radio position FIX TAKING to maintain sufficient navigation ACCURACY to enable tight row dovetailing (critical at end-of-row aircraft turns to initiate start of next row back-sweep) and in deciding the PREFERRED LOCATION of visual fix updates (surveyed retroreflectors).
- In considering future use of GPS both onboard the data collecting aircraft as a navaid adjunct (15 meter CEP, real-time accuracy of $\pm$ 30 meters), perhaps using the differential mode of GPS receiver operation for higher accuracies (in the $\pm$ 5 meter range for real-time use; in the tens-of-centimeters range in the post-processing mode), and for flexibility in quick convenient land-based use in preliminary terrestrial surveying and designating retroreflector placement locations within a patch. (For a

more complete perspective on the potential use of GPS for the ETB application, see Appendix, Section A.4.)

Tables 2 and 3 indicate that use of just position fixes from surveyed retroreflector locations provides as much accuracy as using simultaneous retroreflector and Loran-C VOR/DME position fixes together. The position accuracy availed by taking position fixes every 3 minutes [32] from surveyed retroreflectors is better than twice what is afforded every 15 minutes and three times better than that offered every 30 or 45 minutes. The drawback is that surveying the retroreflector locations for each candidate data collection site is a slow and expensive proposition. GPS land survey equipment could help in this regard. VOR/DME usage should still help in getting the aircraft on station via use of waypoints. The exacting navigation accuracy comparable to the 21 centimeter resolution of our down-looking GaAs line scanner, to date, is only available from differential GPS in the post-processing mode (as possible tags to the imaging data for later orientation).

Two conclusions become apparent from Table 3. It is apparent that, as compared to the use of exclusive VOR/DME position fixes as depicted in Section 7.2.1 (at the sample rates lower than every 3 minutes), (1) it is better to not use these relatively coarse fixes (coarse as compared to the inherent accuracy embodied within the LASERNAV II itself and only slowly degraded by the drift rates that are also inherent) since, except for using VOR/DME every 3 minutes, the use of VOR/DME fixes at the slower rate tends to hasten the corruption of navigation position accuracy. In all cases of using external position fixes (even when using the high accuracy GaAs line scanner position fixes from surveyed retroreflector locations), (2) the tilt errors are more degraded when position fixes are used than they would be without position fixes being used to improve the accuracy of position determination. Therefore, we are in a compromise situation were external position fixes are needed to improve the net navigation position accuracy yet use of these very position fixes aggrevates the psi-angle tilts and causes them to be larger than would otherwise be the case.

9.3 Impact on Data Collection Missions

In collecting ETB data at a nominal altitude of 500 ft from each designated 10 km $\times$ 10 km patch through overflights by the G-1 Gulfstream aircraft at 140 kts ($\sim$ 70 meters/sec), the GaAs laser line-scanner uses a wide Field-of-View (FOV)=$\pm$ 45°. The swath-width in performing data collection corresponding to the sensor sweep width of the GaAs laser line-scanner in wide FOV=$\pm$ 45° is 2(500 ft)(0.3048 meters/ft)(tan (45°)) = (1000)(0.3048)(1) = 304.8 meters. Under

[32]We also treated the case of position fixes every 45 seconds in our computer evaluations but refrained from including these further results in this report because of invoking reasonable constraints on avoiding an excessive NAV operator workload. The user manual for our LASERNAV II indicates that automatic VOR/DME fix insertion has been inhibited and that external position fix information can only be incorporated manually using the freeze frame mode.

TABLE 2

Maximum Steady-State 1-sigma Position Error for Airborne LASERNAV II

LASERNAV II INS with the following external navaids	Every 3 minutes	Every 15 minutes	Every 30 minutes	Every 45 minutes
Periodic fixes from VOR/DME	57 meters	88 meters (increasing)	94 meters (increasing)	108 meters (increasing)
Periodic fixes from Surveyed Retroreflector	11	21	29	36
Simultaneous Periodic fixes from both VOR/DME and Surveyed Retroreflector	11	21	29	36

[1]Results displayed here under common assumption that initial steady-state calibration/alignment of INS was performed prior to take-off.

[2]Accuracy Disclaimer: above numerical evaluations are only good $\pm$ 20 % by avoiding greater computational burden of using joint truth model and filter model.

[3]Airborne Differential GPS already demonstrated to provide 1 to 2 meter accuracy in real-time.

[4]Airborne Differential GPS already demonstrated to provide 5 to 12 centimeter accuracy in post-processing mode.

[5]Airborne GPS provides $\sim$ 30 meter accuracy (SEP=16 meters) in real-time (using military P-code, otherwise 100 meters with commercial C/A-code).

TABLE 3

Maximum 1-sigma Tilt Error for Airborne LASERNAV II, After 4 Hours

LASERNAV II INS with the following external navaids	Every 3 minutes	Every 15 minutes	Every 30 minutes	Every 45 minutes
Periodic fixes from VOR/DME	2.6 $\widehat{\text{min}}$ (0.76 milliradian)	5.4 $\widehat{\text{min}}$ (1.57)	5.2 $\widehat{\text{min}}$ (1.51)	6 $\widehat{\text{min}}$ (1.75)
Periodic fixes from Surveyed Retroreflector	2.4 (0.70)	4.8 (1.40)	4.8 (1.40)	5.4 (1.57)
Simultaneous Periodic fixes from both VOR/DME and Surveyed Retroreflector	2.4 (0.70)	4.8 (1.40)	4.8 (1.40)	5.4 (1.57)

[6]Results displayed here under common assumption that initial steady-state calibration/alignment of INS was performed prior to take-off.

[7]Accuracy Disclaimer: above numerical evaluations are only good $\pm$ 20 % by avoiding greater computational burden of using joint truth model and filter model.

[8]Compare results here to situation of no fixes being taken yielding maximum tilt error of 2.8 arcminutes.

[9]GPS phase-differences received over a 1 meter baseline have been used for attitude determination to 1-3 milliradians.

the optimistic assumption of having no between row gaps and no redundant row overlap but instead having perfect dovetailing of rows (as use of the LASERNAV II, with proper external navaid fixes is to facilitate) in performing ETB data collection, each 10 km $\times$ 10 km patch would be partitioned into $\frac{10\text{ km}}{304.8\text{ meters}} = 32.8 \approx 33$ row-wise strips of total path length (neglecting aircraft turns at the end-of-row) of (33)(10 km) = 330 km, which would take (neglecting aircraft turns again, which will be accounted for later) $\frac{330 \times 10^3\text{ meters}}{70\text{ meters/sec}} = 4714$ secs = 1.31 hrs to collect (plus an additional 33(3 minutes) = 99 minutes=1.65 hrs just for end-of-row turns, where $1\frac{1}{2}$ minute turns are possible but are shunned as not being desirable) for a total of 2.96 $=\sim$ 3 hrs to perform data collection for one 10 km $\times$ 10 km patch. A nominal aircraft mission is 4 hrs, thus allowing $\frac{1}{2}$ hr to arrive on-station and another $\frac{1}{2}$ hr for the return trip so that designated patches can be up to $\sim$ (140 kts)(0.5 hrs) = 70 nmi from the local hangar or airfield that the Gulfstream aircraft is to take-off from. This coarse analysis of course neglects the time for take-off and landing, acceleration/deceleration to cruise, possible departures in the nominal velocity, other minor delays and effects of winds that would require compensating actions that would detract from efficiency in data collection (as well as ignoring crew fatigue over such long missions).

Waypoints, to be used as an over all guide as the aircraft traverses the row swaths, can be entered into the LASERNAV II prior to take-off as a primary aspect of mission planning. The LASERNAV II can accommodate 255 waypoints. The constraints on LASERNAV II usage are that these 255 waypoints can be strung out over 20 flight plans, each individual flight plan containing from 2 to 20 waypoints. ETB data can be collected from the 10 km $\times$ 10 km patch by stringing together several consecutive flight plans in transit (as is allowable). Instead of having the last waypoint of one flight plan being in common with the first waypoint of the next flight plan, more efficient waypoint utilization is to switch flight plans "on the fly" after reaching the last waypoint of the former flight plan then activating the next flight plan that starts out with the next waypoint of interest (rather than the waypoint already reached in the last flight plan). In this way more unique waypoints can be strategically placed sequentially throughout the patch to serve as guiding way post markers.

A recommended way to use these waypoints within the ETB data collection mission is to pre-plan the detailed geographic location of the waypoints to occur five per a row swath, one at the beginning, one at the end, and three in the middle at the 2.5 km, 5 km, and 7.5 km points. These are inserted directly into the pre-prepared flight plan and the pilot aims at these while flying down the row. Different waypoints at appropriately corresponding locations are separately planned for each succeeding row, so that 4 rows (of $4 \times 5 = 20$ waypoints) are contained in a single flight plan. The pilot is to execute 3 minute turns in proceeding from the concluding waypoint of the previous (just completed) row to the initial starting waypoint of the next row to be done. Since $\frac{33}{4} = 8.2$, a total of 9 consecutive mission plans (8 with 20 waypoints each) are needed to completely cover a 10 km $\times$ 10 km patch (using a total of 165 waypoints). The remaining waypoints and mission plans may be used to assist the pilot in arriving at the patch to be measured and in returning to the airfield, as well as getting to distant airfields in the first place. While a greater density of waypoints per a row could be used, a likely density that comes to mind corresponds to using a waypoint every 1 km

(as 11 per a row swath), but this corresponds to having $11 \times 33 = 363$ waypoints and LASERNAV II only has 255 waypoints available for use. The above analysis is an optimistic scenario. An alternate approach (also preliminary since it is not yet tested) for maintaining fairly straight rows while collecting the data is offered in [132, Fig. 3] using an airborne GPS receiver and a laptop computer.

9.4 Future Plans and Recommended Refinements

Objectives for the Future (near term):

- In deciding whether or not REAL-TIME NAVIGATION DATA TAGS should also be INSERTED within imaging sensor recording TAPES (for auxiliary scene orientation in post-processing), still need to consider use of:
  - INS with differential GPS [33] (and constraint to have well-surveyed second set nearby with radio intercommunication);
  - INS with differential GPS (and constraint to use and be near one of the many planned (and existing) GPS-RAP ranges);
  - INS with differential GPS and corrections now to be disseminated over broader area via INMARSAT satellite links;
- Survey the more exacting software tools advertised to be available (from NAVSTAR SYSTEMS, from COMPUTING APPLICATIONS SOFTWARE TECHNOLOGY) for providing excruciating detail in predicting effect of satellite locations, effect of atmosphere, effect of motion of host platform, impact of available INS sensor suite, anticipated hierarchy of nest of Kalman filters used, etc. at test site geographic location on specified test date. (Cost of initial offering in 1990 was $35,000.00 (as compared to Optimization Software's more general version of Kalman filtering for $200.00, where user has to supply the model) but expect this price to come down when there are no takers. Rationale in pricing appears to be "how much would it cost for half a years effort to build one yourself?")
- Appealing to analogies in use of navigation info with airborne SAR. Considering utility of real-time compensation of camera tilts using INS info and what form this would take and what convention/mechanization would be most efficient.

Objectives for the Future (long term beyond just this supporting ETB navigation analysis role):

---

[33] GPS status, timetables, considerations and principles of operation are discussed in Section A.4 of Appendix

- Consider use of Kalman-filter-based alignment technology (normally used for in-air alignment of missiles to mothership) for boresite alignment of several participating sensors in sensor fusion suites, each to be equipped with its own cheap [34], low quality INS, and with various lever-arm corrections accounted for. Compensating effect of flexure of non-rigid members is difficult to handle (as is aircraft flutter) and other vibration effects but use of INS/Kalman Filter alignment techniques are expected to help;
- Pursue new variations on how to use a Kalman filter for image enhancement ([129], [130], [131]);
- Pursue some new inroads made that use a Kalman filter within the back propagation approach to neural network (NN) learning [84] for target detection and discrimination in these imaging applications [59], [60];
- Contribute further to the evolution of tracking approaches (angle-only and conventional) based on Extended Kalman filters (and related batch processing variations) using imaging sensors (as in [136]);
- Pursue ideas similar to those contained in Rob Ender's '89 MIT Ph.D. thesis [61], in its refinement by Bob Mentle in [93], and in IR target tracking approach trailblazed by AFIT/WPAFB for handling optics applications involving Poisson and other doubly stochastic point- or counting-processes representative of optical applications ([62]-[81], [88]).

[34]According to the Acting Manager of Advanced Systems Precision Products Division of Northrop in Norwood, MA, slave INS alignment to a master INS to within 40 arcsec can be achieved in 5 minutes (using a few S-turn maneuvers), otherwise a gyrocompassing mode using the earth's rotation to accomplish this alignment would take much longer. (For more detail about calibration/alignment procedures, see Section 6.2.)

APPENDIX A
NAVIGATION SENSOR SUBSYSTEMS

This section describes major features and operating modes of a collection of navigation sensors comprising likely candidate navigation data sources to be used to support flight accuracy in the creation of the terrain board data base. Three candidate navigation aid (navaid) reference subsystems are described first: Air Data System, and two alternative radio navigation candidate subsystems VOR/DME and TACAN [35]. GPS is also briefly described below as a radio navigation sensor candidate likely to eventually be selected to augment the first cut implementation in the proposed navigation sensor suite of the test aircraft to be used to support terrain board data collection. The principles of Relative Navigation or (RNAV) will also be reviewed since this is the principle normally used in developing an aircraft's flight plan or in establishing an aircraft's anticipated trajectory by using a sequence of pre-planned way-points as intermediate stepping stones on the way to the ultimate destination. Extending this approach to use pre-surveyed retroreflectors in a similar manner had been discussed. More detail on each of these systems can be found in [21], [22], [23], and [24].

Table A-1 offers a concise overview comparison of accuracies, capabilities, and limitations of the various systems mentioned above. Please notice that the INS characteristics depicted in this table are not specifically those of the HONEYWELL LASERNAV II Inertial Navigation System but those of a comparable airborne 0.1 nmi/hr system.

A.1 Air Data System/Baro-Altimeter

The Air Data System (ADS) typically provides the following outputs:

- Angle-of-attack,
- Indicated airspeed,
- True airspeed,
- Altitude,
- Altitude rate.

---

[35]Short descriptions and delineations of principles of operation (POP's) for Inertial Navigation Systems (INS) and ILS/MLS are offered in [43]. A recent easy to read update on ILS/MLS is available in [44]. The Loran and Omega radionavigation systems are described in recent Special Issues of *Navigation, Journal of the Institute of Navigation* devoted exclusively to each of these two systems. Detailed analytical error models of typical airborne navaids, as needed in the specification of Kalman navigation filters, are provided in [112].

TABLE A-1

Navigation System Accuracies Table (from Collins/RI marketing publication No. 074-3993-000/5M-BAR-2-90)

System	Position Accuracy (Meters)	Velocity Accuracy (M/Sec)	Time Accuracy (Seconds)	Range of Operation	Operation
Navstar GPS (P-Code)	16 M 3-Dimensions	0.1	.0000001 (100 nanoseconds)	Worldwide	Longitude, Latitude, Altitude 24-hour, all-weather
Transit Satellite	200 M	—	—	Worldwide	Longitude, Latitude, degraded performance in Polar areas
Loran	180 M	—	—	Regional, 10% of world	Longitude, Latitude
Omega	2,200 M	—	—	Nearly 90% Worldwide	Longitude, Latitude
Inertial Navigation Systems	1,500 M max after first hour	0.8 after 2 hours	—	Worldwide	24-hour, all-weather degraded performance in Polar areas
TACAN	400 M	—	—	Line of sight	3° Angular error
ILS/MLS	5-10 M	—	—	Line of sight	Only at properly-equipped airports

The ADS consists of aerodynamic sensors (such as a number of static ports and a Pitot tube), temperature probes, and a computer for performing the requisite intermediate calculations of free-stream outside-air temperature, and Mach number. For the altitude damping of the effective altitude channel of an INS, only the indicated altitude and possibly altitude-rate are used, and are denoted here as being from a baro-altimeter (a subset of the ADS).

A.2 VOR/DME

The VHF omni-range (VOR) system is the mainstay of civilian air navigation both within the U.S. (since 1946, currently with more than 1000 U.S. stations), and worldwide (since 1947). Using VOR, the bearing from the VOR station to the aircraft can be determined. This information can be used to set a course to the VOR station. Once the course has been established, the VOR indicator will show whether the aircraft is to the left or right of the selected course.

Two other forms of radio navigation aid are often placed at a VOR station location to be used in conjunction with a VOR transmission. These are distance measuring equipment (DME) and the military navigation system called TACAN (tactical air navigation). When a TACAN facility and a VOR facility are co-located, the combined facility is called a VORTAC station. A VORTAC station or a VOR/DME station can provide both bearing and distance data that can be used together to determine aircraft horizontal position. The VOR is relatively immune to degradations due to propagation and atmospheric effects because it operates at the VHF radio band; however,

its range is thereby limited (particularly at low altitudes) to the line-of-sight signal horizon. VOR signals also cannot be used in the "cone of confusion" directly above the station.

In determining range, the airborne interrogator radiates coded pulse pairs at a frequency within the band 978 to 1213 MHz from an omnidirectional antenna. A ground transponder (the beacon) within range of the aircraft and tuned to the interrogator's channel automatically triggers a beacon response after a 50 nanosec delay, on a frequency differing by 63 MHz from that of the original interrogator. After receiving the reply, the aircraft's DME performs the necessary processing to determine the round-trip travel time from which the range is easily deduced.

Once every 30 seconds, the DME beacon transmits its identity, which is detected by the pilot as a Morse code burst of three letters in an audio tone of 1350 Hz. (Unlike the random time intervals that exist between the pulse pairs of beacon replies to interrogations, the time intervals between identification pulse pairs is always 1/1350 seconds.) A technique for aircraft to automatically select appropriate VOR/DME stations enroute is offered in [33].

A.3 TACAN

TACAN (tactical air navigation) is a military system which gives both range and bearing with respect to a fixed beacon. The ranging portion of TACAN has the same characteristics as civil DME, described above. However, there are more channels available to TACAN, which utilizes an extended frequency range from 962 to 1213 MHz. TACAN/VOR/DME outputs are as follows:

- Digital: 32-bit serial BCD word at least five times per second; resolution is 0.01 nautical mile;
- Range Rate Pulse: transmitted for each 0.01 nautical mile change in range;
- Range Output Accuracy: From $\pm$ 0.1 to $\pm$ 0.3 nautical miles, depending on signal strength and time since acquisition.

A.4 Global Positioning System

The Global Positioning System (GPS) is a satellite-based multilateration system that generates signals capable of providing extremely accurate 16 meter spherical error probable (SEP) three dimensional position and 0.1 m/sec velocity navigation data for suitably equipped users. The fundamental computation frame for GPS is an earth-centered earth fixed (ECEF) frame, although the derived navigation data are usually transformed to WGS-72 or WGS-84 Local Level coordinates for the end user.

The baseline GPS satellite constellation is to consist of 21 satellites (and three active spares) in six orbital planes. The satellites transmit two (three) spread spectrum signals at 1227 and 1575 MHz (L-band) (and a third slightly higher NDET frequency) to allow corrections for ionospheric delays to be implemented. The signal modulation includes both P (Precision) and C/A (clear/acquisition) pseudo-random sequences at 10.23 Mbps and 1.023 Mbps, respectively. The signals are further data

modulated with a 50 bps message frame. The data consists of clock correction, satellite ephemeris and health, message, and satellite almanac data. A considerable measure of jamming immunity is provided through use of a Gold code for GPS signals. The satellite navigation data are based on data uploaded to the satellite from a ground based segment (Ground Segment/Monitoring Stations) charged with precision tracking of the constellation (and providing periodic corrections of satellite ephemeris as conveyed via S-band uplink transmissions).

Fundamental to the operation of GPS navigation is the requirement for the user to estimate and track "GPS system time". A GPS user with an estimate of system time can then compute pseudo-range to each given satellite. Three components of range in the ECEF coordinate system plus the user clock drift (user/GPS) are the fundamental parameters of the navigation solution that can be subsequently determined. The satellite clock drifts are estimated by the ground segment; the signal propagation delays are estimated and corrected by the user via the differences in pseudo-ranges at the two different GPS frequencies [92].

To achieve a continuous ideal GPS navigation solution requires that at least four visible satellites be present, thus allowing determination of the four unknowns of "three position coordinates and time" in the equations. If more than four satellites are visible at one time, an optimal set of four satellites can be selected to provide the best navigation performance in terms of the smallest geometric dilution of precision (GDOP) incurred. If fewer than 4 satellites are available, any available onboard navaids can be used to supplement the GPS derived solution. Algorithms to select the optimal satellites for use in determining the GPS navigation solution are based on the almanac data transmitted by the satellites (concerning its own ephemeris as it was informed of by the Monitoring Stations) plus the user's present geodetic position. The launch schedule/time-table for GPS satellite orbit insertion (roughly one new launch every 60 days) and associated GPS set capabilities are depicted in Fig. A-1. As of December 1990, there are 10 Block II satellites in orbit and 6 of the Block I's for a total of 16 operational GPS satellites. There is to first be a 24 hour 2-D GPS capability for all of North America, as achieved in December 1990.

The differential mode of GPS has the capability of providing more exacting accuracies in the vicinity of 5 to 12 cm for airborne applications [40] (in post-processing only) [36]. In differential GPS usage, there are two GPS receivers in reasonable proximity (but one of these being ground-based at a fixed surveyed location) using the exact same satellites and experiencing the same atmospheric degradations, which are then successfully compensated for via the differential mode of operation where the two GPS receivers work in concert. Commencing on 25 March 1990, the normal benign GPS signals were intentionally corrupted under a DOD program entitled "Selective Availability" (SA) (previously entitled "Denial of Accuracy," a term that was more inflammatory) so that civilian

[36]This approach is also being pursued (in 1990) by Army Cold Region Research Laboratory in Hanover, NH, and is being considered (in 1990) for use in follow-on versions of Motorola's existing *Golden Eagle* receivers (using these techniques of double- and triple-differencing).

GPS BLOCK II LAUNCH SCHEDULE

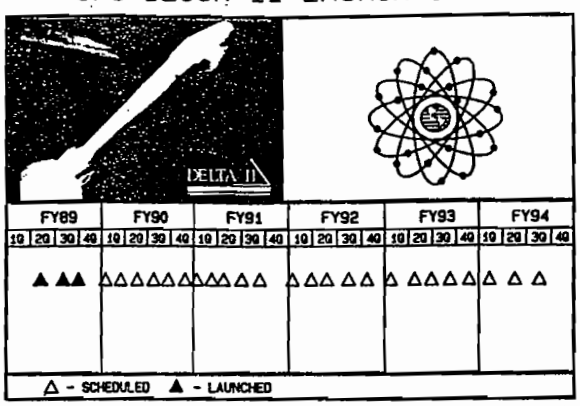

AS OF: 15 SEP 89

CONSTELLATION SIZE/ACCURACY/COVERAGE

- 12 SPACECRAFT EVENLY SPACED IN 6 PLANES
  - 10 m WORLDWIDE CEP
  - LARGE AREAS OF REDUCED 2D ACCURACY
- 18 SPACECRAFT EVENLY SPACED IN 6 PLANES
  - FULL 2D COVERAGE WITH NO AREAS OF REDUCED ACCURACY
  - 15 m WORLDWIDE SEP
  - LARGE AREAS OF REDUCED 3D ACCURACY
- 21 SPACECRAFT OPTIMALLY PLACED IN 6 PLANES
  - 15 m WORLDWIDE SEP WITH SMALL AREAS OF REDUCED ACCURACY
- 24 SPACECRAFT EVENLY OR OPTIMALLY PLACED IN 6 PLANES
  - FULL 3D COVERAGE WITH NO AREAS OF REDUCED ACCURACY

CONSTELLATION BUILDUP DESIGNED TO OPTIMIZE WORLDWIDE COVERAGE

THE GPS FIRST LAUNCH CHALLENGE

- NEW SATELLITE (BLOCK II)
- NEW BOOSTER (DELTA II)
- NEW FACILITY (CSOC/MCC-1)
- NEW LAUNCH ORGANIZATION (1SCS)
- NEW COMMAND AND CONTROL SYSTEM (DSM)

Figure A-1. GPS Satellite Insertion Schedule and Consequential GPS User Receiver Set Capabilities

users would only have 200 meter accuracy [37] instead of 25 to 30 meters. However, approved military users and their support programs still have no problem since they are supplied with the key and, moreover, differential GPS use almost completely cancels the deleterious effect of SA [41]. The Range Application Program (RAP) will avail airborne military users and their support with pod mounted differential GPS receivers (loosely integrated with a low quality conventional INS), gratis, but with 65 lbs. of useless ballast (100 lbs total) just to maintain the same center-of-gravity as an identical pod containing its usual armaments. The RAP also provides the existing (and planned) surveyed sites outfitted with a second GPS receiver in conjunction with a transmitter for broadcasting differential corrections; however, user must be within about 30 km (while research by others is underway to increase this to 100 miles) for these to be useful in the presence of SA. Alternatively, work is also underway by others (for the Coast Guard) to extend the range for possible use of differential GPS mode by disseminating necessary GPS corrections over broader area via INMARSAT satellite links. Civil aviation use of GPS is currently being pursued [92, Figs. 11, 14], [90, Fig. 5-6, p. 238]. GPS satellite failure or premature obsolescence should not be an issue, as demonstrated in [94] within a detailed reliability analysis using measured failure rates actually exhibited *in situ* rather than those merely theoretically projected. Use of GPS in conjunction with Microwave Landing System (MLS) in a joint receiver for FAA Category 3 (exclusively instrument) landing systems for aircraft is currently underway. Miniature Airborne GPS Receiver program recently awarded (January 1991) is to produce 2,400 receivers each being 11 lbs. and being $3 \times 7 \times 12$ in. in size. As a final clarification, prior to 1990, GPS users had to contend with merely a 4 hr window of satellite availability sufficient for navigation (often in the middle of the night). However, by the beginning of 1991, due to a string of 10 successful Delta rocket launches to insert GPS satellites, 15 hrs of 3-D coverage is now available on a daily basis thus enhancing the practical utility of current GPS. The 3-D GPS availability will continue to improve and grow to the goal of 24 hrs as the remainder of the GPS satellites are inserted.

A.5 Area Navigation

The Area Navigation (RNAV) function provides the pilot with the capability to navigate (guide the vehicle) relative to a selectable sequence of way-points. This function comprises a standard capability currently available on any properly instrumented commercial or military aircraft. The necessary instrumentation consists of any sufficiently accurate source of horizontal position

---

[37] GPS has received an accelerated boost or development push due to Iraq hostilities since it is hard to navigate from landmarks in the featureless desert. Because of the shifting sands, TERCOM-like systems are way off or useless as well as Doppler radar. The U.S. government is buying up all available GPS receivers with certified accuracy (both military and commercial) and has actually officially dispensed with SA for awhile in order to squeeze out the tighter preferred accuracy from commercial GPS sets.

data (e.g., TACAN, VOR/DME, INS with periodic position updates, GPS, etc.), plus an RNAV processor.

Any RNAV system used for IFR (instrument flight rules) operation in the National Air Space must meet operational and airworthiness requirements established by the FAA. Required cross-track and along-track accuracy values for RNAV avionics must be within the following 95% confidence limits:

Phase	Cross-Track	Along-Track
Enroute	1.5 nmi	1.5 nmi
Terminal	1.1	1.1
Approach	0.3	0.3

The anticipated accuracy of navigation system falls well within these limits when GPS is available. TACAN and VOR/DME generally provide adequate accuracy as well.

The Area Navigation function performs the following processing. It accepts a sequence of way-point locations as input by the pilot. These can be input either as longitude-latitude coordinates, or as range-bearing coordinates relative to a specified TACAN or VOR/DME station. In the latter case, the input data are used to compute the longitude-latitude coordinates.

Thereafter, the RNAV function computes way-point related data for display to the pilot to aid in guiding the vehicle. The computed data include bearing and range to way-point, heading deviation left or right of way-point bearing, and time-to-arrival at way-point based on current velocity. The RNAV function automatically cycles to the next way-point whenever the vehicle arrives within a specified minimum distance of the current way-point. (Other conditions may also apply to way-point cycling to handle off-nominal cases.)

For an INS aided set, the line-of-sight velocity can be computed from a combination of filter estimated velocity and INS delta-V's (ΔV's or changes in velocity) as projected along the line-of-sight. The INS delta-V's provide current information on the vehicle dynamics to improve extrapolation between filter estimates.

For an unaided set, only the filter estimates can be used for velocity projection along the line-of-sight. The resultant aiding information is of lower quality, due to filter processing delays and errors in estimating acceleration. These aiding techniques have been successfully used for the Phase I and II GPS sets.

The GPS receiver acquisition process is that of finding and locking onto the signals in both frequency and position. Typically, pre-positioning data consisting of the expected frequency bin and code position is computed and provided to the receiver for initiating the signal search.

Given the best estimate of GPS time, user position and velocity, plus satellite ephemeris data (possibly almanac data), the expected doppler shift and line-of-sight distance can be computed. This data is then translated to frequency bin and code positioning data. The uncertainties in these quantities directly affect the time to first fix, because multiple frequency bins and longer code intervals may need to be searched.

REFERENCES

1. Richman, J., and Friedland, B., "Design of Optimum Mixer-Filter for Aircraft Navigation Systems," *Proceedings of the National Aerospace Electronics Conference-NAECON*, Dayton, OH, pp. 429-438, 15-17 May 1967.

2. Nash, R. A., D'Appolito, J. A., and Roy, K. J., "Error Analysis of Hybrid Inertial Navigation Systems," *Proceedings of AIAA Guidance and Control Conference*, Paper No. 72-848, Stanford, CA, August 1972.

3. Maybeck, P. S., *Stochastic Models, Estimation, and Control,* Vol. 1, Academic Press, N.Y., 1979.

4. Widnall, W. S., and Grundy, P. A., *Inertial Navigation System Error Models,* Intermetrics Technical Report TR-03-73, 11 May 1973.

5. Sinha, P. K., *Integrated GPS/Inertial Simulator Computer Program,* Intermetrics Technical Report IR-236/253, 26 August 1977.

6. Haque, I., *Army GPS/132 Navigation Integration: A Covariance Analysis Study-Volume I,* Intermetrics Technical Report IR-MA-214-2, 14 October 1983.

7. Farrell, J. L., *Integrated Aircraft Navigation,* Academic Press, N.Y., 1976.

8. Britting, K. R., *Inertial Navigation System Analysis,* Wiley-Interscience, N.Y., 1971.

9. Pitman, G. R., (Ed.) *Inertial Guidance,* John Wiley and Sons, N.Y., 1962.

10. Mamon, G., Youmans, D. G., et al, "Pulsed GaAs Laser Terrain Profiler," *Applied Optics (USA)*, Vol. 17, No. 6, pp. 868-877, 15 March 1978.

11. Brown, R. H., Chapman, W. H., et al, "Inertial Instrument System for Aerial Surveying," *U.S. Geological Survey Professional Paper*, Vol. 1390, 103 pages, 1987.

12. Chapman, W. H., Cyran, E. T., et al, "Airborne Precision Mapping System-The New Generation," *Proceedings of the Symposium on Gyro Technology*, pp. 6.0-9.18, Stuttgart, FRG, 1988.

13. Kerr, T. H., "Decentralized Filtering and Redundancy Management for Multisensor Navigation," *IEEE Transactions on Aerospace and Electronic Systems,* Vol. AES-23, No. 1, pp. 83-119, January 1987.

14. Britting, K. R., and Smith, M. A., "Effect of Gyro Drift in an Inertial Navigation System in which the Stable Member is Assumed to be Inertially Nonrotating," MIT Instrumentation Laboratory (now C. S. Draper Laboratory) Technical Report No. E-1661, Cambridge, MA, July 1964.

REFERENCES
(Continued)

15. Kerr, T. H., "Idempotent Matrices to Validate Linear Systems Software," *IEEE Transactions on Aerospace and Electronic Systems*, Vol. AES-26, No. 6, pp. 935-952, 1990.

16. Koopman, B. O., *Search and Screening: General Principles with Historical Applications,* Pergamon Press, N.Y., 1979.

17. Washburn, A. R., *Search and Detection,* Military Applications Section, Operations Research Society of America, Arlington, VA, 1981.

18. Aasnaes, H. B., and Kailath, T., "Initial-Condition Robustness of Linear Least Squares Filtering Algorithms," *IEEE Transactions on Automatic Control*, Vol. AC-19, No. 4, pp. 393-397, August 1974.

19. Bar-Itzhack, I. Y., and Berman, N., "Control Theoretic Approach to Inertial Navigation Systems," *AIAA Journal of Guidance, Control, and Dynamics*, Vol. 11, No. 3, pp. 237-245, May-June 1988.

20. Bar-Itzhack, I. Y., and Goshen-Meskin, D., "Observability Studies of Inertial Navigation Systems," *Proceedings of AIAA Journal of Guidance, Navigation, and Control Conference*, Part 2, pp. 1283-1289, Boston, MA, 14-16 August 1989.

21. Spitzer, C. R., *Digital Avionics Systems,* Prentice-Hall, Englewood Cliffs, NJ, 1987.

22. Bose, K. W., *Aviation Electronics,* 4^{th} Edition, Howard W. Sams and Co., Inc., Indianapolis, IN, 1981.

23. Kayton, M., and Fried, W. R., *Avionics Navigation Systems,* John Wiley and Sons, Inc., N.Y., 1969.

24. Helfrick, A., *Modern Aviation Electronics,* Prentice-Hall, Englewood Cliffs, NJ, 1984.

25. Linkwitz, K., and Hangleiter, U. (Eds.), *High Precision Navigation: Integration of Navigational and Geodetic Methods,* Springer-Verlag, N.Y., 1988.

26. Bowditch, N., *American Practical Navigator,* Vol. II, Defense Mapping Agency Hydrographic/Topological Center, 1981 edition.

27. Keel, G., et al, "A Test of Airborne Kinematic GPS Positioning for Aerial Photography," *Photogrammetric Engineering and Remote Sensing,* Vol. LV, No. 12, pp. 1727-1730, December 1989.

28. *Navigation Management System INSTALLATION MANUAL,* Honeywell Inc. Publication No. 95-8211B, Revision 3, 15 January 1985 (Revised 1 April 1989).

REFERENCES
(Continued)

29. Friedland, B., "Analysis of Strapdown Navigation Using Quaternions," *IEEE Transactions on Aerospace and Electronic Systems,* Vol. AES-14, No. 5, pp. 764-768, September 1978.

30. Giardina, C. R., Heckathorn, J., and Krasnjanski, D., "A Comparative Study of Strapdown Algorithms," *Navigation: Journal of the Institute of Navigation,* Vol. 28, No. 2, pp. 101-106, Summer 1981.

31. Hyslop, G. L., "A Norm and Orthogonality Preserving Algorithm," *IEEE Transactions on Aerospace and Electronic Systems,* Vol. AES-23, No. 6, pp. 731-737, November 1987.

32. Miller, K. S., *Some Eclectic Matrix Theory,* Robert E. Krieger Publishing Company, Malabar, FL, 1987.

33. Ruhnow, W. B., and Goemaat, M. L., "VOR/DME Automated Station Selection Algorithms," *Navigation: Journal of the Institute of Navigation,* Vol. 29, No. 4, pp. 289-299, Winter 1983.

34. Center, J. L., "Navigation Task Partitioning in Distributed-Processing Avionics Systems," *Navigation: Journal of the Institute of Navigation,* Vol. 28, No. 2, pp. 93-100, Summer 1982.

35. Hopkins, J. J., "Integrated Satellite Navigation and Strapdown Attitude and Heading References for Civil Air Carriers," *Navigation: Journal of the Institute of Navigation,* Vol. 28, No. 3, pp. 189-198, Fall 1981.

36. Bachman, K. L., "Ring Laser Gyro Navigator Flight Test Results," *Navigation: Journal of the Institute of Navigation,* Vol. 28, No. 3, pp. 214-223, Fall 1981.

37. Majure, R. G., "Demonstration of a Ring Laser Gyro System for Pointing and Stabilization Applications," *Proceedings of IEEE Position, Location, and Navigation Symposium (PLANS),* pp. 219-225, Las Vegas, NV, 20-23 March 1990.

38. Lynch, M. F., and Weber, D. J., "Flight Test Results of a Tightly Integrated RLG-based Global Positioning System/Inertial Navigation System," *Proceedings of Position, Location, and Navigation Symposium (PLANS),* pp. 421-428, Las Vegas, NV, 20-23 March 1990.

39. Farrell, J. L., "Strapdown Inertial Navigation System Requirements Imposed by Synthetic Aperture Radar," *Control and Dynamic Systems: Advances in the Theory and Applications,* C. T. Leondes (Ed.), Vol. 33: Advances in Aerospace System Dynamics and Control Systems, Part 3 of 3, Academic Press, N.Y., 1990.

REFERENCES
(Continued)

40. Krabill, W. B., Martin, C. F., Swift, R. N., "Applying Kinematic GPS to Airborne Laser Remote Sensing," *Proceedings of ION GPS-89: The Second International Technical Meeting of the Satellite Division of The Institute of Navigation,* Colorado Springs, CO, pp. 39-43, 27-29 September 1989.

41. Kremer, G. T., Kalafus, R. M., and Loomis, P. V. W., and Reynolds, J. C., "The Effect of Selective Availability on Differential GPS Corrections," *Navigation: Journal of the Institute of Navigation,* Vol. 37, No. 1, pp. 39-52, Spring 1990.

42. Kerr, T. H., "Update of Discussions with Honeywell on our Questions about LASERNAV II Characteristics, as Published in the Installation Manual," MIT Lincoln Laboratory Group 53 Memo (to P. J. Kolodzy), 11 April 1990.

43. Kerr, T. H., "Position Accuracy Considerations to support Test Aircraft IR Measurements for a Realistic IR Data Base (that can Later be Exercised in Numerous Ways)," MIT Lincoln Laboratory Group 53 Memo No. 53.89-5 (to R. J. Hull), 20 November 1989.

44. *IEEE Aerospace and Electronic SYSTEMS Magazine,* Vol. 5, No. 5, May 1990.

45. Kistosturian, H. G., "On-Orbit Calibration of Satellite Antenna-Pointing Errors," *IEEE Transactions on Aerospace and Electronic Systems,* Vol. AES-26, No. 1, pp. 88-112, January 1990.

46. Ignagni, M. B., "Optimal Strapdown Integration Algorithms," *AIAA Journal of Guidance, Control, and Dynamics*, Vol. 13, No. 2, pp. 363-369, March-April 1990.

47. Ignagni, M. B., "Errata for 'Optimal Strapdown Integration Algorithms'," *AIAA Journal of Guidance, Control, and Dynamics*, Vol. 13, No. 2, p. 576, May-June 1990.

48. Fisk, J. W., Rue, A. K., "Confidence Limits for the Pointing Error of Gimbaled Sensors," *IEEE Transactions on Aerospace and Electronic Systems,* Vol. AES-2, No. 6, pp. 648-654, November 1966.

49. Bar-Itzhack, I. Y., Idan, M., "Recursive Attitude Determination from Vector Observations: Euler Angle Estimation," *AIAA Journal of Guidance, Control, and Dynamics*, Vol. 10, No. 2, pp. 152-157, March-April 1987.

50. Lee, J. G., Yoon, Y. J., and Mark, J. G., Tazartes, "Extension of Strapdown Attitude Algorithms for High-Frequency Base Motion," *AIAA Journal of Guidance, Control, and Dynamics*, Vol. 13, No. 4, pp. 738-743, July-August 1990.

REFERENCES
(Continued)

51. "IEEE Standard Specification Format Guide and Test Procedure for Single-Axis Laser Gyros," *IEEE Std 647-1981*, Published by the Institute of Electrical and Electronics Engineers, N.Y., 14 December 1981 (Currently being updated by the Gyro and Accelerometer Panel of the IEEE Aerospace and Electronic Systems Society, a group having voluntary monthly meetings and incorporating new approaches and characterizations such as use of Allan Variance measurement calculations to further characterize essential RLG performance).

52. "IEEE Standard Specification Format Guide and Test Procedure for Nongyroscopic Inertial Angular Sensors: Jerk, Acceleration, Velocity, and Displacement" *IEEE Std 671-1985*, Published by the Institute of Electrical an Electronics Engineers, N.Y., 9 September 1985.

53. Krabill, W. B., Martin, C. F., "Aircraft Positioning Using Global Positioning System Carrier Phase Data," *Navigation: Journal of the Institute of Navigation,* Vol. 34, No. 1, pp. 1-21, Spring 1987.

54. Lapine, L. A., "Practical Photogrammetric Control by Kinematic GPS," *GPS World,* Vol. 1, No. 3, pp. 44-49, May/June 1990.

55. Quist, T. M., (Ed.) "Aircraft Multisensor System Progress and Plans," Progress Report SW-1, Lincoln Laboratory of Massachusetts Institute of Technology, Lexington, MA, 26 May 1989.

56. Novak, L. M., Burl, M. C., "Optimal Speckle Reduction in Polarimetric SAR Imagery," *IEEE Transactions on Aerospace and Electronic Systems,* Vol. AES-26, No. 2, pp. 293-305, March 1990.

57. "System Theory Manual Fire Power Control System for USAF Series F-111D Aircraft," AF Serial No. 68-085 thru 68-180, T. O. 1F-111D-2-5-1-1, General Dynamics Fort Worth Division, 20 June 1975 (CHANGE 15, 17 October 1987).

58. Brogan, D., (Ed.), *Visual Search (Proceedings of the First International Conference on Visual Search),* Taylor & Francis, N.Y., 1988.

59. Rogers, S. K., Ruck, D. W., Kabrisky, M., and Tarr, G. L., "AFIT Neural Network Research," *IEEE AES Magazine,* Vol. 13, No. 9, pp. 17-19, Sept. 1990.

60. Dreyfus, S. E., "Artificial Neural Networks, Back Propagation and the Kelley-Bryson Gradient Procedure," *AIAA Journal of Guidance, Control, and Dynamics,* Vol. 13, No. 5, pp. 926-928, October 1990.

REFERENCES
(Continued)

61. Enders, R. H., "Laser Radar Tracking Theory: Track-While-Image Operation," Ph.D. Thesis in Department of Electrical Engineering and Computer Science, MIT, February 1989.

62. Snyder, D. L., and Fishman, P. M., "How to Track a Swarm of Fireflies by Observing Their Flashes," *IEEE Transactions on Information Theory*, Vol. IT-21, No. 6, pp. 692-695, November 1975.

63. Tobin, D. M., and Maybeck, P. S., "Enhancements to a Multiple Model Adaptive Estimator/Image-Tracker," *IEEE Transactions on Aerospace and Electronic Systems*, Vol. AES-24, No. 4, pp. 417-426, July 1988.

64. Johnson, B. A., and Maybeck, P. S., "Stochastic Adaptive Tracker Based on Noise-Corrupted Space-Time Measurement Process," *Proceedings of the IEEE 1988 National Aerospace and Electronics Conference (NAECON)*, Vol. 1, pp. 352-359, Dayton, OH, 23-27 May 1988.

65. Tobin, D. M., and Maybeck, P. S., "Substantial Enhancements to a Multiple Model Adaptive Estimator from Target Image Tracking," *Proceedings of the* 26^{th} *IEEE Conference on Decision and Control*, Vol. 3, pp. 2002-2011, Los Angeles, CA, 9-11 December 1987.

66. Maybeck, P. S., and Hentz, K. P., "Investigation of Moving-Bank Multiple Model Adaptive Algorithms," *AIAA Journal of Guidance, Control, and Dynamics*, Vol. 10, No. 1, pp. 90-96, January-February 1987.

67. Maybeck, P. S., and Hentz, K. P., "Investigation of Moving-Bank Multiple Model Adaptive Algorithms," *Proceedings of the* 24^{th} *IEEE Conference on Decision and Control*, Vol. 3, pp. 1874-1081, Fort Lauderdale, FL, 11-13 December 1985.

68. Maybeck, P. S., and Suizu, R. I., "Adaptive Field of View Expansion via Multiple Model Filtering for Tracking Dynamic Target Images," *Proceedings of the IEEE 1985 National Aerospace and Electronics Conference (NAECON)*, Vol. 1, pp. 364-373, Dayton, OH, 20-24 May 1985.

69. Maybeck, P. S., and Suizu, R. I., "Adaptive Tracker Field-Of-View Variation Via Multiple Model Filtering," *IEEE Transactions on Aerospace and Electronic Systems*, Vol. AES-21, No. 4, pp. 529-539, July 1985.

70. Meer, D. E., and Maybeck, P. S., "Multiple Model Adaptive Estimation for Space-Time Point Process Observations," *Proceedings of the* 23^{rd} *IEEE Conference on Decision and Control*, Vol. 2, pp. 811-818, Las Vegas, NV, 12-14 December 1984.

REFERENCES
(Continued)

71. Maybeck, P. S., and Zicker, W. L., "MMAE-Based Control with Space-Time Point Process Observations," *IEEE Transactions on Aerospace and Electronic Systems*, Vol. AES-21, No. 3, pp. 292-300, May 1985.

72. Roemer, W. A., and Maybeck, P. S., "An Optically Implemented Multiple-Stage Kalman Filter Algorithm," *Proceedings of SPIE International Society of Optical Engineering: Real Time Signal Processing VI*, Vol. 431, pp. 221-228, San Diego, CA, 23-25 August 1983.

73. Maybeck, P. S., and Rogers, S. K., "Adaptive Tracking of Multiple Hot-Spot IR Images," *IEEE Transactions on Automatic Control*, Vol. AC-28, No. 10, pp. 937-943, October 1983.

74. Kendrick J. D., Maybeck, P. S., and Reid, J. G., "Estimation of Aircraft Target Motion Using Orientation Measurements," *IEEE Transactions on Aerospace and Electronic Systems*, Vol. AES-17, No. 2, pp. 254-260, March 1981.

75. Maybeck, P. S., Jensen, R. L., and Harnly, D. A., "An Adaptive Extended Kalman Filter for Target Image Tracking," *IEEE Transactions on Aerospace and Electronic Systems*, Vol. AES-17, No. 2, pp. 173-180, March 1981.

76. Maybeck, P. S., Jensen, R. L., and Harnly, D. A., "An Adaptive Distributed-Measurement Extended Kalman Filter Tracker," *Proceedings of the* 19^{th} *IEEE Conference on Decision and Control Including the Symposium on Adaptive Processes*, pp. 554-559, Albuquerque, NM, 10-12 December 1980.

77. Maybeck, P. S., Harnly, D. A., and Jensen, R. L., "Robustness of a New Infrared Target Tracker," *Proceedings of the IEEE 1980 National Aerospace and Electronics Conference (NAECON)*, pp. 639-644, Dayton, OH, 20-22 May 1980.

78. Maybeck, P. S., and Mercier, D. E., "A Target Tracker Using Spatially Distributed Infrared Measurements," *IEEE Transactions on Automatic Control*, Vol. AC-25, No. 2, pp. 222-225, April 1980.

79. Maybeck, P. S., and Mercier, D. E., "A Target Tracker Using Spatially Distributed Infrared Measurements," *Proceedings of the* 18^{th} *IEEE Conference on Decision and Control including the Symposium on Adaptive Processes*, pp. 285-289, Fort Lauderdale, FL, 12-14 December 1979.

80. Maybeck, P. S., and Mercier, D. E., "An Extended Kalman Filter for Use in a Shared Aperture Medium Range Tracker, *Proceedings of the IEEE 1979 National Aerospace and Electronics Conference (NAECON)*, p. 1040, Dayton, OH, 15-17 May 1979.

REFERENCES
(Continued)

81. Kendrick, J. D., Maybeck, P. S., and Reid, J. G., "Estimation of Aircraft Target Motion Using Pattern Recognition Orientation Measurements," *Proceedings of the 1978 IEEE Conference on Decision and Control Including the* 17^{th} *Symposium on Adaptive Processes*, pp. 953-959, San Diego, CA, 10-12 January 1979.

82. Kerr, T. H., "Rationale for Monte-Carlo Simulator Design to Support Multichannel Spectral Estimation and/or Kalman Filter Performance Testing and Software Validation/Verification Using Closed-Form Test Cases," MIT Lincoln Laboratory Report No. PA-512, Lexington, MA, 22 December 1989.

83. Kerr, T. H., "An Invalid Norm Appearing in Control and Estimation," *IEEE Transactions on Automatic Control*, Vol. AC-23, No. 1, pp. 73-74, February 1978 (Correction on pp. 1117-1118, December 1978).

84. Simpson, P. K., *Artificial Neural Networks:* Foundations, Paradigms, Applications, and Implementations, Pergamon Press, N.Y., 1990.

85. *Kalman Filtering Software: User's Guide*, Optimization Software, Inc. Publications Division, N.Y., 1984.

86. Arshal, G., "Error Equations of Inertial Navigation," *AIAA Journal of Guidance, Control, and Dynamics*, Vol. 10, No. 4, pp. 351-358, July-August 1987.

87. Kerr, T. H., "Computational Techniques for the Matrix Pseudoinverse in Minimum Variance Reduced-Order Filtering," in *Control and Dynamic Systems: advances in theory and Applications*, C. T. Leondes (Ed.), Vol. 28: Advances in Algorithms and Computational Techniques in Dynamic Systems Control, Part 1 of 3, Academic Press, N.Y., pp. 57-107, 1988.

88. Kliemann, W. H., Koch, G., and Marchetti, F., "On the Unnormalized Solution of the Filtering Problem with Counting Process Observations," *IEEE Transactions on Information Theory*, Vol. IT-36, No. 6, pp. 1415-1425, November 1990.

89. Bobick, J. C., and Bryson, A. E., "Updating Inertial Navigation Systems with VOR/DME Information," in *NAVIGATION: Land, Sea, Air, & Space*, M. Kayton (Ed.), IEEE Press, N.Y., pp. 250-2357, 1990.

90. Kayton, M., "Introduction to Aircraft Navigation," in *NAVIGATION: Land, Sea, Air, & Space*, M. Kayton (Ed.), IEEE Press, N.Y., pp. 229-244, 1990.

91. Welfald, K. M., and McClary, C. R., "Autocalibration of a Laser Strapdown Inertial Reference/Navigation System," in *NAVIGATION: Land, Sea, Air, & Space*, M. Kayton (Ed.), IEEE Press, N.Y., pp. 258-266, 1990.

REFERENCES
(Continued)

92. Teasley, S. P., Hoover, W. M., and Johnson, C. R., "Differential GPS Navigation," in *NAVIGATION: Land, Sea, Air, & Space*, M. Kayton (Ed.), IEEE Press, N.Y., pp. 131-138, 1990.

93. Mentle, R. E., "Laser Radar Performance Theory: Track-While-Image Operation," M.S. and E.E. Thesis in Department of Electrical Engineering and Computer Science, MIT, June 1990.

94. Durand, J.-M., and Caseau, A., "GPS Availability, Part II: Evaluation of State Probabilities for 21 Satellites and 24 Satellite Constellations," *Navigation: Journal of the Institute of Navigation*, Vol. 37, No. 3, pp. 285-297, Fall 1990.

95. Hutchinson, C. E., and Nash, R. A., Jr., "Comparison of Error Propagation in Local-Level and Space-Stable Inertial Systems," *IEEE Transactions on Aerospace and Electronic Systems*, Vol. AES-7, No. 6, pp. 1138-1142, November 1971.

96. Pinson, J. C., "Inertial Guidance for Cruise Vehicles," in *Guidance and Control of Aerospace Vehicles*, C. T. Leondes (Ed.), Chapter 4, McGraw-Hill, N.Y., 1963.

97. Widnall, W. S., and Bryson, A. E., "Comments on 'Optimizing the Gains of the Baro-Inertial Vertical Channel'," *AIAA Journal of Guidance and Control*, Vol. 3, No. 3, pp. 286-288, May-June 1980.

98. Gelb, A. (Ed.), *Applied Optimal Estimation*, MIT Press, Cambridge, MA, 1974.

99. Benson, D. O., "A Comparison of Two Approaches to Pure-Inertial and Doppler-Inertial Error Analysis," *IEEE Transactions on Aerospace and Electronic Systems*, Vol. AES-11, No. 4, pp. 447-455, July 1975.

100. Weinreb, A., and Bar-Itzhack, I. Y., "The Psi-Angle Error Equation in Strapdown Inertial Navigation Systems," *IEEE Transactions on Aerospace and Electronic Systems*, Vol. AES-14, No. 3, pp. 539-542, May 1978.

101. Benson, D. O., "Comments on 'The Psi-Angle Error Equation in Strapdown Inertial Navigation Systems'," *IEEE Transactions on Aerospace and Electronic Systems*, Vol. AES-15, No. 1, pp. 168-170, January 1979.

102. Huddle, J. R., "Advances in Strapdown Systems for Geodetic Applications," in *High Precision Navigation: Integration of Navigational and Geodetic Methods,* Linkwitz, K., and Hangleiter, U. (Eds.), Springer-Verlag, N.Y., pp. 496-530, 1988.

103. Deyst, J. J., Jr., and Sutherland, A. A., Jr., "Strapdown Inertial System Alignment using Statistical Filters: A Simplified Formulation," *AIAA Journal*, Vol. 11, No. 4, pp. 452-456, April 1973.

REFERENCES
(Continued)

C. T. Leondes (Ed.), Vol. 38: Advances in Aeronautical Systems, Academic Press, N.Y., pp. 273-306, 1990.

137. Bar-Itzhack, I. Y., "In-Flight Alignment of Inertial Navigation Systems," in *Control and Dynamic Systems: Advances in Theory and Applications,* C. T. Leondes (Ed.), Vol. 38: Advances in Aeronautical Systems, Academic Press, N.Y., pp. 369-396, 1990.

138. Jiang, Y. F., and Lin, Y. P., "On the Rotation Vector Differential Equation," *IEEE Transactions on Aerospace and Electronic Systems*, Vol. AES-27, No. 1, pp. 181-183, January 1991.